

University of Windsor

Scholarship at UWindor

Electronic Theses and Dissertations

Theses, Dissertations, and Major Papers

2003

MEMS microphone design.

James Sliepenbeek
University of Windsor

Follow this and additional works at: <https://scholar.uwindsor.ca/etd>

Recommended Citation

Sliepenbeek, James, "MEMS microphone design." (2003). *Electronic Theses and Dissertations*. 2701.
<https://scholar.uwindsor.ca/etd/2701>

This online database contains the full-text of PhD dissertations and Masters' theses of University of Windsor students from 1954 forward. These documents are made available for personal study and research purposes only, in accordance with the Canadian Copyright Act and the Creative Commons license—CC BY-NC-ND (Attribution, Non-Commercial, No Derivative Works). Under this license, works must always be attributed to the copyright holder (original author), cannot be used for any commercial purposes, and may not be altered. Any other use would require the permission of the copyright holder. Students may inquire about withdrawing their dissertation and/or thesis from this database. For additional inquiries, please contact the repository administrator via email (scholarship@uwindsor.ca) or by telephone at 519-253-3000ext. 3208.

In compliance with the
Canadian Privacy Legislation
some supporting forms
may have been removed from
this dissertation.

While these forms may be included
in the document page count,
their removal does not represent
any loss of content from the dissertation.

MEMS Microphone Design

by

James Sliepenbeek

A Thesis

Submitted to the Faculty of Graduate Studies and Research through the
Department of Electrical and Computer Engineering in Partial Fulfillment
of the Requirements for the Degree of Master of Applied Science at the
University of Windsor

Windsor, Ontario, Canada
2003



National Library
of Canada

Bibliothèque nationale
du Canada

Acquisitions and
Bibliographic Services

Acquisitons et
services bibliographiques

395 Wellington Street
Ottawa ON K1A 0N4
Canada

395, rue Wellington
Ottawa ON K1A 0N4
Canada

Your file *Votre référence*
ISBN: 0-612-86709-9
Our file *Notre référence*
ISBN: 0-612-86709-9

The author has granted a non-exclusive licence allowing the National Library of Canada to reproduce, loan, distribute or sell copies of this thesis in microform, paper or electronic formats.

L'auteur a accordé une licence non exclusive permettant à la Bibliothèque nationale du Canada de reproduire, prêter, distribuer ou vendre des copies de cette thèse sous la forme de microfiche/film, de reproduction sur papier ou sur format électronique.

The author retains ownership of the copyright in this thesis. Neither the thesis nor substantial extracts from it may be printed or otherwise reproduced without the author's permission.

L'auteur conserve la propriété du droit d'auteur qui protège cette thèse. Ni la thèse ni des extraits substantiels de celle-ci ne doivent être imprimés ou autrement reproduits sans son autorisation.

Canada

© 2003 James Sliepenbeek

All Rights Reserved. No Part of this document may be reproduced, stored or otherwise retained in a retrieval system or transmitted in any form, on any medium or by any means without prior written permission of the author.

Abstract

This thesis presents an overview of microelectromechanical (MEMS) capacitive type microphone design for use in hearing instruments. A cohesive methodology is achieved via a mechanical equation of motion. Resulting in displacement, change in capacitance, sensitivity and pull-in voltage. All derived from one equation. From this investigation it is apparent that sensitivity is the most important factor in MEMS microphone design. The topics covered in the overview are: MEMS microphone design considerations, comparison of microphone types, signal detection methods, sources of dampening, modeling methods, sensitivity estimation, pull-in voltage estimation, bias voltage, ultimate tensile strength, design space optimization and MEMS microphone design flow.

A current state of the art design is used as an example throughout the overview. The current state of the art design utilizes a square diaphragm with width 2600, thickness 3 and air gap 4 μm , with 361 vent holes of effective radius 33.9 μm in a 13 μm thick backplate. The results from this overview highlight the importance of the various design parameters and their effect on the change in capacitance and the corresponding sensitivity of the microphone. An improvement in sensitivity from 8 to 12 mV/Pa was achieved while maintaining the diaphragm width and thickness values. By adjusting thickness of the diaphragm while maintaining the width, sensitivities of around 42 mV/Pa can be achieved.

With the initial modeling conclusions in place, two new MEMS capacitive microphone designs are introduced, modeled and analyzed. The first of these designs involves a di-

ABSTRACT

aphragm freely supported by cantilever springs. This type of design is sometimes referred to as a suspended design. It has the inherent advantage of being more flexible; thus it has a higher mechanical sensitivity. Expected sensitivities are around 81 mV/Pa. Finally a ring type microphone design is introduced and compared to the current state of the art. This ring microphone design utilizes capacitive edge detection methods to detect acoustic signals. It has the advantage of no pull-in voltage and an extremely high sensitivity in the range of 340 mV/Pa at only 3 V bias. The analysis methods used solids modeling in MATLAB and finite element analysis concepts in IntelliSense, where applicable, to analyze the proposed three-dimensional micro structure geometries.

For My Mother

Acknowledgments

The author wishes to thank the following for their patience and assistance with this thesis,

Dr. W. C. Miller
P. I. Makrygiannis
Dr. E. Liasi
N. S. Chana
T. Kuendiger
S. Sliepenbeek
Dr. S. Chowdhury
Dr. E. Lang
Dr. W. Altenhof
Dr. N. Zamani
Dr. R. Bowers

Contents

Abstract	iv
Dedication	vi
Acknowledgments	vii
List of Figures	xi
List of Tables	xiv
1 Introduction	1
1.1 Thesis Introduction	1
1.2 Thesis Objective	1
1.3 Introduction to MEMS Microphone Design Issues	2
1.4 Thesis Organization	4
2 Clamped MEMS Microphone Design	6
2.1 MEMS Microphone Design Considerations	6
2.2 Comparison of Microphone Types	7
2.3 Signal Detection Methods	8
2.4 Sources of Dampening	10
2.5 Modeling Methods	12
2.6 Sensitivity Estimation	18
2.7 Pull-In Voltage Estimation	23

CONTENTS

2.8	Bias Voltage	29
2.9	Ultimate Tensile Strength	31
2.10	Discussion of Current State of the Art	35
3	Clamped MEMS Microphone Design Optimization	37
3.1	Design Space Optimization	37
3.2	MEMS Microphone Design Flow	42
3.3	Discussion of Optimized Clamped Microphone Results	44
4	A Suspended Microphone Design	46
4.1	Suspended Microphone Modeling	46
4.2	Suspended Microphone Stress and Strain	57
4.3	Suspended Design Space Optimization	57
4.4	Suspended FEA Analysis Results	58
4.5	Discussion of Suspended Microphone Results	62
5	A Ring Microphone Design	64
5.1	Ring Microphone Introduction	64
5.2	Ring Microphone Design Modeling	66
5.3	Discussion of Ring Microphone Results	72
6	Conclusion	73
6.1	Conclusions	73
	References	75
A	Program 1	78
B	Program 2	82
C	Program 3	86
D	Program 4	90

CONTENTS

E Program 5	95
F Program 6	100
G Program 7	103
H Program 8	108
I Program 9	112
J Program 10	117
K Program 11	121
VITA AUCTORIS	126

List of Figures

2.1	The Hearing Range of the Human Ear	7
2.2	A Typical Clamped MEMS Microphone Design Cut-away View	8
2.3	An Example of the Frequency Shifting and Dampening on Displacement	11
2.4	Illustrating Couette Flow Dampening	12
2.5	Illustrating Squeeze Film Dampening	12
2.6	An Electrical Equivalent Circuit	13
2.7	A Mechanical Equivalent Circuit	13
2.8	Sum of the Forces Acting on the Diaphragm	15
2.9	Displacement $X_m(s)$ vs Frequency	16
2.10	Piston Like (Left) vs Actual Plate Deflection (Right)	17
2.11	Displacement vs Node Number	18
2.12	Displacement vs Node Number Illustrating Convergence	19
2.13	Displacement vs Delta	19
2.14	Displacement vs Delta	20
2.15	A Typical Detection Circuit	20
2.16	Capacitance vs Frequency	22
2.17	Sensitivity vs Voltage	23
2.18	Displacement X_m vs Voltage	24
2.19	Displacement X_m vs Voltage for Various Air Pressures	25
2.20	Displacement X_m vs Voltage for Various Residual Tensions	26
2.21	Pull-In Voltage vs Delta	27

LIST OF FIGURES

2.22 Pull-In Voltage vs Delta	28
2.23 Isuite Displacement For an Applied Voltage to 1/4 Microphone	28
2.24 Isuite Displacement vs Voltage	29
2.25 Isuite Capacitance vs Voltage	30
2.26 Stress Invariant SP1	32
2.27 Stress Invariant SP2	33
2.28 Stress Invariant SP3	33
2.29 Coulomb-Mohr Theory of Failure	34
3.1 A Design Space	38
3.2 Design Space Resolution Problems	39
3.3 The Sensitivity for an Optimized Clamped Microphone Design	40
3.4 The Sensitivity for an Optimized Clamped Microphone Design	41
3.5 The Stress Invariant SP3 Showing the Maximum Stress	42
3.6 Clamped MEMS Microphone Design Flow Chart	45
4.1 A Suspended MEMS Microphone Design	47
4.2 A Suspended MEMS Microphone Design	47
4.3 Spring Combinations	48
4.4 Common Types of MEMS springs	49
4.5 Displacement Results for Thin Structure Spring Analysis	49
4.6 Frequency Results for Thin Structure Spring Analysis	50
4.7 Displacement Results for Thick Structure Spring Analysis	52
4.8 Frequency Results for Thick Structure Spring Analysis	53
4.9 A Suspended Design Displacement vs Frequency	54
4.10 A Suspended Design Capacitance vs Frequency	55
4.11 A Suspended Design Sensitivity vs Frequency	55
4.12 Suspended Displacement vs Voltage for $P = 0$ and 1 Pa	57
4.13 FEA Displacement for the Optimized Suspended Design	59
4.14 FEA Displacement for the Optimized Suspended Design	59

LIST OF FIGURES

4.15 FEA SP1 For Optimized Design	60
4.16 FEA SP2 For Optimized Design	60
4.17 FEA SP3 For Optimized Design	61
4.18 FEA Frequency response	61
5.1 A Ring MEMS Microphone Design	65
5.2 Ring Design Showing Cross Section of Center Ring	66
5.3 Ring Design Showing Cross Section of Center Ring	67
5.4 Ring Design Showing Cross Section of Center Ring	67
5.5 Ring Design Showing Cross Section of Center Ring	68
5.6 Ring Design Showing Offset in Horizontal Plane	68
5.7 Ring Design Showing Offset in Vertical Plane	69
5.8 Ring Microphone Mechanical Equivalent	69
5.9 Ring Design Displacement vs Frequency	71
5.10 Ring Design Capacitance vs Frequency	71
5.11 Ring Design Sensitivity vs Frequency	72

List of Tables

2.1	Comparison of the Different Detection Methods	10
2.2	FEA Pull in Voltage Results for Various Mesh Sizes	30
3.1	Design Space Results for The Clamped Microphone	40
4.1	FEA Results for Various Plate Thickness	52
4.2	Design Space Optimization Results for Suspended Microphone	58
4.3	FEA Results for the Suspended Microphone	62
5.1	Ring Design Space Optimization Results	70
6.1	Comparison of the Designs	74

Chapter 1

Introduction

1.1 Thesis Introduction

Micro Electro Mechanical Systems (MEMS) were first conceived by legendary physicist Richard Feynman, who theorized in 1959 that size was not a barrier to advanced technology. MEMS technology utilizes VLSI design principles to create micro scale machines which are primarily used as sensors in various systems from accelerometers in automobile air bags to small microphones in hearing aids. Some of the advantages of MEMS devices are, durability, size and the potential for cost savings due to mass production. Currently size is the primary advantage of MEMS. In the ear hearing aids have a size restriction of about 4 square millimeters. MEMS microphones can fulfill this size constraint and still provide a high sensitivity.

1.2 Thesis Objective

This thesis will investigate the current state of the art in MEMS microphone design. With the objective of creating an improvement in sensitivity over the current state of the art designs. New microphones will be investigated to further this goal. A higher sensitivity

will reduce the needed bias voltage magnitude and required diaphragm surface area. Both of which increase MEMS microphone applicability to on chip integration for hearing aid applications.

1.3 Introduction to MEMS Microphone Design Issues

The majority of MEMS microphone designs focus on a parallel plate type of structure. One or both plates are deflected by the air pressure difference of the incoming sound wave. In some designs the top plate deflects and the bottom plate is kept ridged. The plate that moves is sometimes referred to as the membrane or diaphragm. the gap separating the two plates is referred to as the air gap. The backplate typically contains vent holes that serve to reduce air pressure built up by plate displacement.

Commonly used materials for the diaphragm are, polysilicon, silicon nitride or even a man made material such as parylene. If the material used is brittle then its fracture strength must be taken into consideration. Exceeding the ultimate tensile strength will result in fracture and failure of the diaphragm. The choice of material depends mainly on flexibility and the signal detection method desired.

Signal detection methods typically are achieved by, piezoelectric, piezoresistive, electrolytic and capacitive means. Piezoelectric and piezoresistive designs utilize materials whose properties change due to applied stress. Piezoelectric materials create a voltage when a stress is applied. Piezoresistive materials have a change in resistance when stress is applied. Both of these detection methods detect the bending stress found at the edge of the diaphragm. Electrolytic microphones utilize a material that contains charges. Capacitive microphones require a bias voltage to operate. The bias voltage creates an electric field in the gap between the plates. Deflecting the diaphragm causes an increase in the electric field between the plates for both electrolytic and capacitive microphone types. This electric field causes a detectable change in voltage. The diaphragm and backplate need to be conductive for the capacitive detection method. This conductivity is obtained by metalization or heavy doping. Metalization can be done with aluminum and phosphorus is a typical dopant. Electrolytic and capacitive microphones provide the best sensitivity.

Microphone designs are compared by sensitivity and base capacitance. Base capacitance of the microphone is the capacitance with no plate deflection. Sensitivity is the change in output voltage per air pressure difference applied and is measured in mV/Pa. The base capacitance needs to be stated so that capacitive voltage divider losses can be evaluated. Capacitive voltage divider losses occur when a capacitive microphone is connected to an amplifier circuit. The amplifier circuit has an intrinsic capacitance which adds together in series with the microphone's capacitance. This creates a capacitive voltage divider circuit that attenuates the magnitude of output signal. Stating the base capacitance allows any researcher to compare another design with the measured sensitivity of their design. Another method of comparing microphone designs is to state the change in capacitance along with the base capacitance. The change in capacitance is directly proportional to sensitivity and is equivalent.

The use of a bias voltage in capacitive microphones results in a phenomenon called pull-in. Pull-in occurs when the electrostatic force, between the parallel plates of a microphone, overcomes the spring forces supporting the diaphragm. When this happens the diaphragm collapses to the backplate. It is for this reason that the bias voltage cannot be increased on capacitive microphones without limit. The voltage at which pull-in occurs is called the pull-in voltage, V_p . An additional benefit of using a bias voltage on capacitive microphones is that the change in capacitance can be increased for a given displacement. This is because of the non-linear nature of pull-in. Bias voltage must also be kept below the pull-in value to avoid non-linear distortion of the output signal. The force created by a typical 1 Pa air pressure difference is much smaller than the electrostatic force. In effect this means that capacitive microphones are dominated by electrostatic forces.

Another dominant feature in MEMS microphone design is residual tension. Residual tension arises in the diaphragm during manufacturing. The effect of residual tension is to increase the stiffness of the diaphragm. This affects pull-in voltage and sensitivity. Pull-in voltage is increased because the spring forces on the diaphragm are larger. The electrostatic force needed to overcome this larger spring force then needs to be larger. Which then requires a higher voltage. Sensitivity is decreased because there is less displacement for a

given air pressure difference. It is important to reduce the residual tension so that sensitivity can be maximized. There are two approaches to reducing residual tension. The first is to use high temperature annealing to relax the diaphragm. The second method involves changing the diaphragm geometry by adding ribbing. This allows for expansion of the diaphragm.

1.4 Thesis Organization

Chapter 1 provides an introduction to the area of research carried out in the thesis. The second section provides an introduction to MEMS microphone design. This section is intended to provide a general overview of design issues in MEMS microphone design. The third section in the introduction presents an overview of the thesis organization.

Chapter 2 begins with an overview of MEMS microphone design considerations, including a comparison of microphone types, design constraints, signal detection methods, sources of dampening, modeling methods, sensitivity estimation, pull-in voltage estimation, bias voltage and ultimate tensile strength. The chosen state of the art design is used as a design example throughout. The chapter is concluded with a discussion of the results from the investigation.

Chapter 3 introduces the fundamental concepts involved in design space optimization. From this a clamped MEMS microphone design flow will be proposed. Following this an optimized clamped microphone will be presented and supported by MATLAB and FEA results. Finally there is a section discussing the results of the chapter, emphasizing the utility of this design space approach.

Chapter 4 will apply the theoretical foundation from Chapter 2 to a suspended plate microphone design. This design utilizes a square plate that is supported by a number of cantilever type springs at the edges. As with the state of the art investigation a mechanical model is developed and its MATLAB simulation results are shown. Next the stress and strain in the supporting springs will be evaluated to ensure that structural failure will not occur. From the mechanical model a design space optimization program is developed and used to optimize the design. FEA results from the optimized suspended microphone are presented in the following section. Finally a section discussing the suspended plate

microphone results is presented.

Chapter 5 will investigate an innovative ring type MEMS microphone. This design utilizes a series of rings that are suspended by springs above a back plate. Capacitive edge detection is used to sense air pressure differences. The analysis proceeds as in Chapter 2 with the development of a mechanical model. This design evolved from suggested improvements from the two previous designs deficiencies. Those design deficiencies center around the flexibility of the diaphragm and the limitations of pull-in voltage. The chapter begins with a introduction discussing the details of the design and its various advantages over the current state of the art and suspended microphone designs. Next a section covers developing a mechanical model of the ring microphone and showing its MATLAB simulation results. Finally a discussion section concludes the chapter where the results for the ring type microphone are covered.

Chapter 6 is the concluding chapter. This chapter presents an overall summary of the results from Chapters 2 to 5. The various designs are compared.

Chapter 2

Clamped MEMS Microphone Design

2.1 MEMS Microphone Design Considerations

Various design issues must be addressed when designing a MEMS microphone. The first design constraint is the ear itself. The human ear can hear from 100 to 20 kHz and from around 0 to 100 dB as can be seen in Figure 2.1. Most hearing aids are designed for a maximum frequency of around 10 kHz. The dynamic range is from 4×10^{-4} to 1 Pa of pressure difference [1]. For hearing aids the size of the microphone must be less than 4 mm so that it can physically fit in the ear canal. The second area of constraints arises from the battery that will provide the hearing aid with voltage and current. Most hearing aid batteries are in the range of only 3 V. As is seen in Section 2.6 and 2.7 voltage plays an important role in microphone operation. Finally material selection is constrained in MEMS design. Most MEMS microphones are made of polysilicon or silicon nitride; as such, a design must not exceed the maximum stress that the structure can handle, as will be shown in Section 2.9.

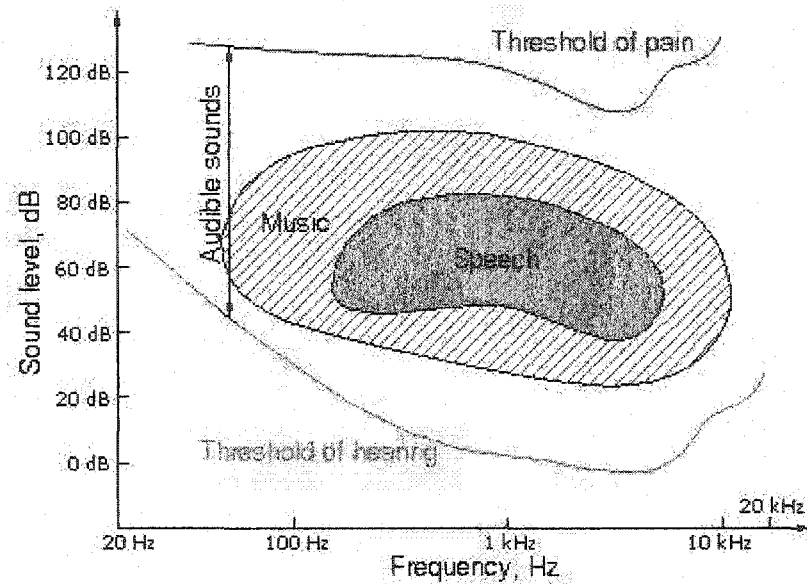


Figure 2.1: The Hearing Range of the Human Ear

2.2 Comparison of Microphone Types

MEMS microphones follow traditional microphone design in that they utilize a diaphragm that is deflected by a sound wave. This diaphragm is supported by a backplate that contains numerous vent holes, which reduce air resistance due to diaphragm motion. This air resistance dampens out the diaphragm's motion, which results in a smoother frequency response. The diaphragm is separated from the backplate by a thin layer of insulation. The backplate and diaphragm are usually made of polysilicon that has been heavily doped with phosphorus making them conductive. The diaphragm and the backplate together constitute a capacitance. The impinging sound waves change this capacitance and thus cause a change in voltage and charge that can be detected. A typical design can be seen in Figure 2.2.

This thesis will use the work of Hsu, Mastrangelo and Wise,[2] as an example of a typical state of the art design. The following sections will use this paper as an example to illustrate the various topics discussed there in. It presents the analysis, design, fabrication and testing of a square condenser microphone and is considered typical of the state of the art in MEMS microphone design.

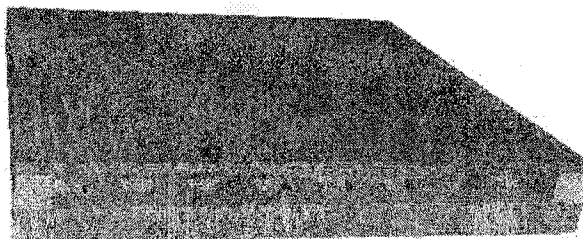


Figure 2.2: A Typical Clamped MEMS Microphone Design Cut-away View

Two additional microphones that will also be investigated are shown in Figure 4.1 and Figure 5.1. The first of these designs is known as a suspended or spring supported microphone. Although it is not very common, it was desired to determine its behavior and whether it is suitable for microphone applications. The second design is a ring microphone and has been developed based upon improvements suggested by the analysis of the current state of the art. This design will be referred to as a ring type capacitive microphone.

2.3 Signal Detection Methods

Diaphragm motion detection in MEMS falls into five primary categories: piezoelectric, piezoresistive, electret, FET and capacitive microphones [3], [5]. Piezoelectric microphones utilize a material that creates a voltage due to bending stresses. This material is mounted on the surface of the microphone where the greatest bending stresses occur, which is around the edges of the diaphragm. Piezoelectric microphones have low sensitivities of around $25 \mu\text{V}$ to 1 mV/Pa with a frequency response of 10 to 10 kHz. One problem with piezoelectric microphones is a relatively high noise level.

Piezoresistive microphones utilize a material whose resistance changes due to bending stresses. Typically four piezoresistors are arranged in a Wheatstone bridge configuration, with two resistors placed in the middle and the other two placed at the edge of the diaphragm. When the diaphragm deflects, the strains at the middle and edge of the diaphragm are of opposite signs causing an inverse change in the piezoresistors. Piezoresistive

microphones typically have a low sensitivity of around 25μ to 10 mV/Pa with a frequency range of 100 to 5 kHz [6], [7]. Noise in piezoresistive microphones comes mainly from thermal noise at high frequencies and $1/f$ noise at lower frequencies. One advantage of the piezoresistive microphone is the relatively low output impedance [3]. This changing resistance can be turned into a varying current or voltage as desired.

Capacitive microphones are the most popular of all the microphones and as such will be the focus of this thesis. The reason for this popularity is ease of manufacture and high sensitivity. In typical designs two parallel plates are charged and an impinging sound wave causes one or both plates to deflect. This deflection causes a change in capacitance which in turn can result in a change in voltage or current. Once again capacitive microphones have high sensitivities of around 0.1 mV to 25 mV/Pa with a frequency response of 10 to 15 kHz [3]. Capacitive microphone noise is primarily dominated by amplifier $1/f$ noise [5]. One disadvantage of capacitive microphones is the decreased sensitivity for high frequencies due to the air-streaming resistance of the narrow air gap [3]. Unlike the other designs, capacitive microphones need a bias voltage to operate. This bias voltage is in the range of 3 to 15 V. Hearing aid batteries typically operate around 3 V; voltages higher this require a voltage multiplier stage in order to boost the voltage. Bias voltage is selected to ensure maximum sensitivity yet prevent a phenomena called pull-in, which will be discussed in Section 2.7. Also bias voltage should be kept within the linear range of deflection of the microphone.

Electret microphones have a similar arrangement as capacitor microphones in that two parallel plates are separated by an air gap; electret microphones, however, do not require an external bias voltage. It is supplied by a layer of material containing built in charges, which provides an electric field and in turn creates a voltage. Electret microphones have a relatively high sensitivities of around 1 to 10 mV/Pa with a frequency response around 10 to 10 kHz. Primary sources of noise once again come from the amplifier.

The FET microphone utilizes a integrated field-effect transistor [4]. Its metalized diaphragm serves as the movable gate of the field-effect transistor. FET microphones have a sensitivity of 0.2 to 6 mV/Pa with a frequency range of 100 to 30 kHz. An advantage of the FET microphone is its low output impedance. A disadvantage is the absence of a bias

Table 2.1: Comparison of the Different Detection Methods

	Piezoelectric	Piezoresistive	Electrolytic	Capacitive	FET
Sensitivity	Low	Low	Low	High	Low
Frequency Range	Large	Small	Small	Small	High
Impedance	High	Low	Low	Low	Low
Polarizing Voltage	No	Yes	No	Yes	Yes
Noise Level	High	High	Low	Low	High

element; which defines a stable gate potential of the FET. As such the long-term stability of the microphone is affected due to drift. Noise shows a $1/f^{1/2}$ dependence due to flicker noise in the channel of the FET [3]. Table 2.1 compares the differences between the various signal detection methods.

2.4 Sources of Dampening

Ideally a microphone will create a voltage or current proportional to the audio signal impinging upon it. However, the actual case is that various dampening effects cause the microphone to distort the corresponding amplitude of the signal at various frequencies. Figure 2.3 shows an example of this frequency shifting and dampening effect. The curve represents the displacement versus frequency for a suspended microphone design as will be introduced in Chapter 4. The estimated resonant frequency for this design was 8550 Hz. The actual resonant peak was found at the much higher frequency of 18.3 kHz. The magnitude of the frequency peak is far less than expected for a resonant mode. Microphone dampening comes from two sources, squeeze film dampening and Coulett flow dampening [8]. Couette flow dampening arises in MEMS structures when a layer of air is between two plates, where one plate is moving relative to the other. This effect is illustrated in Figure 2.4, where h is the air gap height, U is the velocity of the above plate and τ is the shear stress acting on the plate. The flow profile can be seen in the plot to the right of the Figure.

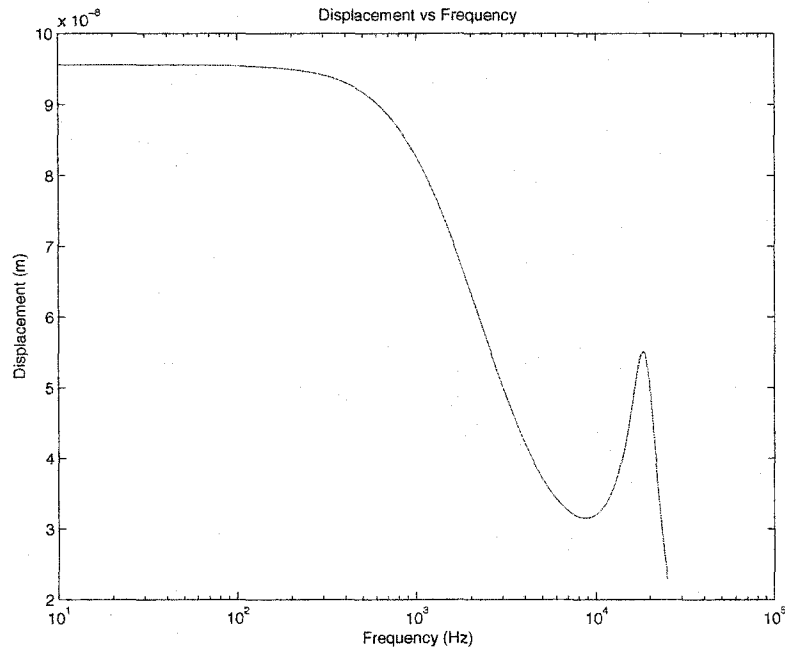


Figure 2.3: An Example of the Frequency Shifting and Dampening on Displacement

The formula governing this effect is given in Equation 2.1.

$$R_{Couette} = \frac{\eta A}{h} \quad (2.1)$$

The other source of dampening, squeeze film dampening, occurs when air is squeezed between two plates where either one or both plates are moving perpendicularly to the air gap as is illustrated in Figure 2.5. Here, a time varying force, F , applied to the top plate causes the air gap height, $h(t)$, to change, squeezing the air out the sides. The equations governing this source of dampening when there are no vent holes in the back plate are,

$$b = \frac{96\eta LW^3}{\pi^4 h_0^3} \quad (2.2)$$

$$\omega_c = \frac{\pi^2 h_0^2 P_0}{12\eta W^2} \quad (2.3)$$

Where b is the damping constant, η is the viscosity of air, and ω_c is the cutoff frequency. Finally the resultant dampening is calculated as,

$$R_{sq} = b \quad (2.4)$$

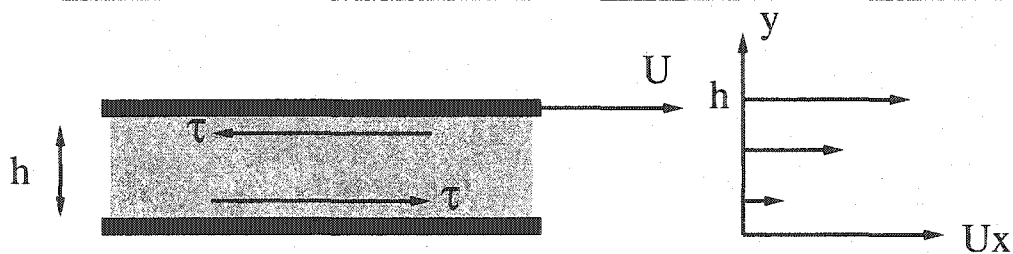


Figure 2.4: Illustrating Couette Flow Dampening

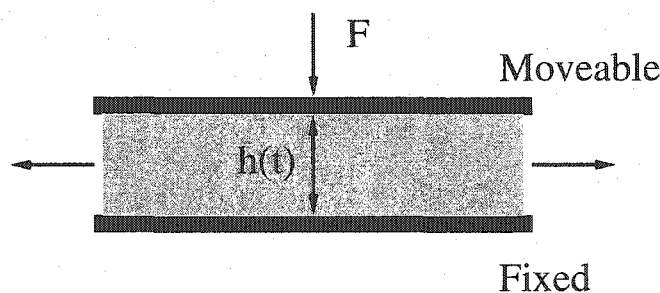


Figure 2.5: Illustrating Squeeze Film Dampening

and, is calculated as

$$K_{sq} = b\omega_c. \quad (2.5)$$

If the air gap has vent holes, a different set of equations is used to describe the dampening and spring constants. These equations will be covered in Section 2.5.

2.5 Modeling Methods

Modeling methods can be divided into two groups, analytical and finite difference/element. Analytical modeling methods can be divided into two groups, mechanical and electrical equivalents. Electrical equivalents utilize capacitors, resistors and inductors to model the mechanical behavior of a microphone. An example of an electrical equivalent circuit is given in Figure 2.6. This electrical equivalent circuit is from Reference [2]. Mechanical equivalents simplify a structure into fundamental units such as mass, dampeners and spring constants, [9], [10], [11], [12], [13]. An example of a mechanical equivalent is given in Figure 2.7. The microphones modeled in this thesis will be modeled as mechanical equivalents.

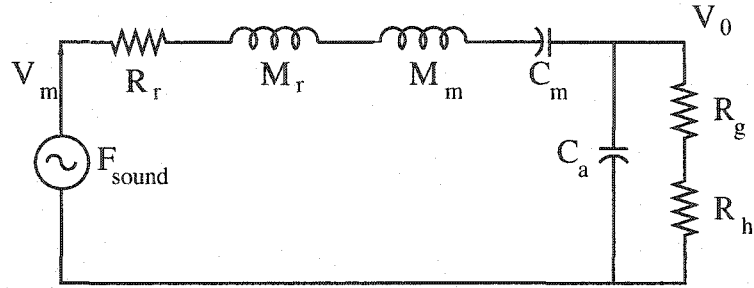


Figure 2.6: An Electrical Equivalent Circuit

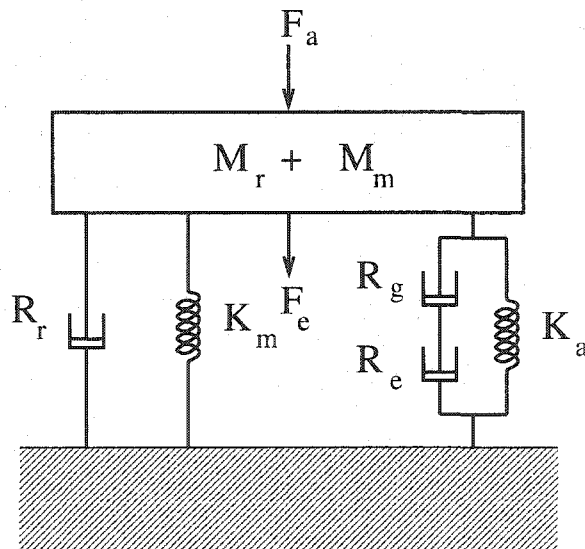


Figure 2.7: A Mechanical Equivalent Circuit

This is felt to be more intuitive. The mechanical equivalent shown in Figure 2.7 is actually the equivalent for the chosen state of the art design given in reference [2]. The various parameters are as follows.

$$R_r = \frac{\rho_0 a^4 \omega^2}{2\pi c} \quad (2.6)$$

$$M_r = \frac{8\rho_0 a^3}{3\pi\sqrt{\pi}} \quad (2.7)$$

R_r is the radiative resistance and M_r is the mass of the air in contact with the vibrating diaphragm. ρ_0 is the air density; c is the sound velocity; ω is the angular vibration frequency ($2\pi f$); and a is the diaphragm width. The diaphragm stiffness, K_m , is given by the inverse of the compliance as given in Reference [2].

$$K_m = \frac{\pi^6(2\pi^2 D + a^2 T)}{32a^2} \quad (2.8)$$

The equivalent mass element M_m of the square diaphragm is,

$$M_m = \frac{\pi^4 \rho (2\pi^2 D + a^2 T)}{64T} \quad (2.9)$$

D is the flexural rigidity, and T is the residual tension of the diaphragm. The viscosity loss in the air gap, R_g , is given by,

$$R_g = \frac{12ua^2}{nd^3\pi} \left(\frac{\alpha}{2} - \frac{\alpha^2}{8} - \ln \frac{\alpha}{4} - \frac{3}{8} \right). \quad (2.10)$$

its stiffness, K_a , is given by the inverse of the air gap compliance, C_a , as

$$K_a = \frac{d}{\rho_0 c^2 \alpha^2 a^2} \quad (2.11)$$

Where n is the hole density in the backplate, α is the surface fraction occupied by the holes, u is the air viscosity coefficient, and d is the average air gap distance. The viscosity loss of the back plate holes R_h is,

$$R_h = \frac{8uha^2}{\pi nr^4} \quad (2.12)$$

where h is the back plate height and r is the radius of the air gap vent holes. There is some confusion as to what is meant by r . Hsu et al., [2] refer to this parameter as the radius of the vent holes; however, the fabricated microphones have backplate holes that are $60\mu\text{m}$ by

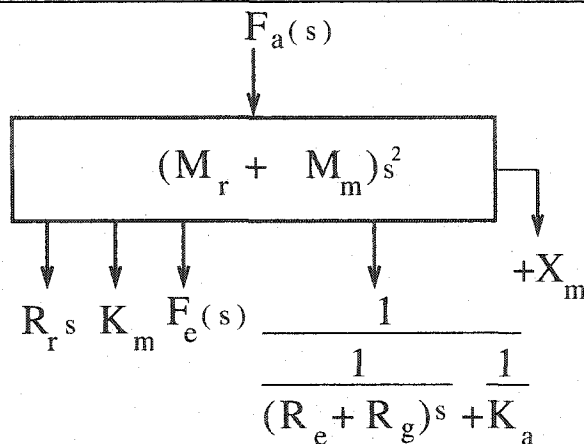


Figure 2.8: Sum of the Forces Acting on the Diaphragm

60 μm square. It is assumed that r in this case means the effective radius of a circular hole that is of the same area. Also the number of vent holes used in the 2.6 mm diameter design is unclear. This thesis has assumed that since the 2 mm design has 17 by 17 holes, giving 289 total, that the 2.6 mm design must be approximately 19 by 19 giving 361 holes by linear scaling. The number of holes on the 2 mm design has been determined from Figure 2 in the paper [2]. From the mechanical equivalent, the forces acting on the diaphragm are derived as shown in Figure 2.8. From Figure 2.8 the sum of the forces can be obtained, and the equation of motion in the frequency domain for the clamped microphone can be derived by solving for $X_m(s)$.

$$X_m(s) = \frac{F_a + F_e}{(M_m + M_r)s^2 + R_r s + K_m + \frac{1}{\frac{1}{(R_g + R_h)s} + \frac{1}{K_a}}} \quad (2.13)$$

where $X_m(s)$ is the displacement of the diaphragm with the down direction considered positive. $X_m(s)$ is a function of s ; the absolute value of $X_m(s)$ is the magnitude of the response; and the phase is the \tan^{-1} of the ratio of the real and imaginary parts. Further references to X_m in this thesis imply the absolute value of $X_m(s)$. F_a is the force due to the applied air pressure difference, and F_e is the force due to the electrostatic attraction between the plates. The MATLAB implementation of the above Equations can be found in Appendix A. The first output plot from this program can be seen in Figure 2.9, which displays the displacement $X_m(s)$ versus frequency. An average displacement of 3.67 nm is

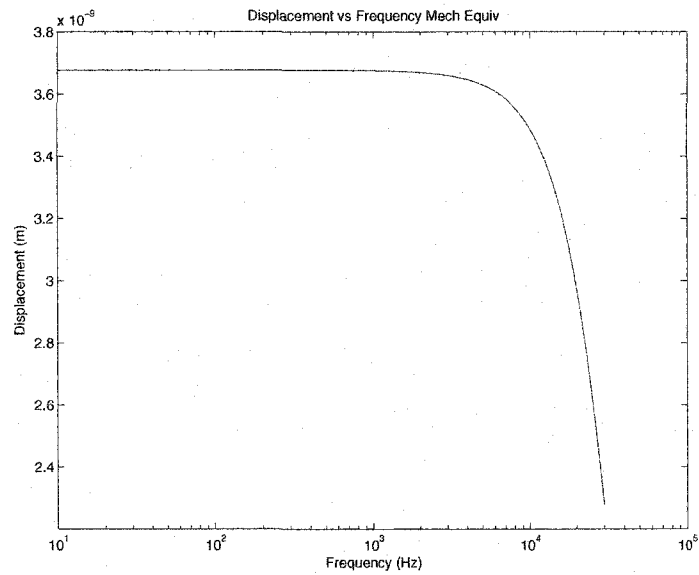


Figure 2.9: Displacement $X_m(s)$ vs Frequency

noted with a quick drop off in amplitude above 10 kHz due to back plate viscosity losses at higher frequencies. Hsu et al., [2] estimate the resonant frequency of the microphone by,

$$F_{res} = \sqrt{\frac{1}{\rho} \left(\frac{D\pi^2}{a^2} \frac{T}{2a^2} \right)} \quad (2.14)$$

Evaluating Equation 2.14 gives 25 kHz for the resonant frequency. Both electrical and mechanical models are using lumped parameter values to predict the approximate behavior of the system based upon the derived transfer function of the model. As will be seen this equation can predict the behavior of these systems with reasonable accuracy for almost all behaviors. The limitations of this method are discussed in the following sections.

Where lumped parameter models fail, finite difference/element models are used. With clamped microphones, the diaphragm does not deflect like a piston; most lumped parameter models assume this behavior. In actuality the diaphragm deforms in a continuous manner as shown in Figure 2.10. The dashed structures represent the initial positions before and the solids are after displacement. For this reason that lumped parameter models fail to predict pull-in voltage with any accuracy.

In microphone design, finite difference can be used to model the bending plate problem

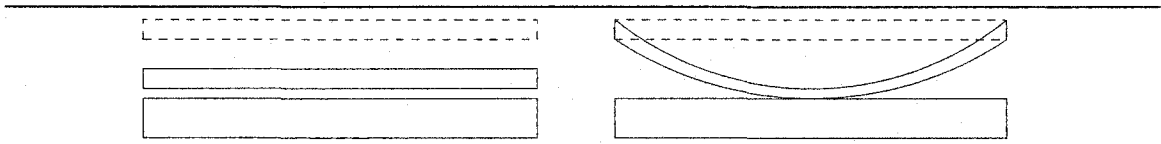


Figure 2.10: Piston Like (Left) vs Actual Plate Deflection (Right)

as seen in Equation 2.15. The method of finite differences can be used to solve partial differential equations [14].

$$D \nabla^4 W + T \nabla^2 W = P_{\text{applied}} \quad (2.15)$$

where P_{applied} is the applied pressure difference to the top plate [15]. The applied pressure can also include electrostatic forces which can be viewed as an applied pressure. A solution to this equation would allow the correct calculation of displacement or change in capacitance versus applied pressure. Section 2.7 discusses some problems with finite difference modeling. The MATLAB m code for this can be found in Appendix B. An output plot of deflection versus node number can be seen in Figure 2.11. This plot is at 1 Pa with 1 V applied to the diaphragm. Finite difference reveals how the diaphragm has been deflected and the limitations of the piston-like displacement assumption, as can be seen in Figure 2.13.

A MATLAB program was written to investigate the deflection of the diaphragm for a range 0 to 1 Pa pressure differences, Figure 2.14; the program to generate the plot can be found in Appendix C. The nodes correspond to how the diaphragm has been broken up by the program: the higher the number of nodes, the more finely divided the diaphragm. With finite difference, the question arises as to how many nodes are needed for accuracy. A MATLAB program written to investigate this question can be found in Appendix D. The output of this program is seen in Figure 2.12, which illustrates the convergence of the displacement with the number of nodes. The number of nodes equals the number of pieces the diaphragm has been divided from side to side; thus a number of nodes of 40 means that the diaphragm has been divided into 40 pieces. As is seen in the figure, the larger the number of nodes the better. At around 100 nodes the solution begins to converge. As such at least 100 nodes are needed in order to ensure accuracy of the solution. However, the computation time needed at 100 nodes can be significant. Running the MATLAB program

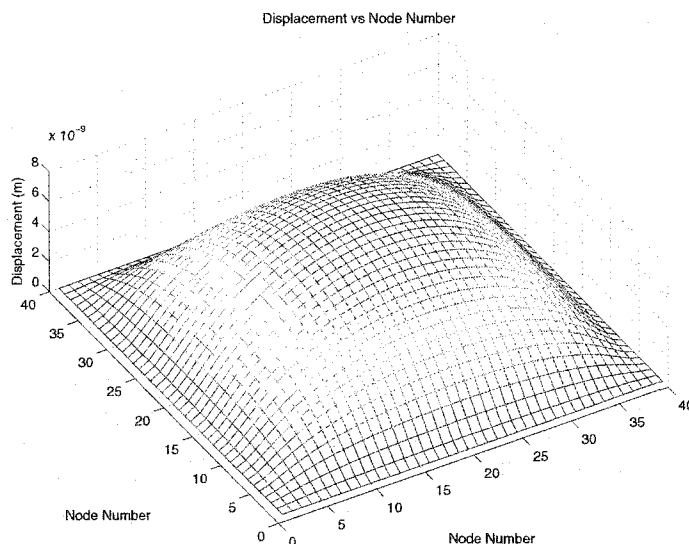


Figure 2.11: Displacement vs Node Number

in Appendix D required 2 weeks of computation time on a Sun Blade 1000, at 900 MHz.

2.6 Sensitivity Estimation

An important design parameter in microphone design is sensitivity. The sensitivity of a microphone is given in Volts per Pascal referenced to 1mV/Pa , which corresponds to the lowest sound pressure humans can hear. This sensitivity is measured at 1 kHz for all microphones. Sensitivity can be broken into mechanical and electrical sensitivity.

$$S = S_m S_e \quad (2.16)$$

The mechanical sensitivity S_m corresponds to how much the diaphragm deforms per Pascal and is measured in m/Pa . Electrical sensitivity S_e corresponds to the change in V per meter and is measured in V/m . When comparing microphones, sensitivity only becomes meaningful when discussing open circuit sensitivity. Open circuit sensitivity is the change in voltage for a given pressure for a microphone that is not connected to any other amplification circuitry. If a microphone is connected to an amplifier then any sensitivity can be obtained simply by increasing outside amplification.

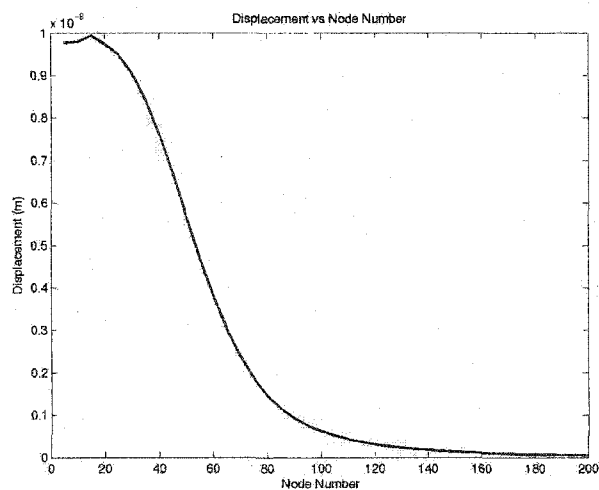


Figure 2.12: Displacement vs Node Number Illustrating Convergence

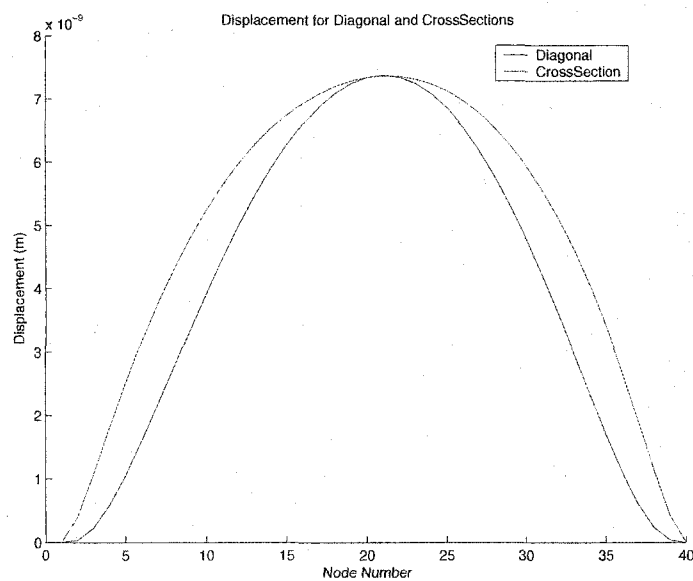


Figure 2.13: Displacement vs Delta

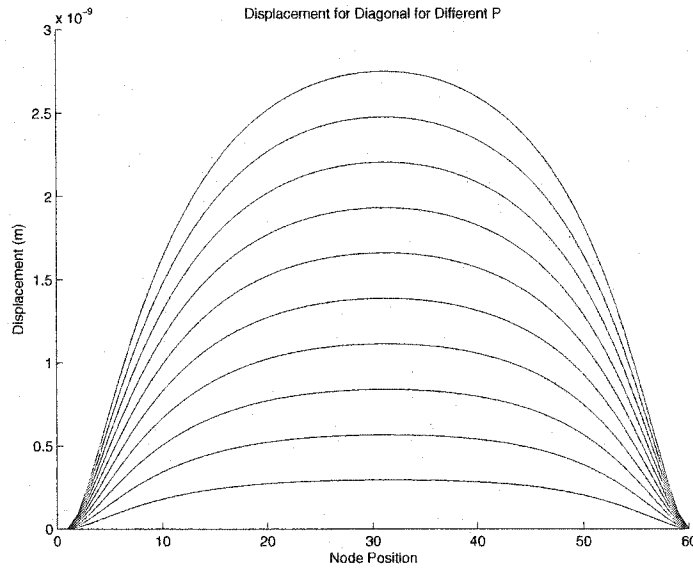


Figure 2.14: Displacement vs Delta

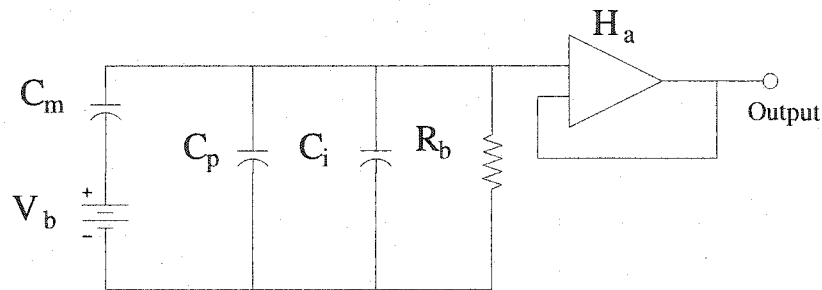


Figure 2.15: A Typical Detection Circuit

Another microphone property that is required when comparing microphones is the microphones capacitance. It is important because the capacitance of the microphone combines with parasitic and preamplifier intrinsic capacitance, which reduce the voltage that is detected by the amplifier. A typical detection circuit is show in Figure 2.15. C_m corresponds to the capacitance of the microphone. C_p is parasitic capacitance including the capacitance of the bonding pad, approximately 3 pF. C_i and R_b is the intrinsic capacitance of the amplifier and the bias resistor respectively.

In order to estimate the actual measured sensitivity, S_{meas} , the open circuit sensitivity, S_{oc} , is required as well as the capacitance of the microphone. The intrinsic capacitance, C_i ,

of the preamplifier connected to the microphone, and the parasitic capacitance, C_p , that will be encountered. Knowing these values allows an estimate of the capacitive signal attenuation, H_c , due to the input capacitance of the preamplifier and the parasitic capacitance.

It is given by,

$$H_c = \frac{C_m}{C_m + C_i + C_p}. \quad (2.17)$$

The measured sensitivity can be calculated finally as,

$$S_{meas} = -S_m S_e H_c H_a \quad (2.18)$$

where H_a is the gain of the preamplifier, with a value usually around one. Most MEMS microphones give an open circuit sensitivity in the range of a few millivolts per Pascal with a capacitance of around 1 to 10 pF. Another way to estimate sensitivity is to derive it from fundamentals. Starting with

$$Q_0 = V_0 C_0 \quad (2.19)$$

where Q_0 is the initial charge on the MEMS microphone capacitor, V_0 , the applied initial voltage supplied by the battery, C_0 , the initial capacitance with no displacement. Applying a displacement and assuming conservation of charge gives,

$$Q_n = V_n C_n \quad (2.20)$$

where Q_n is equal to Q_0 , V_n , the new voltage and C_n , the new capacitance created by the displacement. Equating Equation 2.19 to Equation 2.20 and rearranging gives,

$$V_n = \frac{V_0 C_0}{C_n} \quad (2.21)$$

noting that,

$$C_0 = \frac{\epsilon_0 A}{d_0} \quad (2.22)$$

and,

$$C_n = \frac{\epsilon_0 A}{(d_0 - X_m)} \quad (2.23)$$

subbing 2.22 and 2.23 into 2.21 gives,

$$V_n = \frac{V_0(d_0 - X_m)}{d_0} \quad (2.24)$$

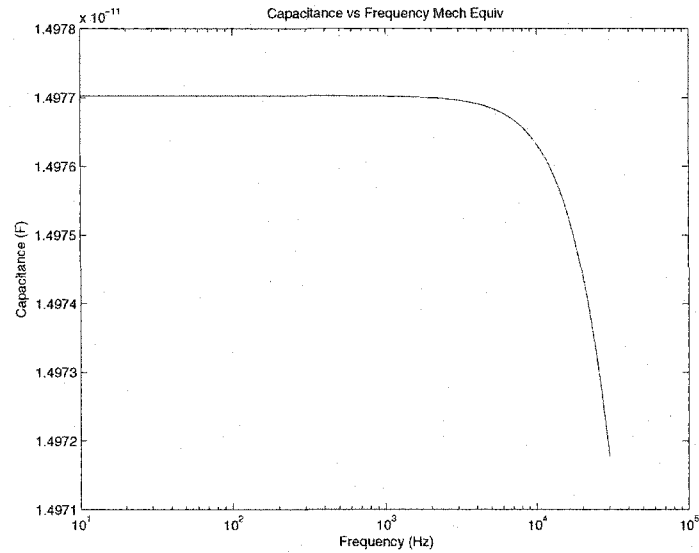


Figure 2.16: Capacitance vs Frequency

where d_0 , the original air gap distance and X_m , the displacement of the diaphragm. The fundamental definition of sensitivity is the change in voltage for a given change in pressure,

$$S = \frac{\Delta V}{\Delta P} \quad (2.25)$$

subbing in 2.24 for the change in voltage and $P = 1$ Pa as the change in pressure gives,

$$S = \frac{V_0(d_0 - X_m)}{d_0} \quad (2.26)$$

Which shows that the sensitivity is proportional to the ratio of the old and new capacitance. Which, ultimately becomes the air gap height of the new capacitance divided by the old air gap. From which can be concluded, the larger the change in capacitance the larger the sensitivity. From $X_m(s)$ the change in capacitance can be calculated by Equation 2.23 as seen in Figure 2.16. The base capacitance can be seen at 0 Hz to be around 15 pF. This capacitance is close to the papers stated capacitance 16.2 pF. Applying Equation 2.26 to Equation 2.13 and calculating the absolute value of the sensitivity from 0 to 30 kHz gives Figure 2.17. As with figures 2.9, 2.16 and 2.17 were generated by the program listed in Appendix A. This is the sensitivity for a clamped microphone based upon the lumped parameter mechanical model. The predicted sensitivity for the design is around 9.2 mV/Pa

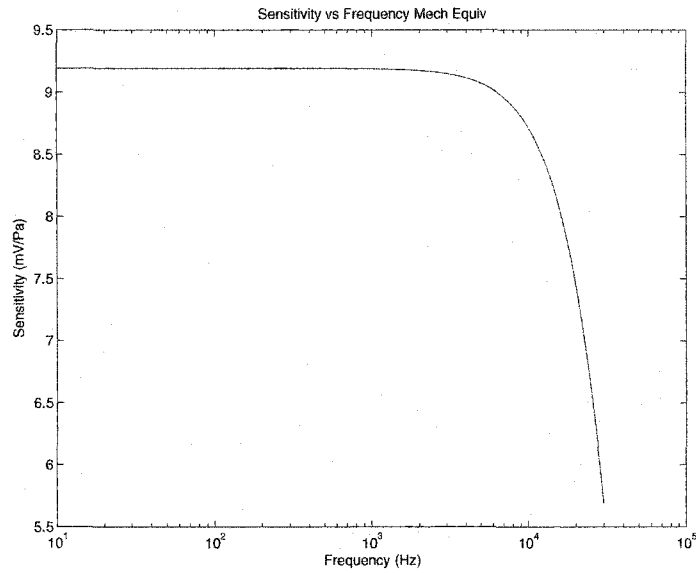


Figure 2.17: Sensitivity vs Voltage

which is close to the reference papers 8 mV/Pa. As expected from the derivation the capacitance and sensitivity plots follow the basic trend as the displacement.

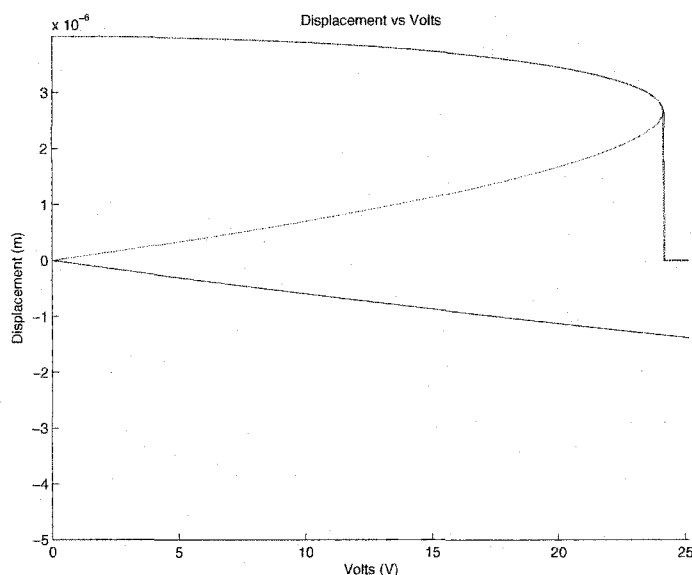
2.7 Pull-In Voltage Estimation

Another important design requirement is pull-in voltage [16]. Pull-in occurs when the bias voltage on capacitive type microphones is too high and causes the electric field to pull down the diaphragm onto the backplate. Effectively the spring forces supporting the diaphragm have been overcome by the electrostatic attractive forces. Knowing the bias voltage is important since it has a direct effect on the sensitivity of the microphone. Pull-in voltage can be derived directly from the mechanical model of the microphone. By setting the applied frequency $s = 0$ gives,

$$X_m = \frac{F_a + F_e}{K_m} \quad (2.27)$$

Subbing in for $F_e(s)$, [17],

$$F_e = \frac{\epsilon_0 A V_0^2}{2(d_0 - X_m)^2} \quad (2.28)$$

Figure 2.18: Displacement X_m vs Voltage

solving for X_m gives,

$$K_m X_m^3 - (2d_0 K_m + F_a) X_m^2 + (K_m d_0^2 + 2d_0 F_a) X_m - \frac{F_a d_0^2 + \epsilon_0 A V_0^2}{2} \quad (2.29)$$

This displacement of the diaphragm is considered positive down. Plotting Equation 2.29 gives the curve shown in Figure 2.18. This plot shows three lines corresponding to the three roots of Equation 2.29. The first root shows a straight line going down. This corresponds to the diaphragm moving away from the backplate and it is discarded as a nonsensical solution. The second root is the line that curves up from the center of the plot up to the third root and corresponds to the unstable solution. Unstable means that if the diaphragm lies anywhere along this curve it would then quickly collapse. The third root is the remaining curve. It represents the stable solution. The intersection of the second and third root actually corresponds to the pull-in point. It is the maximum voltage that can be applied to the diaphragm and still not have it collapse. A voltage greater than this will cause the diaphragm to immediately collapse. The third root curve indicates that the diaphragm initially drops down in an almost linear fashion until it approaches the pull-in point at which it then collapses to the back plate. A range of air pressures can be applied to our model and the effects can be seen as in Figure 2.19. This pressure is applied differentially

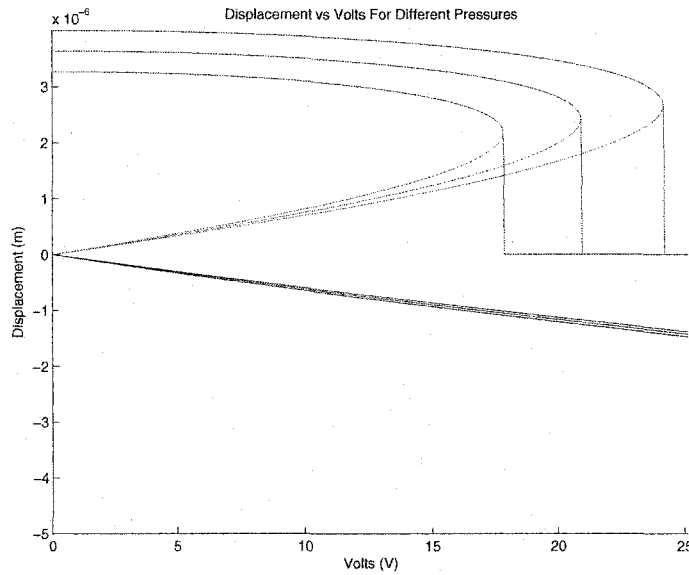


Figure 2.19: Displacement X_m vs Voltage for Various Air Pressures

to the microphone. That is the pressure is the difference between the front and back of the diaphragm. The range of pressures applied is 0, 100 and 200 Pa. The curve for 0 Pa is to the right followed by the other two in order. As can be seen the pressure needs to be significantly higher than the range of pressure that a microphone needs to work with. Our expected range of operation is around 1 Pa. So it is apparent that pull-in voltage is not greatly affected by applied air pressure. The MATLAB m code used to generate Figure 2.19 and Figure 2.19 can be found in Appendix E. Due to the manufacture of MEMS microphones, a residual tension is often left in the diaphragm. This residual tension will affect the pull-in voltage as can be seen in Figure 2.20. Here there are three pull-in curves for 100, 200 and 300 N for an applied pressure of 1 Pa. As the residual tension increases the pull-in voltage also increases. This is because the diaphragm is stiffer and bends less to applied pressure. From this it is clear that MEMS clamped diaphragm microphones are very dependent on remaining residual tension in the diaphragm. Various methods can be implemented to reduce residual tension. The first and foremost method is using high temperature annealing. This relaxes the diaphragm by allowing the stresses to flex. The second method involves adding a ribbing like structure around the diaphragm that stretches and relieves residual tension. The MATLAB m code

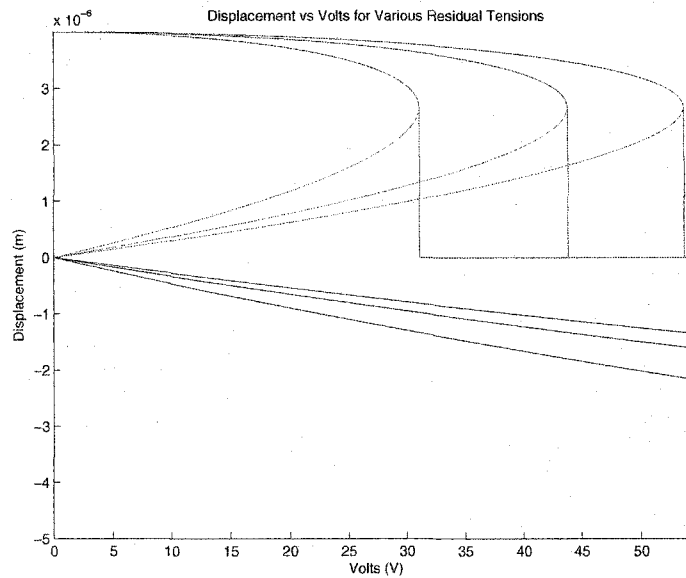


Figure 2.20: Displacement X_m vs Voltage for Various Residual Tensions

for Figure 2.20 can be found in Appendix F. The predicted pull-in voltage for the design can be seen from Figure 2.29 to be about 24 V. This estimate is found to be at least 5 V too large. The reason for which was discussed in Section 2.5. In this case the assumption of piston like motion has underestimated the amount of displacement. A finite difference model was developed to better estimate pull-in voltage. However it was found that the method of finite differences is not able to estimate pull-in voltage. As can be seen in Figure 2.21, each curve represents the pull-in voltage for various node sizes ranging from 10 to 100 nodes, going up by 10 nodes each step. Figure 2.22 is another representation of the data shown in Figure 2.21. Here the pull-in voltage is plotted versus delta, which is the number of nodes. As can be seen in either Figure, the pull-in voltage is increasing with increasing number of nodes. This is counter intuitive since the simulation should be converging to a final solution like in Figure 2.12. Thus the conclusion is that finite differences prediction of pull-in voltage diverges instead of converges and as such is inaccurate. The reason for this is that the partial differential equation describing plate motion is only accurate for small plate deflections. Small plate deflections is defined as a deflection that is less than the thickness of the plate. The behavior of pull-in voltage is a distinctly large scale deflection and as

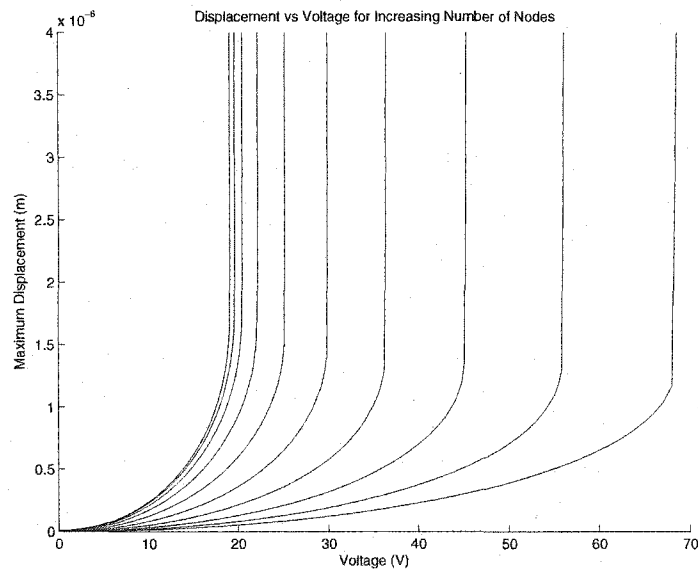


Figure 2.21: Pull-In Voltage vs Delta

such cannot be modeled via Equation 2.15. In order to solve this problem a finite element package, Intelisuite, was used to predict pull-in voltage. A quarter model was made in the package and a voltage range was applied to the plates. Figure 2.23 illustrates displacement for an applied voltage. The generated displacement versus voltage for the node at the tip of the plate is shown in Figure 2.24. Here the range of applied voltage is from 0 to 25 V. As can be seen the diaphragm collapses around 20 to 21 V. The normal operating voltage should be kept within the linear range of this curve which can be seen to be around 19 V. In order to confirm the accuracy of the FEA results a series of pull-in voltage runs were performed for various mesh sizes on a 1/4 of square microphone plate. A plate 1/4 the size of the desired diaphragm can be setup with the proper boundary conditions to give the same results for a full plate but at 1/4 the run time. Often there are advantages in exploiting symmetry in a FEA problem. The results for the different mesh sizes are shown in table 2.2. Here pull-in voltage values are shown for various mesh sizes. The results show that for mesh sizes finer than $40 \mu\text{m}$ the pull-in voltages remain within 0.1 volt. The values for pull-in voltage are consistently have been found to be consistently 20% less than what was predicted by the lumped parameter mechanical equivalent [18], [3]. Accordingly the values

2. CLAMPED MEMS MICROPHONE DESIGN

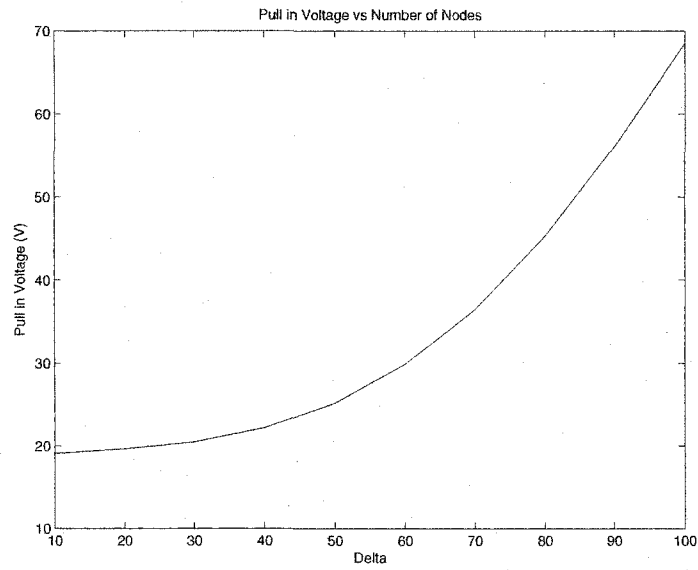


Figure 2.22: Pull-In Voltage vs Delta

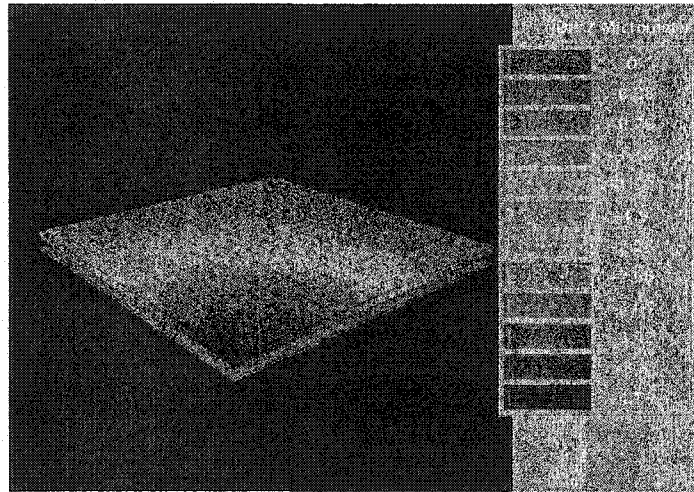


Figure 2.23: Isosurface Displacement For an Applied Voltage to 1/4 Microphone

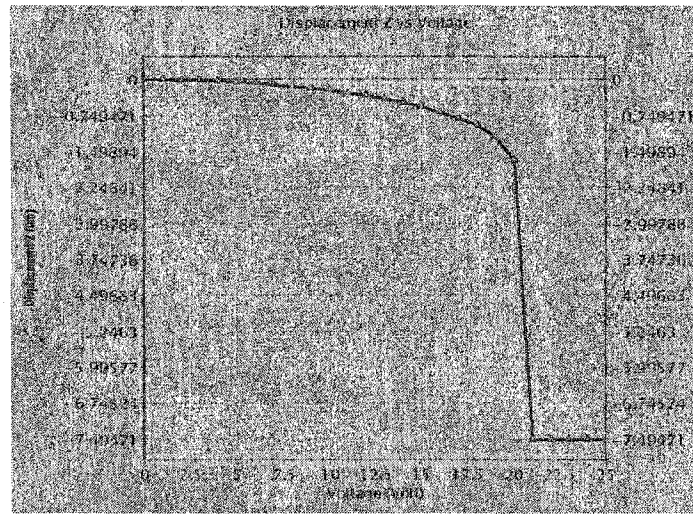


Figure 2.24: Isuite Displacement vs Voltage

used in all clamped microphone lumped parameter programs will use this modification.

2.8 Bias Voltage

Capacitor microphones need a bias voltage in order to function. The sensitivity analysis has made it clear that this bias voltage should be large but as shown in Section 2.7 the voltage cannot be too large to cause collapse of the diaphragm from electrostatic forces. The change in capacitance is also another important parameter since sensitivity is directly proportional to this. Applying Equation 2.13 to the capacitance Equation 2.23 and plotting the result gives Figure 2.25. This Figure shows the change in capacitance versus bias voltage and is generated by the program in Appendix E. In order to avoid the distortion of additional harmonics, the bias voltage should be in the linear range of the pull-in voltage. This can be seen to be around 19 V as shown in Figure 2.18. This should be considered the actual maximum operating voltage and should also incorporate the %20 difference as discussed in the previous Section 2.7 giving a total difference of 30% less voltage. It is this voltage that is used in the following Section 3.1, Design Space Optimization.

Table 2.2: FEA Pull in Voltage Results for Various Mesh Sizes

Mesh Size μm	Pull-In Voltage Range V
100	20.1 - 20.2
80	20.0 - 20.1
60	19.9 - 20.0
40	19.9 - 20.0
20	20.1 - 20.2

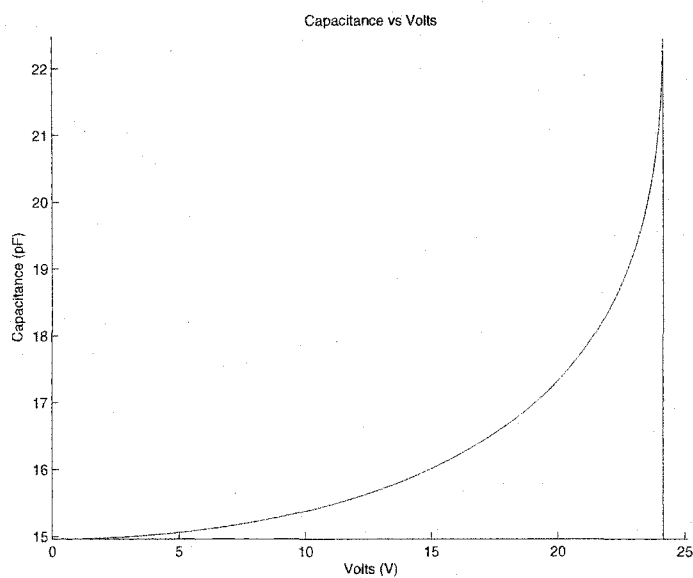


Figure 2.25: Isuite Capacitance vs Voltage

2.9 Ultimate Tensile Strength

Polysilicon can withstand an ultimate tensile strength S_{UT} of 1.21 GPa before it fractures [19][20]. Accordingly a MEMS microphone design must keep the maximum value of stress below this value. Polysilicon is a brittle material and as such a theory of its failure needs to take this behavior into account. There are several theories describing brittle fracture as can be found in references [21] and [22]. Of which the two most relevant will be discussed here. The first theory is the maximum-principal-stress theory. This theory states that brittle fracture is reached when the maximum principal stress reaches the ultimate tensile yield strength. The total value of stress is the sum of residual tension and the stress created by deformation of the diaphragm. Once this value exceeds S_{UT} fracture is expected to occur. The formula for estimating this bending stress can be found in reference [23] and is,

$$\sigma_{bend} = 1.47 \sqrt[3]{\frac{q^2 L^2 E}{h^2}} \quad (2.30)$$

where q is the applied pressure, L is side length and h the thickness of the diaphragm. E is Young's Modulus. The Poisson ratio used here is 0.25. However this should have a minimum effect on the calculations. In order to include electrostatic forces the total pressure can be considered the sum of applied air pressure difference and the effective electrostatic pressure. The electrostatic pressure varies over the deformed diaphragm. In order to conservatively estimate the effective pressure the maximum electrostatic force on the diaphragm at a voltage of 19 V, which is less than pull-in. This is conservative since this maximum value of electrostatic pressure is found at the center of the diaphragm. It is less at the edges. Taking the maximum electrostatic pressure at the center and assuming it is the same across the diaphragm will then give a value for the stress that is greater than expected. Applying this formula to the state of the art design would give $\sigma_{bend} = 35.27$ MPa. The total stress would then be the residual tension, $\sigma_r = 20$ MPa, plus this bending tension, which gives 55.27 MPa total. The IntelliSense results for the stress invariants can be seen in Figures 2.26, 2.27, 2.28. These plots are also based upon the chosen state of the art design. The maximum value from the stress invariants can be seen in Figure 2.28 to be 24.5 MPa. This already includes the 20 MPa residual tension assumption via the FEA setup. The lower

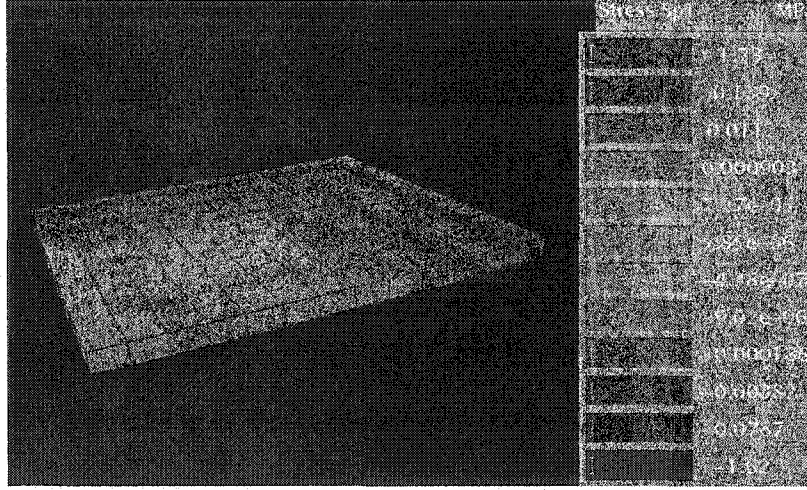


Figure 2.26: Stress Invariant SP1

value of 24.5 MPa instead of 55.27 MPa is as expected because of the assumption of uniform maximum electrostatic pressure. These results indicate that this method can be used to conservatively estimate the maximum bending stress that will be encountered. The second theory to be discussed is the modified Coulomb-Mohr failure theory for brittle materials. Consider a general three-dimensional state of stress at a point given by,

$$[\sigma] = \begin{bmatrix} \sigma_x - \sigma_p & \tau_{xy} & \tau_{zx} \\ \tau_{xy} & \sigma_y - \sigma_p & \tau_{yz} \\ \tau_{zx} & \tau_{yz} & \sigma_z - \sigma_p \end{bmatrix} = 0 \quad (2.31)$$

There will be, by a three-dimensional transformation, a coordinate system x', y', z' , where the state of stress at the same point can be described by the matrix

$$[\sigma] = \begin{bmatrix} \sigma'_x & 0 & 0 \\ 0 & \sigma'_y & 0 \\ 0 & 0 & \sigma'_z \end{bmatrix} \quad (2.32)$$

Evaluating the determinant of matrix 2.31 results in,

$$\begin{aligned} & \sigma_p^3 - (\sigma_x + \sigma_y + \sigma_z)\sigma_p^2 + (\sigma_x\sigma_y + \sigma_y\sigma_z + \sigma_z\sigma_x - \tau_{yz}^2 - \tau_{zx}^2 \\ & - \tau_{xy}^2)\sigma_p - (\sigma_x\sigma_y\sigma_z + 2\tau_{yz}\tau_{zx}\tau_{xy} - \sigma_x\tau_{yz}^2 - \sigma_y\tau_{zx}^2 - \sigma_z\tau_{xy}^2) = 0 \end{aligned} \quad (2.33)$$

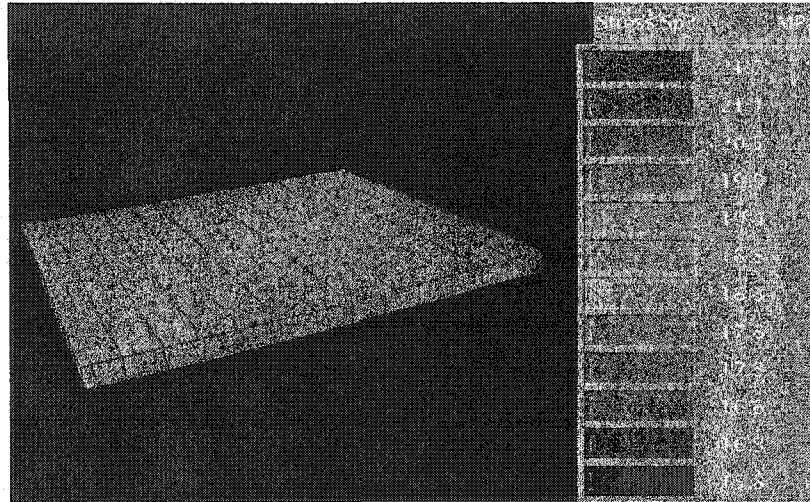


Figure 2.27: Stress Invariant SP2

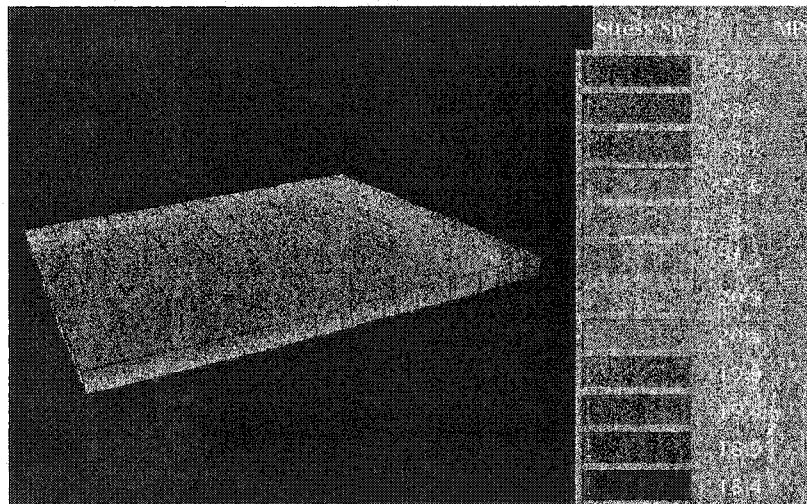


Figure 2.28: Stress Invariant SP3

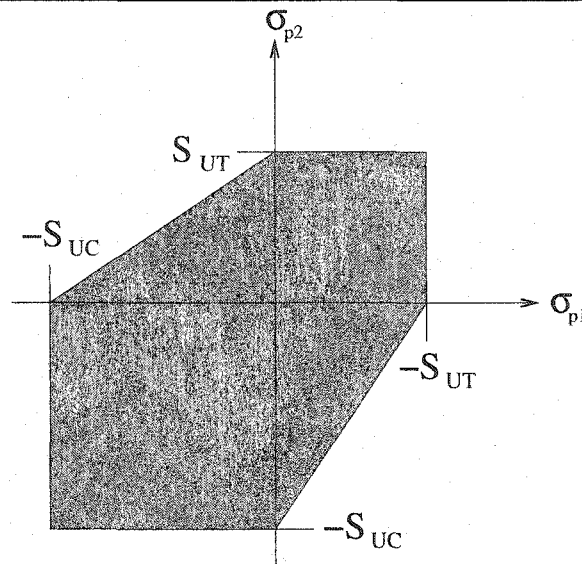


Figure 2.29: Coulomb-Mohr Theory of Failure

The solutions σ_p are independent of the coordinate system used to define the coefficients of the cubic equation for σ_p . Thus the coefficients of σ_p in Equation 2.33 are constant and are referred to as the stress invariants. These are the stress invariants SP1, SP2, SP3 given by the IntelliSense software. For polysilicon only the ultimate tensile strength is listed. For typical brittle materials the ultimate compressive strength, S_{UC} , is equal to or greater than the ultimate strength in tension, S_{UT} . From this it is a conservative estimate to set the S_{UC} equal to the S_{UT} . The Coulomb-Mohr theory of failure is graphically illustrated by Figure 2.29. Here only two of the principal stresses are shown for simplicity. The remaining principal stress would form the third dimension in this Figure. Referring back to the IntelliSense results for the stress invariants shown in Figures 2.26, 2.27, 2.28 it is clear that the maximum value for the invariant principal stresses is around 25 MPa for any point on the diaphragm. SP1, SP2 and SP3 form points well within a three-dimensional box defined by the ultimate tensile strength S_{UT} of 1.21 GPa. Since all of the principal stress values for the diaphragm lie within this box then the diaphragm shall not experience fracture.

2.10 Discussion of Current State of the Art

This chapter has covered in detail the major design issues in MEMS microphone design. The design constraints discussed layout the fundamental design criteria that must be met by the microphone. A comparison of microphone signal detection methods revealed that capacitive and electrolytic microphones were the most sensitive. It is for this reason capacitive microphones were chosen to be investigated. Sources of dampening were investigated and their effect on the sensitivity was noted. Modeling methods were examined and a mechanical equivalent representation was chosen as the best representation. The chosen current state of the art design, Hsu, et al., was used as an example in the modeling sections. The fundamental equation of motion, Equation 2.13, was derived. Limitations due to the piston like motion assumption were discussed. A investigation into the usefulness of finite difference models was presented. Sensitivity was derived from fundamentals via $Q = CV$ and Equation 2.13. The effect of an external amplifier circuit on output voltage was investigated. It was found that a capacitive voltage divider circuit could significantly reduce the sensitivity of the the microphone. It is for this reason that MEMS microphones should have at least 1 pF of capacitance. The expected sensitivity versus frequency for the chosen state of the art was reproduced with reasonable accuracy. Verifying the mechanical model representation. Pull-in voltage was evaluated directly from Equation 2.13. The effect of air pressure and residual tension on pull-in voltage was investigated. It was found that air pressure has an insignificant effect and residual tension has a strong effect on pull-in voltage. In effect, MEMS microphones are dominated by electrostatic forces and residual tension. The inaccuracy of the pull-in voltage estimate was explained to be due to the aforementioned piston-like displacement assumption. It is for this reason that alternative methods for estimating pull-in voltage were investigated. An attempt to use finite difference to model pull-in voltage proved ineffective due to the small plate assumption. FEA simulation of pull-in in the IntelliSense software proved effective in calculating a more realistic pull-in voltage. The use of bias voltage was investigated. It was found that bias voltage increases the in change in capacitance due to applied air pressure differences. Finally a detailed investigation into brittle fracture was performed. It was found via the modified Coulomb-Mohr

2. CLAMPED MEMS MICROPHONE DESIGN

theory, that if the principal stress invariants are less than the ultimate fracture strength then the microphone will not fail.

Chapter 3

Clamped MEMS Microphone Design Optimization

3.1 Design Space Optimization

While designing a MEMS microphone, one question that can be asked is which design is the best given the design constraints. There are numerous methods to determine an optimal design of which this thesis will use the simple brute force design space search. The reason for this choice is it's conceptual simplicity and ease of implementation. For a desired device there will be design parameters that can be varied over a range of potential size. These parameters constitute the devices design space. See Figure 3.1 for an example of a 3 parameter design space A, B and C with ranges a, b and c. Of course real devices have a design space of several design parameters and this cannot be easily visualized. The resolution of the design space parameters can affect the outcome of the design space search. As can be seen in Figure 3.2 a coarse resolution will result in missing possible optimal designs. Here a local maximum has been found but a global maximum is missed due to resolution of the design space search. It is for this reason that a possible optimal design is not know to be truly optimal or locally optimal. The finer the resolution the longer the

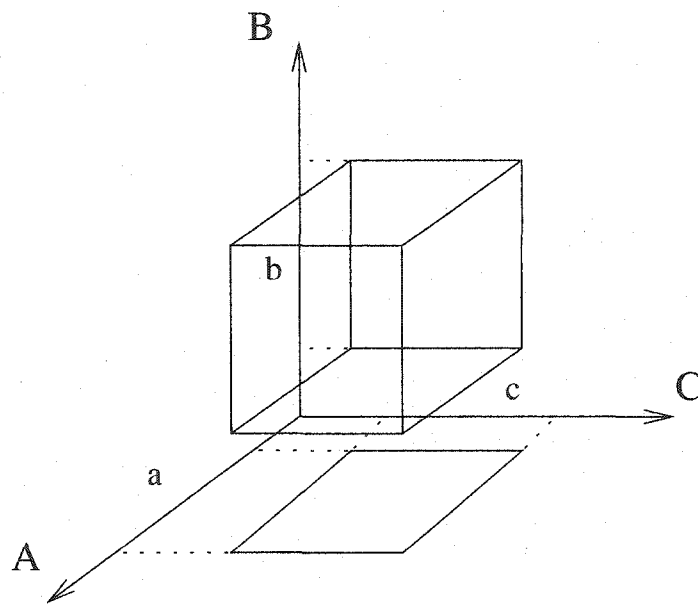


Figure 3.1: A Design Space

design space search takes. Even with the coarse resolution used in this thesis the simulation times could be up to 1/2 hour. A more thorough search could take weeks of simulation time. For the clamped microphone design, the basic mechanical model program given in Appendix A was modified to search over the desired design ranges for the parameters. The design space parameters for this program are as follows: width of the diaphragm, thickness of the diaphragm, residual tension, height of the air gap, number of backplate vent holes and the radius of the back plate vent holes. The design space program for the clamped microphone can be found in Appendix G. The desired optimized result is the sensitivity. Several small logical tests are incorporated into the program to help speed up the search. For example if the vent holes area is less than the available surface area of the back plate then the design is rejected outright. Obviously hole area cannot be larger than available back plate area. Also the design is checked to see if there is at least 1 pF of capacitance. This is to avoid the capacitive voltage divider problems as discussed in Section 2.6. Finally before the results are recorded from a run one of two possible checks are performed. If a spike in the displacement is detected then it is assumed that this is the actual resonant frequency. If no spike is detected then the actual resonant frequency cannot be determined via this

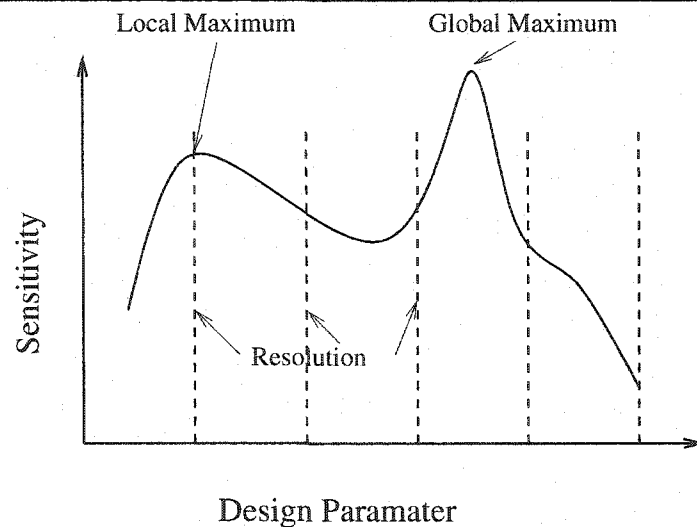


Figure 3.2: Design Space Resolution Problems

method and it is assumed the displacement curves decreases smoothly. If there is an actual resonant frequency then the displacement at that value is checked to see if it is no more than 10% greater than the displacement at 1 kHz. This prevents curves with large spikes from being accepted as valid results. If no actual resonant frequency is detected then the displacement at the desired maximum frequency is checked to see if it is no less than 30% the value at 1 kHz. This is to reject any curves that drop off too quickly to be acceptable. The results from this design space program are listed in table 3.1. For the first results a resonant frequency of at least 10 kHz was desired with Width and thickness fixed to 2600 and 3 μm respectively. Residual tension, air gap distance, number of vent holes and radius of vent holes are all variable. For the second design a resonant frequency of 20 kHz is also desired and only the width of the diaphragm is fixed at 2600 μm . Fixing the width helps to compare the design space results. The second result has a variable diaphragm thickness that can be as low as 0.2 μm . These values can then be entered back into the basic mechanical model and the frequency response for X_m , capacitance and sensitivity can be plotted as before with the current state of the art design. The sensitivity for the optimized clamped microphone design is shown in Figure 3.3 Considering the 10 kHz results, the value of 41.92 mV/Pa for the optimized clamped microphone design is seen to be an improvement over the

3. CLAMPED MEMS MICROPHONE DESIGN OPTIMIZATION

Table 3.1: Design Space Results for The Clamped Microphone

Criteria	Results							
Desired F (kHz)	Sensitivity (mV/Pa)	F_{est} (Hz)	V_p V	Width μm	thickness μm	air gap μm	# Holes	r Holes μm
10.0	12.26	10.14	9.75	2600	3.0	3.0	320	50.0
10.0	41.92	10.62	6.47	2600	0.4	3.8	320	60.0

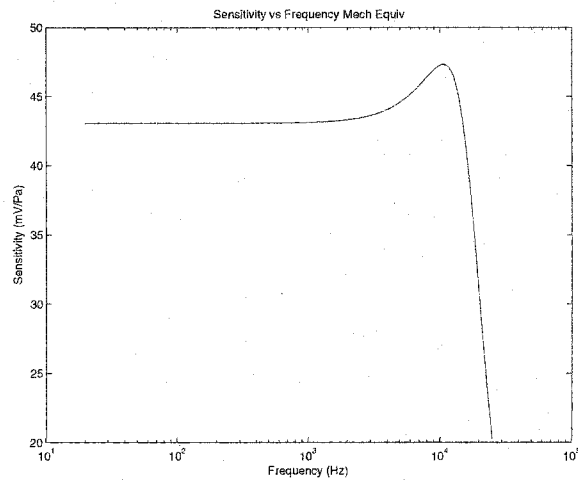


Figure 3.3: The Sensitivity for an Optimized Clamped Microphone Design

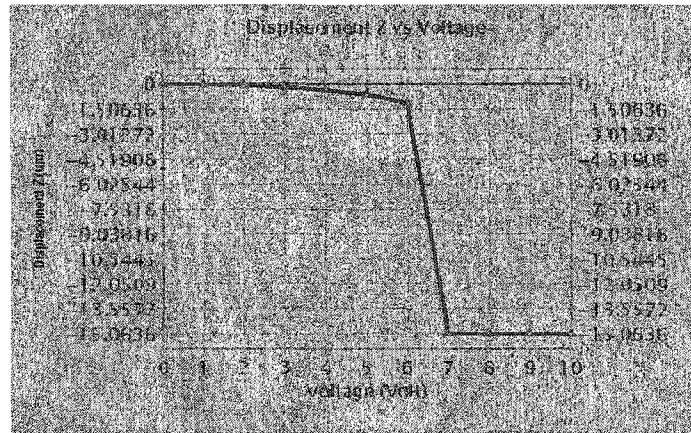


Figure 3.4: The Sensitivity for an Optimized Clamped Microphone Design

current state of the art designs sensitivity of 9 mV/Pa. The estimated pull-in voltage for the optimized design is $V_p = 6.47$ V. The bending stress in the diaphragm was estimated to be $\sigma = 42.7$ MPa. This value is estimated based upon the assumption of 50% air gap displacement and 5.8 V applied to the diaphragm. The 50% air gap distance is meant to be an average displacement since the electrostatic pressure doesn't act over the area uniformly. The electrostatic force displaces the center of the diaphragm more than the edges. The 5.8 V comes from 90 % of the estimated pull-in voltage V_p . The maximum estimated stress was calculated to be 62.4 MPa. This is an extreme case at maximum deflection assuming maximum electrostatic pressure. The maximum electrostatic pressure is normally only found at the center of the diaphragm when it pulls in. Instead the electrostatic pressure has been assumed to be the same over the whole diaphragm. This is expected to give a conservative estimate. In order to confirm these values an FEA analysis was performed in the IntelliSense software. The pull-in curve for the optimized clamped plate design is shown in Figure 3.4. Here the pull-in curve shows a pull-in somewhere in between 6 to 7 V which agrees with the estimated 6.47 V nicely. Figure 3.5 shows the maximum stress invariant for the diaphragm at the bias voltage of 5.8 V. The maximum value is seen to be 31.2 MPa and is shown in Figure 3.5. The estimated value of 62.4 MPa is greater than 31.2 MPa and this is expected since it is a conservative estimate.

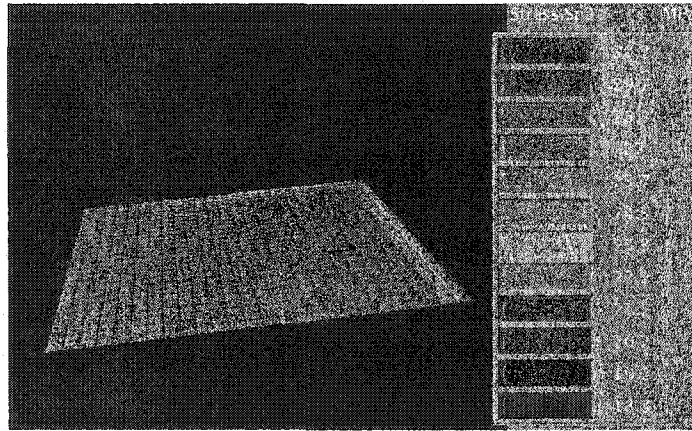


Figure 3.5: The Stress Invariant SP3 Showing the Maximum Stress

3.2 MEMS Microphone Design Flow

From the approach taken in the previous sections, it is possible to come up with a MEMS microphone design flow. The design flow specified in this section is applicable to the clamped type MEMS microphone. Any design flow must start with specifying the required range of the design parameters and design constraints.

It is apparent from the previous sections that diaphragm flexibility is an important design criteria. So this design flow will start with the diaphragm parameter that affects this the most, diaphragm thickness. Here it is assumed that proper stress relief methods have been employed so that the residual tension in the diaphragm is keep to a minimum. For the purpose of this design flow the residual stress is assumed to be 20 MPa as per the fundamental reference paper. Here no special stress relieve geometries will be employed. Just a standard flat square diaphragm will be used. Lowering diaphragm thickness can only be done to the point of maximum sustainable stress or until the pull-in voltage for the desired operating voltage is reached. Diaphragms of $0.2 \mu\text{m}$ have been observed as can be seen at reference [24], [25] and this will be the minimum thickness used.

Evaluating the expected stress and strain requires knowledge of the expected pull-in voltage. At this point the diaphragm width and air gap need to be chosen and the pull-in voltage evaluated. The thinner the diaphragm the higher the mechanical sensitivity.

However this has a direct impact on pull-in voltage. Making the diaphragm too thin will lower the pull-in voltage to the point where the microphone collapses for a very low voltage. At the same time the maximum stress and strain could be exceeded. Even the 3 V used by most hearing aid batteries could be sufficient to cause collapse. The pull-in voltage represents the maximum voltage that can be applied to the diaphragm. The actual voltage used should be at least 10% lower than this to ensure linearity of the output signal. Also lowering the pull-in voltage lowers the electrical sensitivity. Too high a pull-in voltage serves no real purpose since voltages can only be boosted to around 12 V with on chip voltage multipliers. These microphones are electro-statically dominated structures and as such the applied pressure difference from the sound source represents an insignificant effect on diaphragm displacement when considering pull-in issues. So from this it is clear that a balance must be found between diaphragm thickness and a reasonably high pull-in voltage.

Next lets consider diaphragm size. The larger the diaphragm the more acoustical energy that can be gathered by the microphone. However this too will effect the pull-in voltage. The larger diaphragm has more electrostatic force acting upon it that tends to pull it down even more. So once again the diaphragm size needs to be maximized yet its effect on pull-in needs to be considered.

At the same time lets consider the air gap height. This effects pull-in voltage too. A large air gap means a large pull-in voltage and vise versa. However a smaller air gap means larger electric field intensity in the air gap and a higher electrical sensitivity. The air gap can not be too small or else the pull-in voltage will be too low. It is clear that pull-in voltage is the most important design consideration. All design parameters affect this.

A condensation of the above arguments results in the design flow summarized in the flow chart seen in Figure 3.6. After defining the design parameter ranges and design constraints a diaphragm thickness and width is chosen. Followed by an air gap and vent holes size. Finally vent hole radius is selected. Next the estimated pull-in voltage, resonant frequency and stress/strain is evaluated. These values need to be sufficient to satisfy the design. Finally the sensitivity needs to be compared to the previous maximum value. If it is more, then the new design is selected as the best. This procedure repeats for the entire range of

the design parameters. In the end the highest sensitivity will be selected and the optimal design parameters will be known.

3.3 Discussion of Optimized Clamped Microphone Results

This chapter investigated design space optimization. First the concept of a design space was presented and the problem with resolution was discussed. Too coarse a resolution on the design space parameters could result in missing an optimal design. The design space methodology was applied to the mechanical equivalent model for the clamped microphone design. The results of which are summarized in Table 3.1. It was found that the current state of the art designs sensitivity can be improved from 8 to 12 mV/Pa by adjusting the air gap, number of vent holes and vent hole radius. The sensitivity can be further increased to 42 mV/Pa if the thickness is allowed to decrease to 0.4 μm . An FEA analysis was used to confirm the expected pull-in voltage and expected maximum stress. This chapter helps to illustrate the power of using a design space optimization approach. If there exists a lumped parameter model representing a devices behavior, then a design space optimization program can find the best design. Finally a clamped MEMS microphone design flow is proposed. In effect, it represents the steps taken by the design space optimization program.

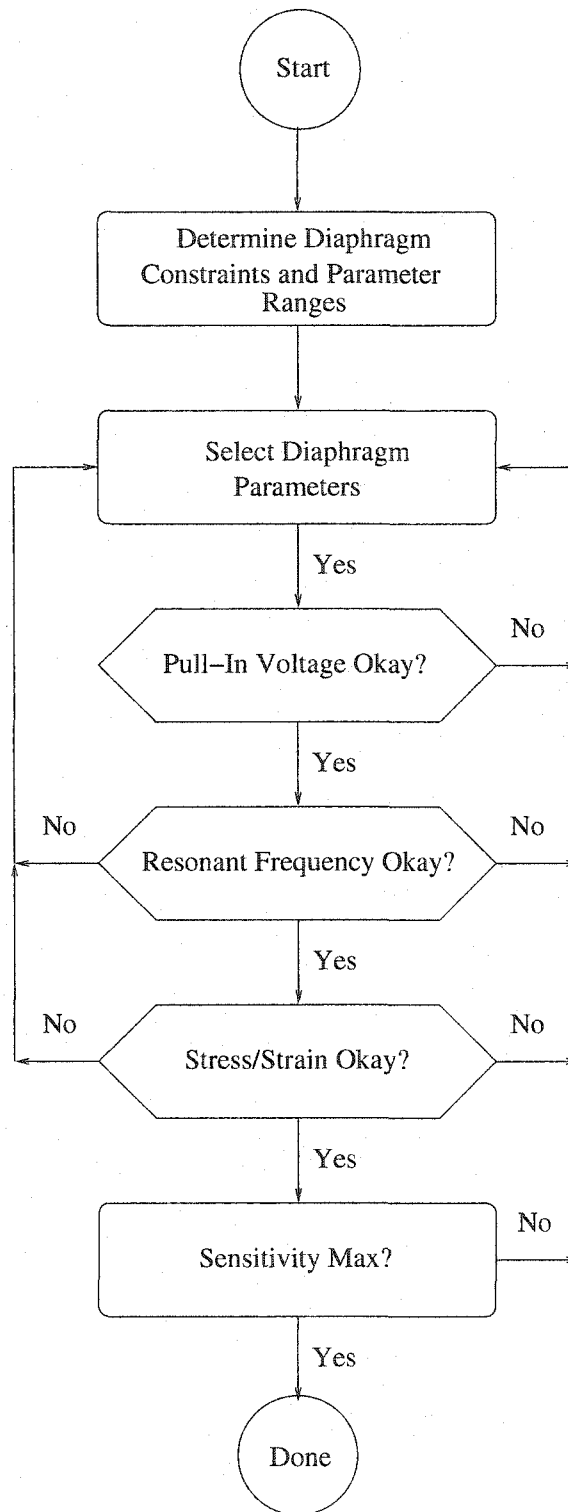


Figure 3.6: Clamped MEMS Microphone Design Flow Chart

Chapter 4

A Suspended Microphone Design

Another possible MEMS microphone design is the suspended design as shown in Figure 4.1. An example of this type of structure can be found in the reference [26], [27], [28]. With this design the diaphragm is supported by cantilever beam springs. An analysis of this microphone is undergone in the same manner as the clamped microphone. There are some unique design issues and these will be covered in detail in section 4.1.

4.1 Suspended Microphone Modeling

As with the clamped microphone design a mechanical model of the suspended microphone was developed. This can be seen in Figure 4.2. The only difference here is that the spring constant of the clamped microphone K_m has been replaced by the spring constant of the supporting springs K_s , [29].

$$K_s = (\#Springs)(EWH^3)/(L^3) \quad (4.1)$$

Where W , H and L are the supporting spring width height and length respectively. The $\#$ springs corresponds to the number of support springs, in this case four. This must be multiplied by the spring constant on one spring to get the total effective spring constant.

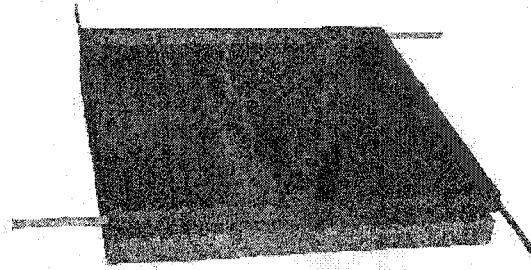


Figure 4.1: A Suspended MEMS Microphone Design

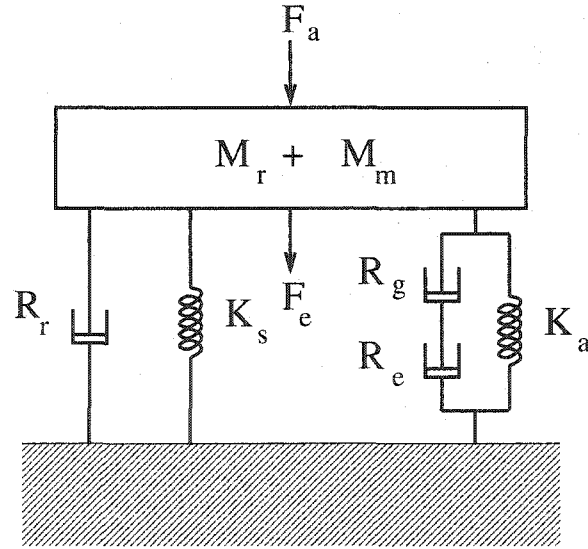


Figure 4.2: A Suspended MEMS Microphone Design

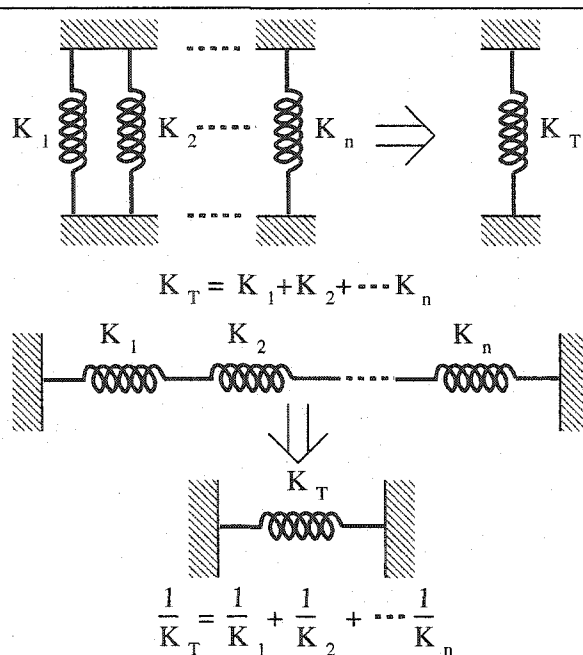


Figure 4.3: Spring Combinations

The springs are acting together and need to be summed to get the total spring constant. If they were acting in series then it would be like adding parallel resistances, [30]. This is shown in Figure 4.3. Choosing the correct model for the support springs becomes critically important for resonant frequency, displacement and corresponding sensitivity estimation. If simple cantilever springs were chosen it would be discovered that the model predicts a more flexible membrane as shown in the lower resonant frequency and larger displacement. The suspended microphone model assumes a rigid membrane and guided cantilever beams should be used to model the support springs. The spring constant for guided cantilever beams is given in Equation 4.1. If the diaphragm is not of sufficient thickness to guarantee rigidity then the perceived spring constants will vary between simple and guided cantilever springs. Typical MEMS springs are shown in Figure 4.4, [31]. As an example of the problems encountered with modeling structures with springs, a structure will be built and analyzed in the IntelliSense Isuite software, shown in Figure 4.5. The figure presents a circular diaphragm $250 \mu\text{m}$ wide with 3 cantilever beam springs arranged at 120° intervals. The springs have dimensions of $120 \mu\text{m}$ long, $5 \mu\text{m}$ wide and $2 \mu\text{m}$ high. Given these dimensions

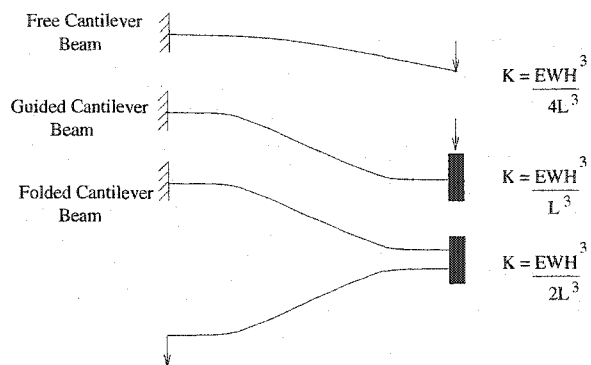


Figure 4.4: Common Types of MEMS springs

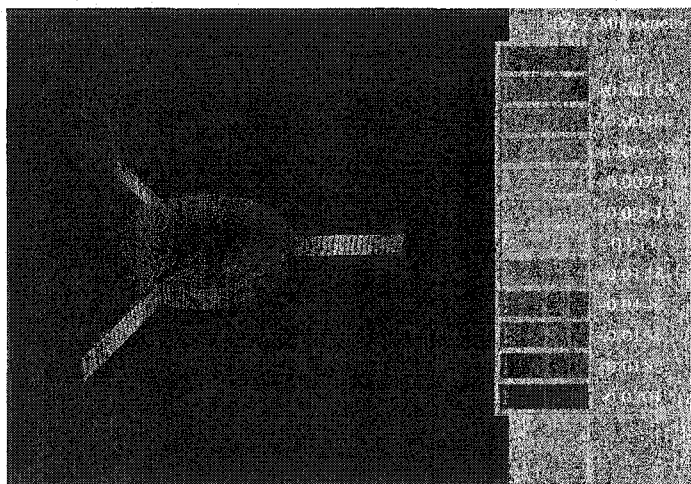
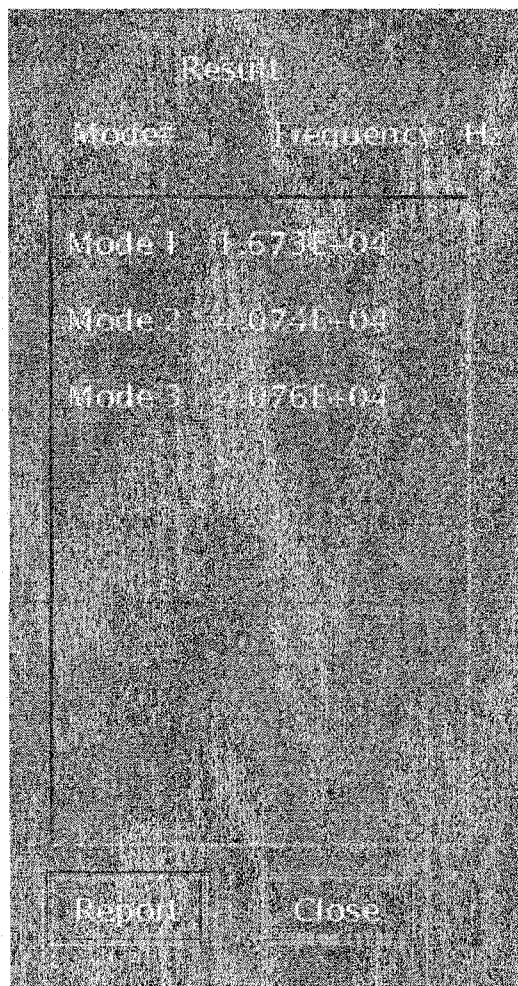


Figure 4.5: Displacement Results for Thin Structure Spring Analysis



Mode#	Frequency	Hz
Mode 1	1.673E+04	
Mode 2	2.074E+04	
Mode 3	2.076E+04	

Figure 4.6: Frequency Results for Thin Structure Spring Analysis

the calculated spring constants for these beams for both free and guided cantilever beams are $K_{free} = 0.33$ N/m and $K_{guided} = 1.30$. Subbing these values into $F = kx$ and solving for the displacement X with an applied pressure of 1 Pa to the top plate gives, $X_{free} = 57.8$ nm and $X_{guided} = 14.7$ nm. The force here corresponds to the pressure times the plate area which gives $F = 5.726 \times 10^{-8}$ N. The spring constants used here correspond to the spring constant multiplied by 3 for 3 springs. The plate diameter is $270 \mu\text{m}$ wide and the initial height is $2 \mu\text{m}$. From this the plate area is 5.73×10^{-8} m², with a mass of 2.63×10^{-10} kg. The expected resonant frequency is $F_{cal} = 19.4$ kHz. Running the analysis in Isuite gives the deflection value of $X_{FEA} = 16.2$ nm shown in Figure 4.5. Running a frequency analysis on the structure will give the primary mode as $F_{FEA} = 16.7$ kHz as can be seen in Figure 4.6. The spring constant of one cantilever beam is $K_x = 0.95$ N/m from the displacement data and $K_f = 0.97$ from the frequency data. This is significantly different from either the free or guided cantilever beam. The reason for this is that the diaphragm is actually deforming and this causes more than expected deflection. Resulting in a lower spring constant than guided but higher than the free spring. To correct for this the diaphragm can be made thicker so that it deforms much less. Setting the structures thickness to $42 \mu\text{m}$, and running this thicker model in Isuite gives the results shown in Figure 4.7. The deflection is 16.6 nm for an applied load of 1 Pa. A frequency response also gives a $F_{FEA} = 4$ kHz. Calculating the spring constant like before for this thicker structure then gives $K_x = 1.15$ N/m from the deflection and $K_f = 1.15$ N/m from the frequency data. Which is much closer to the calculated spring constant for the guided cantilever beam. These results are summarized in table 4.1 below. Also included is intermediate results for plates with thicknesses of 5, 10 and $22 \mu\text{m}$. F_{cal} is based upon the guided spring constant. The spring constant approaches 1.16 for thicknesses of $10 \mu\text{m}$ and up. It's interesting that the spring constant is around 1.16 which is close to K_{guided} of 1.30 but not quite so. This example serves to illustrate the importance of understanding how these springs really behave in actual structures. The assumption of a rigid plate plays as much a role as the assumption of piston like deflection in the accuracy of the models. The development of the mechanical equations of motion

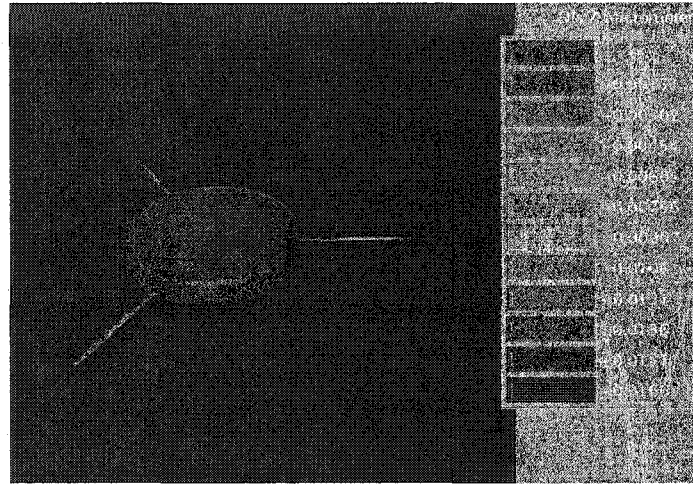
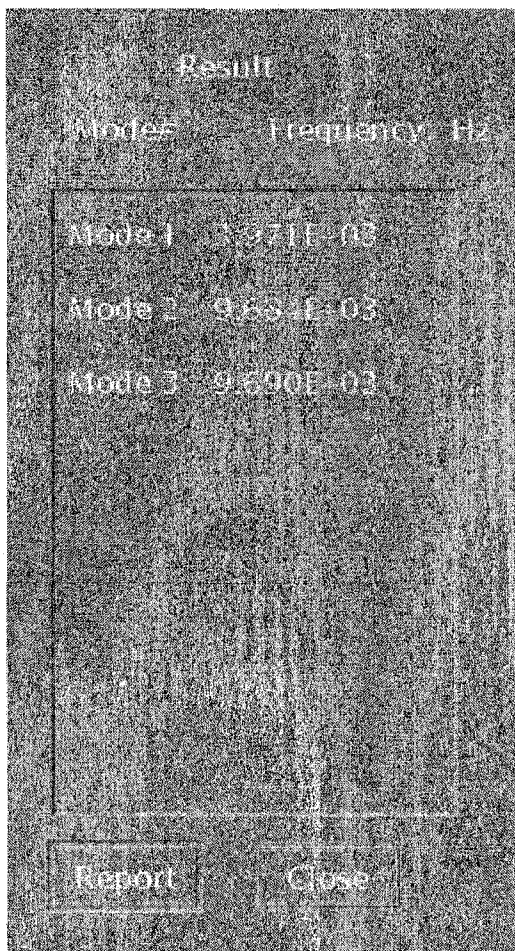


Figure 4.7: Displacement Results for Thick Structure Spring Analysis

Table 4.1: FEA Results for Various Plate Thickness

Plate	Calculated				FEA Results			
t μm	K_{guided} (N/m)	K_{free} (N/m)	F_{cal} (kHz)	Mass (10^{-9} kg)	X_{FEA} (nm)	K_x (N/m)	F_{FEA} (kHz)	K_f (N/m)
2	1.30	0.33	19.4	0.26	20.1	0.95	16.7	0.97
5	1.30	0.33	12.3	0.66	16.9	1.13	11.4	1.13
10	1.30	0.33	8.6	1.32	16.4	1.16	8.1	1.16
22	1.30	0.33	5.9	2.90	16.3	1.17	5.5	1.17
42	1.30	0.33	4.2	5.53	16.6	1.15	4.0	1.15



The image shows a screenshot of a software window titled "Result". The window contains a table with two columns: "Mode#" and "Frequency, Hz". The table lists three modes with their corresponding frequencies in scientific notation. At the bottom of the window, there are two buttons labeled "Report" and "Close".

Mode#	Frequency, Hz
Mode 1	3.271E-03
Mode 2	9.634E-03
Mode 3	9.890E-03

Figure 4.8: Frequency Results for Thick Structure Spring Analysis

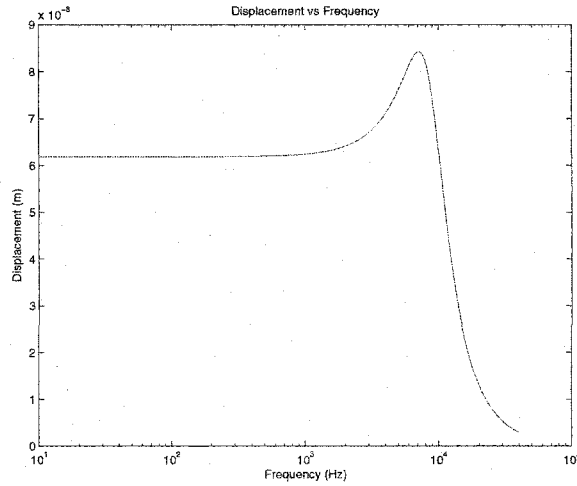


Figure 4.9: A Suspended Design Displacement vs Frequency

follow directly from the diagram just as in Chapter 2 and results in,

$$X_m = \frac{F_a + F_e}{(M_m + M_r)s^2 + R_r s + K_s + \frac{1}{\frac{1}{(R_g + R_h)s} + \frac{1}{K_a}}} \quad (4.2)$$

solving this equation for the desired frequency range gives Figure 4.9 The change in capacitance follows directly from,

$$C_n = \frac{\epsilon_0 A}{(d_0 - X_m)} \quad (4.3)$$

which can be seen in Figure 4.10. Finally the sensitivity of this design can be calculated from,

$$S = V_0 - \frac{d_0 - X_m}{d_0} V_0 \quad (4.4)$$

which is shown in Figure 4.11. The sensitivity is around 81 mV/Pa with a pull-in voltage of 8.7 V. The program that generated these plots can be found in Appendix H. The design parameters for the suspended microphone were once again determined via a design space optimization program, which can be seen in Appendix I. As with the previous design space optimization program covered in 2, this program searches thorough the design space of every parameter. The parameters scanned are: cross sectional diameter of the square diaphragm, support spring length, width and height, diaphragm thickness, air gap height, number of backplate vent holes and radius of the vent holes. Back plate thickness was

4. A SUSPENDED MICROPHONE DESIGN

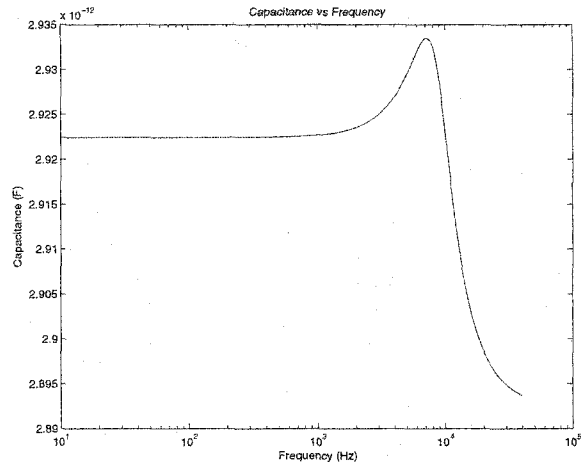


Figure 4.10: A Suspended Design Capacitance vs Frequency

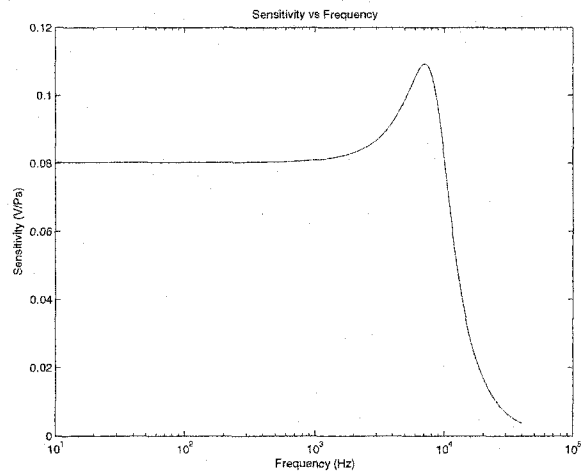


Figure 4.11: A Suspended Design Sensitivity vs Frequency

left at 13 μm . The mechanical model is expected to accurately predict the suspended microphones behavior. The suspended design will deflect in a piston like manner. Unlike the clamped design in which the piston like deflection is a simplifying assumption. The expected accuracy of the model then allows the design space optimization program to incorporate some simplifying assumptions. Firstly that the estimated primary resonant frequency F_{res} ,

$$F_{res} = \sqrt{\frac{K_t}{M_t}} \quad (4.5)$$

can be used to predict the resonant frequency of the microphone. Where K_t is the total spring constant and M_t is the total mass of the system. The displacement at 1 kHz is compared with the displacement at the estimated primary frequency. If the value at the estimated primary frequency is less than or equal to 10% more of the displacement at 1 kHz then there is sufficient dampening. This check allows for the quick elimination of designs without enough dampening to give a smooth frequency response. The program also checks to see if the capacitance is greater than 1 pF and that the area used up by the holes in the back plate is less than the area available. The estimated resonant frequency is checked to see if it is at least 10 kHz. Finally the estimated pull-in voltage is determined via [32],

$$V_{pIdeal} = \sqrt{\frac{8K_t d_0^3}{27\epsilon_0 A}} \quad (4.6)$$

Where d_0 is the air gap height, A is the area of the microphone and K_t is the total spring constant. This formula for pull-in voltage is expected to be accurate for the same reasons that F_{res} is expected to be accurate. The pull-in voltage is used to determine the sensitivity of the microphone if it is less than 10 V. Otherwise 10 V is used. 10 V is considered a reasonable voltage that can be generated from a voltage multiplier circuit. Both voltages are dropped by 10% to avoid linearity problems at pull-in. Using pull-in voltage to estimate the sensitivity then represents a maximum value for the sensitivity. A realistic operating voltage would have to be less than this for reasons covered in previous sections. The pull-in voltage can be determined also by the program in AppendixF and the results are shown in Figure 4.12 for the optimized 10 kHz design. This shows a pull-in voltage of 10.85 V. Reducing this by 20% gives 8.68 V. The ideal equation gives a voltage of 8.65 V. These two values should be similar since the both rely on the assumption of piston like displacement.

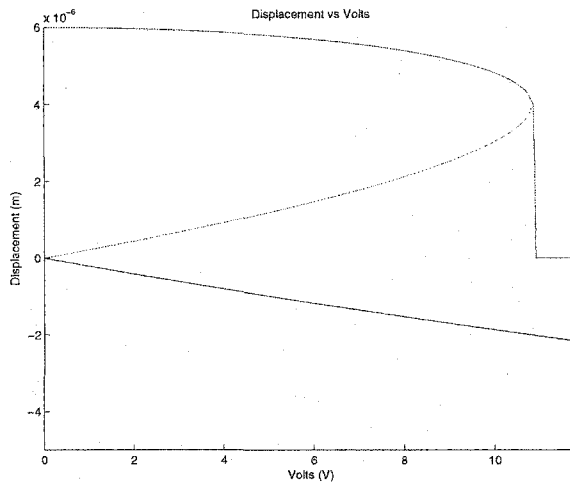


Figure 4.12: Suspended Displacement vs Voltage for $P = 0$ and 1 Pa

4.2 Suspended Microphone Stress and Strain

The maximum stress and strain in the suspended design comes from the supporting cantilever beams. The equation governing these are given below , [33], [34],

$$\sigma_{max} = \frac{6L}{H^2W} \frac{PA}{K \#ofSprings}, \quad (4.7)$$

and

$$\epsilon_{max} = \frac{LH}{2EI} \frac{PA}{K \#ofSprings}, \quad (4.8)$$

where E is young's modulus, H is the thickness of the beam, W is the width, L is the length and F is the applied force at the tip. From these equations the maximum stress that the springs will experience is. Just as with the clamped microphone design this stress must be kept under the maximum of 1.21 GPa.

4.3 Suspended Design Space Optimization

Just as with the clamped microphone, a design space optimization program can be developed for the suspended microphone. In this case the design space program is easier to implement. Since the suspended microphone displaces in a more piston like manner it is seen that the predicted resonant frequency is actually very close to the measure resonant frequency. From

Table 4.2: Design Space Optimization Results for Suspended Microphone

Simulation Results		Diaphragm		Spring			Backplate		
Sensitivity	F_{res}	Diameter	t	L	W	H	# of Holes	r of Holes	d0
mV/Pa	kHz	μm	μm	μm	μm	μm		μm	μm
80.6	10.0	1400.0	1.0	200.0	3.0	5.0	1300	10.0	6.0
41.6	20.0	900.0	1.0	100.0	2.0	3.0	700	9.0	4.5

this knowledge a design space optimization program only needs to evaluate the displacement at 1 kHz and at the expected resonant frequency. This speeds up the program considerably since there is no need to search thorough the entire desired frequency range. The check performed on the results is to see if the resonant frequency is above the desired frequency and that the displacement at the resonant frequency is no more that 10% greater at 1 kHz. The results from the design space optimization are given in Table 4.2 for both 10 and 20 kHz resonant frequencies. The capacitance of the 10 kHz design is 2.9 pF with a pull-in voltage of 8.7 V. The 20 kHz design has a capacitance of 1.6 pF with a pull-in voltage of 9.4 V. Section 4.4 will attempt to confirm some of the predicted results for the 10 kHz lumped parameter model.

4.4 Suspended FEA Analysis Results

The suspended microphone optimized for design 10 kHz was implemented in the IntelliSense software FEA package. The results of which will be covered in this section. Figure 4.13 shows the desired design. The z axis has been zoomed in the Figure to help highlight the sections. The $5 \times 10 \mu\text{m}$ support ring can be seen around the edge. The reasons for this have been given in 4.1. No vent holes can be seen in on the backplate. These have been omitted due to software limitations. The desired design would have used small beams criss-crossing the diaphragm to ensure that the diaphragm acted like a rigid body. However the IntelliSense software would not recognize these elements as being part of the

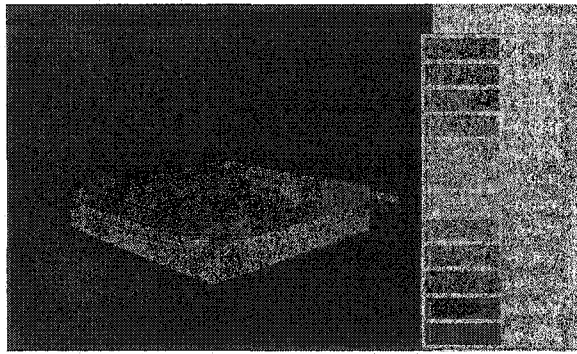


Figure 4.13: FEA Displacement for the Optimized Suspended Design

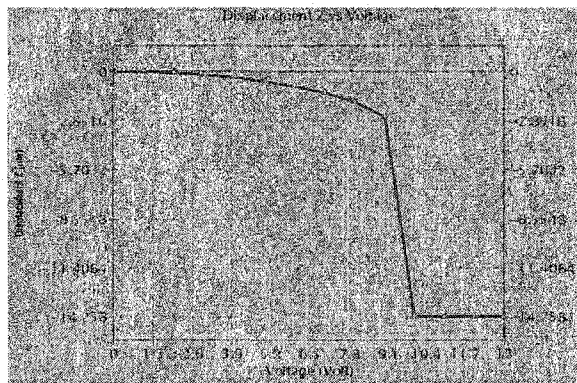


Figure 4.14: FEA Displacement for the Optimized Suspended Design

diaphragm. The reason for this is that the mesh size was not small enough so that the beam mesh matched with the diaphragm mesh. This could not be accomplished due to memory limitations of the software and time constraints. Accordingly the diaphragm was thickened so that it would remain rigid. This should have little effect on these results except for the resonant frequency estimation. The first result to be considered is the displacement due to an applied pressure difference of 1 Pa. This is shown in Figure 4.13. The displacement at the springs is 9.0 nm. This is reasonably close to the expected 61.9 nm. Next the pull-in voltage was determined. The pull-in curve for the optimized suspended microphone is shown in Figure 4.14. The curve shows that pull-in occurred right around 9 V which agrees nicely with the estimated 8.65 V. The ideal value was calculated to be 10.81 V. Taking 20% less than this gives the estimate of 8.65 V. Applying 10% less voltage than this to

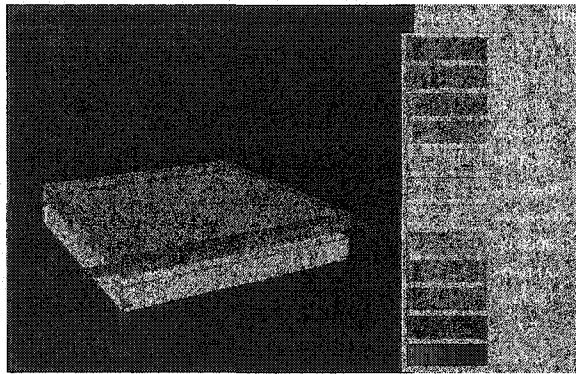


Figure 4.15: FEA SP1 For Optimized Design

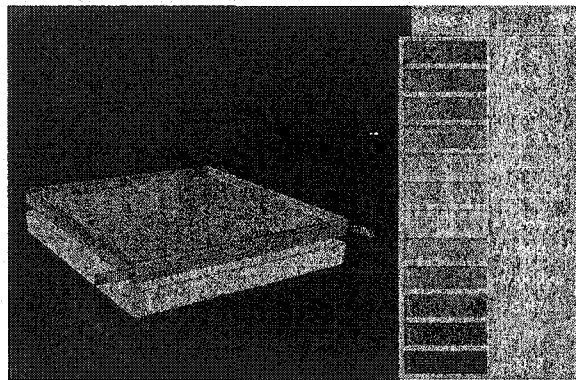


Figure 4.16: FEA SP2 For Optimized Design

the optimized design and observing the invariant stresses from this gives the plot shown in Figures 4.15, 4.16 and 4.17. Here the maximum value of invariant primary stress is seen to be 59.2 MPa. This is much more than the calculated value of 1.68 MPa. The final FEA analysis to be performed is for the resonant frequency as shown in Figure 4.18. Here the FEA resonant frequency is 7.05 kHz which is close to the expected value of 10 kHz. The accuracy of these results implies that the expected sensitivity of 81 mV/Pa is realistic. These results are summarized in Table 4.3.

4. A SUSPENDED MICROPHONE DESIGN

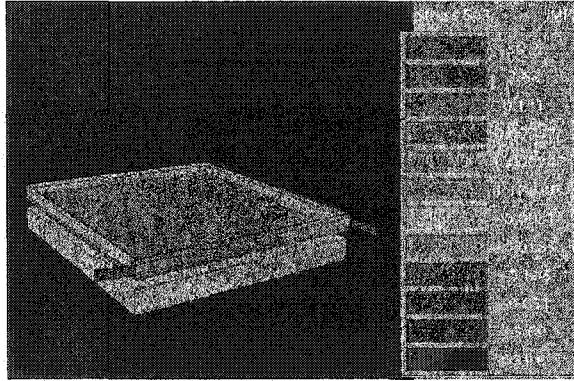


Figure 4.17: FEA SP3 For Optimized Design

Result	
Mode	Frequency Hz
Mode 1	7.047E-03
Mode 2	1.411E-04
Mode 3	1.417E-04
Mode 4	2.338E-04
Mode 5	3.618E-04

Figure 4.18: FEA Frequency response

Table 4.3: FEA Results for the Suspended Microphone

	Expected Results	FEA Results	% Error
Displacement (nm)	62.9	90.3	30.3
F_{res} (kHz)	7.05	10.0	29.5
Stress (MPa)	1.96	59.2	96.7
Pull-in Voltage (V)	8.68	9.0	3.56

4.5 Discussion of Suspended Microphone Results

This chapter introduced a suspended plate type microphone design. As with the clamped microphone design a mechanical model was developed. The first thing to consider when developing this model is to consider the springs used to support the plate. It was determined how to combine these springs and which type of spring to use. An FEA analysis was done to better determine the correct spring type. It was found that the plate rigidity plays an important role in the effective spring constant. With a sufficiently rigid plate the springs were found to be more guided cantilever like, but not exactly. Both FEA frequency response and displacement values were used to confirm this. Expected resonant frequency and sensitivity was evaluated. Next a method for evaluating the stress/strain in the support springs was determined. With this knowledge a mechanical model was created and a design space optimization program was developed from this. It was found that the suspended microphone had an estimated sensitivity of 80.6 mV/Pa for a 10 kHz design and 41.6 mV/Pa for a 20 kHz design. An FEA analysis was done to confirm the estimated displacement, resonant frequency, pull-in voltage and maximum stress. The results are summarized in Table 4.3. The results agree reasonably well except for the evaluated stress which is off by almost 100%. This is most likely due to the coarse mesh used to ensure the rigidity of the plate. The reason for the coarse mesh is due to software limitations. The desired support bars could not be included in the design. They were to criss cross the plate in a X connecting the springs. This was to reinforce the plate and ensure its rigidity.

4. A SUSPENDED MICROPHONE DESIGN

However the software was unable to incorporate them into the mesh. The other FEA results are all within 30% of the estimated values. This error could be due to the fact that the spring constant was not exactly like the guided cantilever beam.

Chapter 5

A Ring Microphone Design

5.1 Ring Microphone Introduction

Building upon the discovered important design considerations from chapter 2 a ring microphone design was conceived and developed. The design can be seen in Figure 5.1. A cross section of the ring design can be seen in Figure 5.5. This figure shows a set of free moving rings supported by three symmetrically located springs and corresponding fixed rings. The edges of the free moving rings make a variable capacitance with the corresponding fixed rings. A dielectric layer provides electrical isolation along the edge of the fixed rings. A blow up of a cross Section for the center ring can be seen in Figure 5.5. As a ring is displaced down by a sound wave the top capacitance decreases and the bottom increases. Assuming conservation of charge in Equation 2.20, if capacitance decreases then voltage must increase. Conversely if capacitance increases then voltage will decrease. With this design there is a need for an offset capacitance. If there is only one capacitance and it is symmetrically located as show in Figure 5.2, then there will only be a decrease in capacitance. This will result in a increase of voltage only, effectively rectifying the input signal. If the capacitance is offset as shown in Figure 5.3, then the capacitance increases and decreases. This will result in a voltage increase and decrease with the applied pressure difference. The final

5. A RING MICROPHONE DESIGN

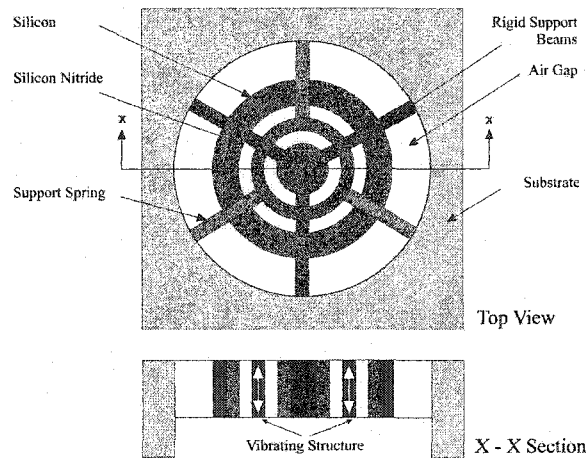


Figure 5.1: A Ring MEMS Microphone Design

design is shown in Figure 5.4. The ring is centered between the two capacitances and is effectively incorporates two offset capacitances. The reason for using two capacitances is that the voltage can be taken differentially off of the capacitors $C1$ and $C2$ as seen in the Figure. A differential arrangement doubles the output voltage for the design at no extra cost. Doubling the output voltage doubles the sensitivity. A squeeze film exists beneath the free moving rings and this space has a minimum of vent holes that are intended for releasing the structure, not dampening. This design attempts to maximize sensitivity by having a large linear change in capacitance and yet still have a large base capacitance to prevent capacitive voltage divider losses as covered in Section 2.6. Also pull-in voltage has been eliminated in the ring microphone so that its linearity over its range of operation can be increased. Electrostatic forces will balance out on the horizontal plane of the microphone. If there is a displacement along the horizontal axis, the total capacitance will still remain the same due to symmetry as can be seen in Figure 5.6. If the cap closes on one side it opens on the opposite so that the total capacitance remains the same. It is expected that this design will have a better directionality since the microphone displaces in only one direction. A sound wave that comes in at an angle will cause the microphone to rotate on an axis and deflect down at the same time. But due to the design the deflection from the rotation will have no effect on the change in capacitance. The deflection down of one side is equal and

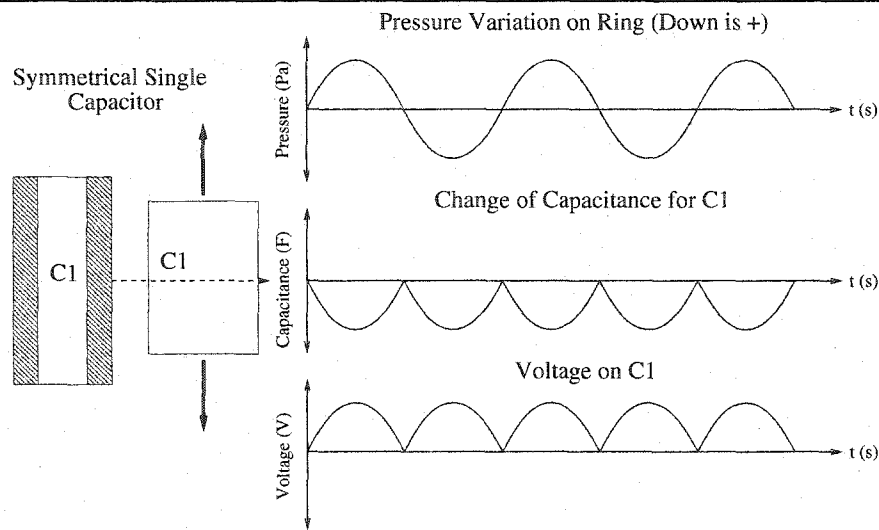


Figure 5.2: Ring Design Showing Cross Section of Center Ring

opposite the the rise of the other side of the capacitor. Balancing out the total effect on capacitance as can be seen in Figure 5.7.

5.2 Ring Microphone Design Modeling

As with the previous designs a mechanical equivalent model was derived for the ring design as shown in Figure 5.8. The differences to note here involve the squeeze film dampening. This model does not use vent holes in the back plate. Also there is the addition of Couette dampening between the rings. The model was implemented in the MATLAB program found in Appendix J. This program models one of the differential capacitors since the opposite capacitor is simply the inverse response. From this program a design optimization program was implemented as can be found in Appendix K. The design parameters of interest were: Spring width, height and length, diameter; moving and stationary conductor width and squeeze film gap distance. Parameters such as air gap distance between the rings and dielectric width were kept constant. The design space search was setup to eliminate designs that have a minimum capacitance less than 1 pF. The theoretical resonant frequency of the microphone also had to be above 10 kHz. A check for large resonant spikes is also

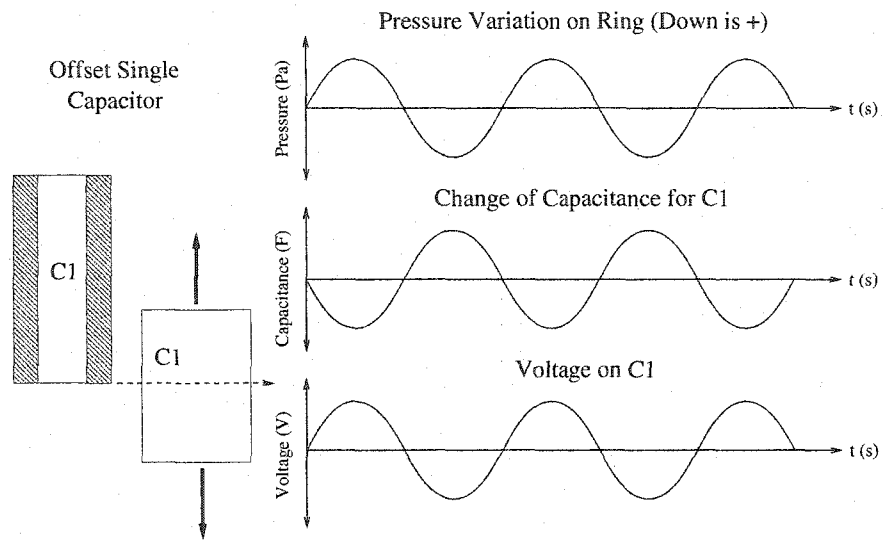


Figure 5.3: Ring Design Showing Cross Section of Center Ring

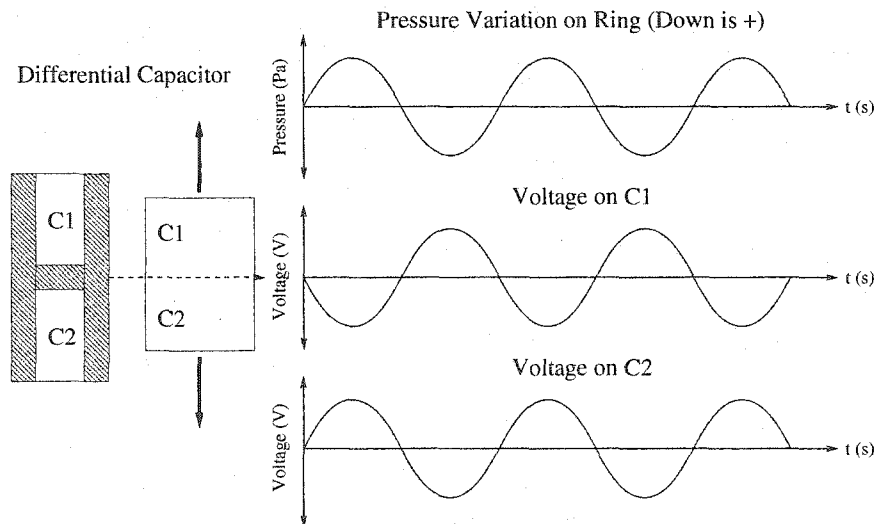


Figure 5.4: Ring Design Showing Cross Section of Center Ring

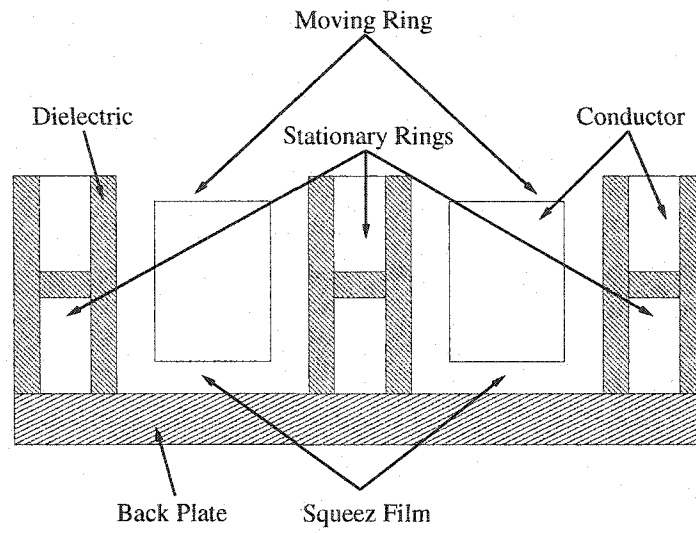


Figure 5.5: Ring Design Showing Cross Section of Center Ring

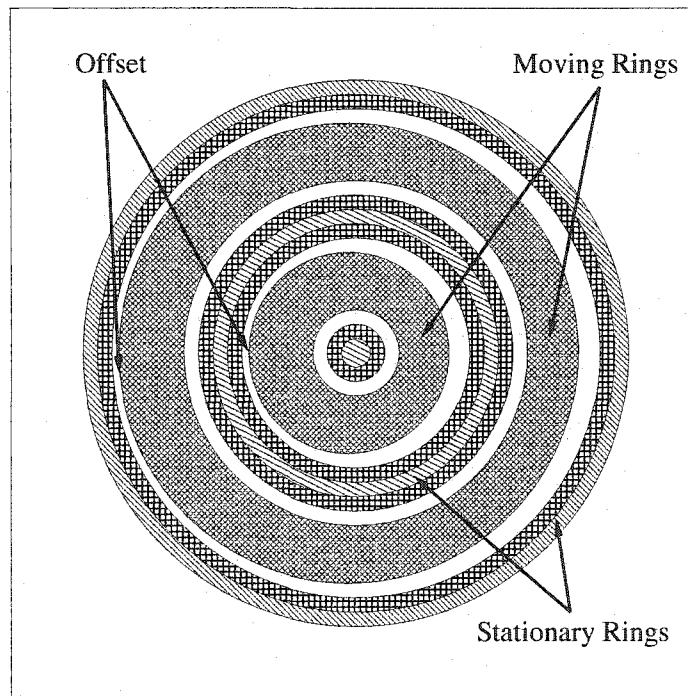


Figure 5.6: Ring Design Showing Offset in Horizontal Plane

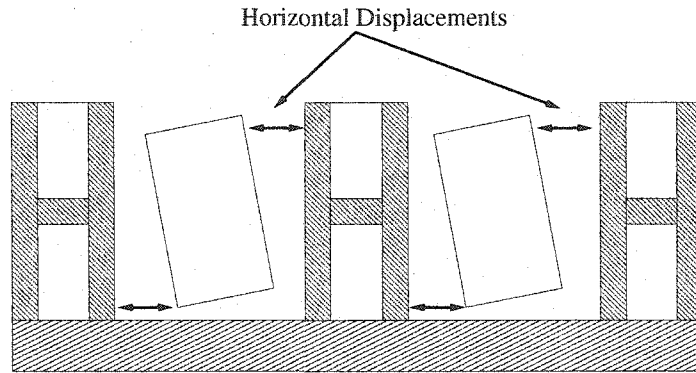


Figure 5.7: Ring Design Showing Offset in Vertical Plane

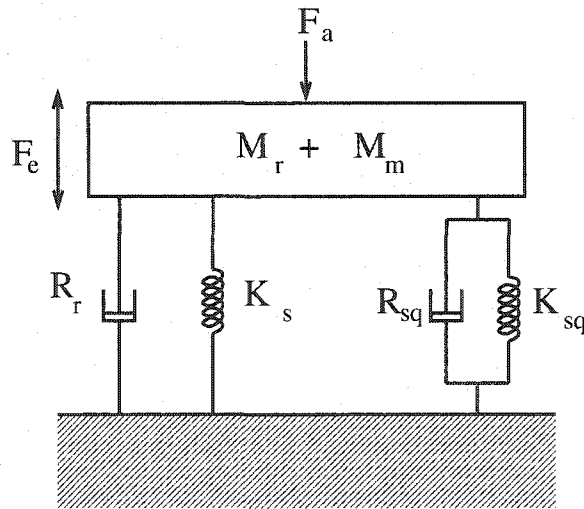


Figure 5.8: Ring Microphone Mechanical Equivalent

Table 5.1: Ring Design Space Optimization Results

Simulation Results		Diaphragm			Spring			Air Gap
Sensitivity	F_{res}	Diameter	t	Cond t	L	W	H	d0
mV/Pa	kHz	μm	μm	μm	μm	μm	μm	μm
340.0	10.0	2600.0	1.0	35.0	200.0	10.0	5.0	4.00
76.6	20.0	2000.0	1.0	18.0	100.0	7.0	3.5	1.75

included. Table 5.1 summarizes the results for 10 and 20 kHz design optimization runs. The optimized design parameters were then entered into the program in Appendix J. This program evaluates the displacement, change in capacitance and sensitivity versus frequency. The resultant displacement can be seen in Figure 5.9, where positive displacement is down. From this displacement the change in capacitance can be evaluated as seen in Figure 5.10. This shows the capacitance decreasing for the top capacitance as the ring deflects down. The lower capacitance would be the opposite of this since its capacitance increases with downward deflection. Finally from the change in capacitance, the change in voltage can be calculated and thus the sensitivity of the microphone, as shown in Figure 5.11. The sensitivity is around 170 mV/Pa for the top capacitor, which results in 340 mV/Pa sensitivity between the top and bottom capacitors. This sensitivity is with a battery voltage of 3.0 V and represents a change of 12 % to the applied voltage. To properly compare this with the state of the art, the sensitivity needs to be evaluated with a bias voltage of 12 V, which would give a sensitivity of in 1.44 V/Pa. The capacitance of both the 10 and 20 kHz ring designs is $C_0 = 1.04$ pF. This needs to be compared to the state of the art designs capacitance, which is around 16 pF. The reason for this is so that voltage divider losses can be estimated as covered in Section 2.6. The 10 kHz ring design utilizes 33 rings of 35 μm width. The 20 kHz design utilizes 43 rings at 18 μm width.

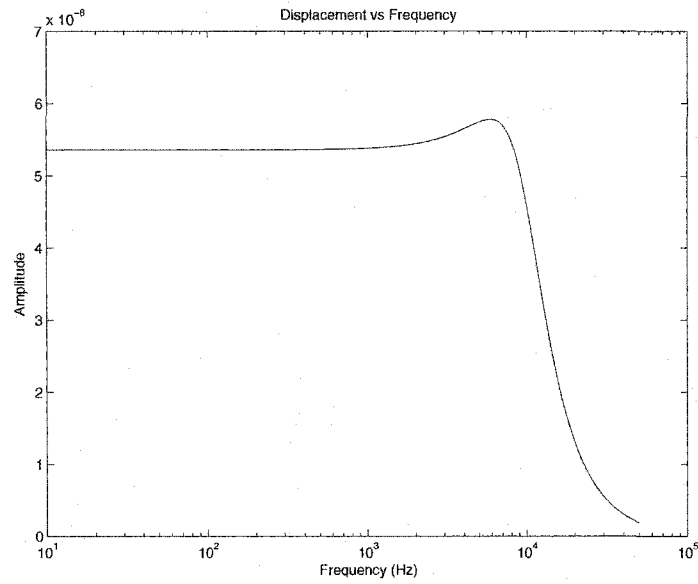


Figure 5.9: Ring Design Displacement vs Frequency

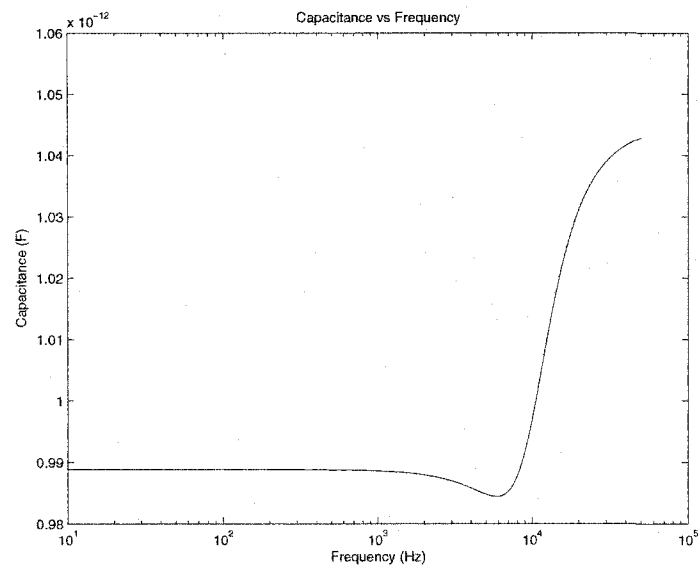


Figure 5.10: Ring Design Capacitance vs Frequency

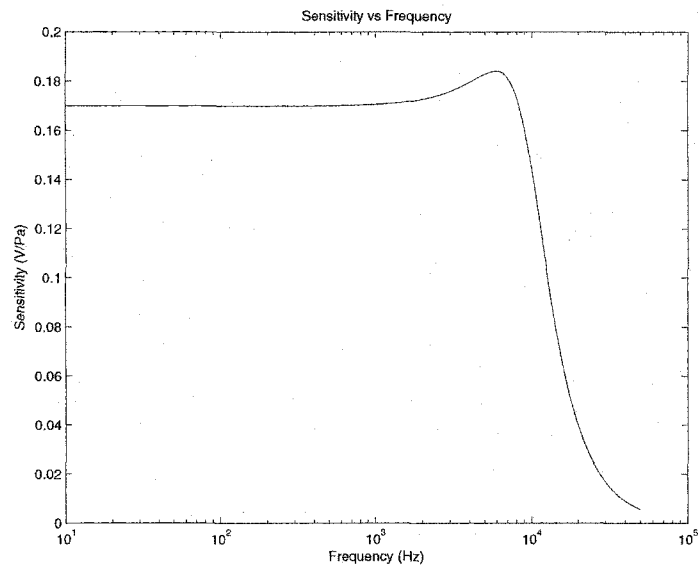


Figure 5.11: Ring Design Sensitivity vs Frequency

5.3 Discussion of Ring Microphone Results

This chapter introduced an innovative ring type MEMS microphone. The first section introduced the basic structure of the ring microphone. Various design advantages were pointed out. Such as the lack of a pull-in voltage and that the capacitance does not change due to offset deflections because of symmetry. The need for an offset detection capacitance was discussed. This is required in order to achieve a full voltage swing. A noted benefit of this design is that the sensitivity is doubled if a differential capacitive setup is used. As with the previous designs the next section presents a mechanical equivalent model of the ring design. The stress/strain in the support springs is expected to be the same as the suspended design. From the mechanical equivalent model a design space optimization program was once again implemented and optimized designs for 10 and 20 kHz resonant frequencies were determined. The results are summarized in Table 5.1. The sensitivities of the designs are significantly above the state of the art design. This is with a low bias voltage of only 3 V, compared to the 12 V used by the state of the art design.

Chapter 6

Conclusion

6.1 Conclusions

In this thesis the design and analysis of three MEMS microphones has been presented. A brief summary of the conclusions from the various chapters and appropriate sections will be presented here.

The first microphone presented is a clamped microphone design which is the current state of the art. A thorough investigation into clamped microphones is presented in chapter 2. The purpose of chapter 2 is to illustrate the design issues and considerations that come into play when designing clamped microphones. The results from this investigation illustrate that clamped microphone sensitivity is dominated by residual tension in the diaphragm and electrostatic forces in the air gap. A chosen basic state of the art design, reference [2], was used as an illustrative example throughout chapter 2.

It was found that the state of the art designs sensitivity could be improved by adjusting parameters other than diaphragm width and thickness. An improvement from 8 mV/Pa to 12 mV/Pa was found for the sensitivity. This represents an improvement of 1.5 times. These results were obtained thorough a design space optimization program. This program was also used to investigate the benefit of reducing diaphragm thickness down to 0.2 μm .

Table 6.1: Comparison of the Designs

Microphone Type	Bias Voltage V	Sensitivity mV/Pa	Capacitance pF
Clamped	10.00	42	16
Suspended	8.65	81	3
Ring	3.00	340	1

An optimal value of 42 mV/Pa was found with a thickness of 0.4 μm , an improvement of over 5 times. A MEMS microphone design flow was developed to illustrate the methodology used.

The second microphone investigated is the suspended microphone design. This design incorporates cantilever type springs supporting a diaphragm. A design space optimization program was also used to find a maximum sensitivity of 81 mV/Pa. This is an improvement of over 5 times compared to the clamped design.

The third and final design is a ring type microphone design composed of a series of rings supported by springs. It was found that the use of capacitive edge detection greatly increases the sensitivity of the microphone. A design space optimization program for this design gave a sensitivity of 170 mV/Pa at only 3 V bias. If differential dual capacitors are used the sensitivity is boosted to 340 mV/Pa. This represents a 42.5 times increase in sensitivity.

These results are summarized in table 6.1. As stated previously these results must include the base capacitance to be meaningful, as covered in Section 2.6.

This thesis has presented a thorough review of the current state of the art in MEMS microphone design. A significant improvement in sensitivity has been made to the current state of the art design. Two additional designs have been investigated and found to have excellent sensitivity. The suspended microphone has a sensitivity that is 5 times greater and the innovative ring design has a sensitivity 42.5 times greater than the current state of the art.

References

- [1] J. A. Voorthuyzen, P. Bergveld, "Semiconductor-based Electret Sensors for Sound and Pressure", IEEE Transactions on Electrical Insulation, Vol. 24 No.2, April 1989.
- [2] P.C. Hsu, C.H. Mastrangelo, K.D. Wise, "A high sensitivity polysilicon diaphragm condenser microphone", Micro Electro Mechanical Systems, 1998, MEMS 98, Proceedings, The Eleventh Annual International Workshop on , 25-29 Jan. 1998, pp 580 to 585.
- [3] P.R. Scheeper, A. G. H. van der Donk, W. Olthuis, P. Bergveld, "A review of silicon microphones", Sensors and Actuators A44 (1994) pp. 1 to 11.
- [4] M.T. Moskowitz, A.M. Hodge, R.W. Newcomb, "A diaphragm-gate transistor for gems microphones", IECON 02 [Industrial Electronics Society, IEEE 2002 28th Annual Conference of the] , Volume: 4 , Nov. 5-8, 2002, pp. 3042 to 3046.
- [5] D. A. Sperring, "On Silicon Microphones and Earphones for Hearing Aids", Sensors and Actuators, 18 (1989) pp. 33 to 44.
- [6] David P. Arnold, "A Piezoresistive Microphone For Aeroacoustic Measurements", Proceedings of 2001 ASME International Mechanical Engineering Congress and Exposition, Nov 11-16, New York, NY.
- [7] Ko Sang Choon, Kim Yong Chul, S.S. Lee, Choi Seung Ho, Kim Sang Ryong, "Piezoelectric membrane acoustic devices", Micro Electro Mechanical Systems, 2002. The Fifteenth IEEE International Conference on , 20-24 Jan. 2002, pp. 296 to 299.
- [8] Stephen D. Senturia, "Microsystem Design", Kluwer Academic Publishers, 2001, Chapter 13, pp. 327 to 339.
- [9] William T. Thomson, "Theory of Vibration with Applications, Third Edition", Prentice Hall, 1988, Chapter 2, pp. 28 to 35, Chapter 3, page 50 to 55.
- [10] Daniel J. Inman, "Engineering Vibration", Prentice Hall, 1994, Chapter 1, pp. 16 to 22.
- [11] Richard C. Dorf, Robert H. Bishop, "Modern Control Systems, 7th ed", Addison-Wesley Publishing Co. Inc., 1995, Chapter 2, pp. 30 to 58.

REFERENCES

- [12] Norman S. Nise, "Control Systems Engineering, 2nd Ed.", Addison-Wesley Publishing Co., 1995, Chapter 2, pp. 64 to 90.
- [13] S.B. Lee, P.V. Loeppert, "An impedance spectroscopic study of MEMS microphones", Sensors, 2002. Proceedings of IEEE , Volume: 2 , 12-14 June 2002 pp. 1250 to 1255 vol.2.
- [14] Steven C. Chapra, Raymond P. Canale, "Numerical methods for Engineers, Second Edition", McGraw Hill, 1988, Chapter 23, pp. 715 and Chapter 26, pp. 774.
- [15] Timoshenko, S., Woinowsky-Krieger, S., "Theory Of Plates And Shells, Second Edition", McGraw-Hill, 1959, Chapter 6, pp. 197 to 202.
- [16] S. Chowdhury, W.C. Miller, M. Ahmadi, "Nonlinear effects in MEMS capacitive microphone design", MEMS, NANO and Smart Systems, 2003. Proceedings. International Conference on July 20-23, 2003, pp. 297 to 302.
- [17] William H. Hayt, Jr., "Engineering Electro-magnetics, Fifth Edition", McGraw-Hill, 1989, Chapter 5, pp. 146.
- [18] Stephen D. Senturia, "Microsystem Design", Kluwer Academic Publishers, 2001, Chapter 20, pp. 543.
- [19] Jiandong Jin and Zhiping Zhou, "Simulation and Modeling of Micro Pressure Sensor Array", Micro-electronics Research Center, Georgia Institute of Technology.
- [20] IntelliSense Isuite software, MEMS material database, version 2.0, 1993.
- [21] Joseph E. Shigley, Charles R. Mischke, "Mechanical Engineering Design, Sixth Edition", Chapter 6, Section 6-6, pp. 337, 2001, McGraw Hill.
- [22] Richard G. Budynas, "Advanced Strength and Applied Stress Analysis, Second Ed", McGraw-Hill, 1999, Chapter 7, pp. 507, 513 to 515.
- [23] Cees van Rijin, Michiel van der Wekken, Wietze Nijdam, and Miko Elwenspoek, "Deflection and maximum Load of Micro-filtration Membrane Sieves Made with Silicon Micro-machining", Journal of MicroElectroMechanical Systems, Vol. 6, No. 1, March 1997.
- [24] MEMS Clearing house, material database, <http://www.memsnet.org/>, 2003.
- [25] Rombach, P.; Mullenborn, M. Klein, U. Rasmussen, K., "The first low voltage, low noise differential silicon microphone, technology development and measurement results", Micro Electro Mechanical Systems, 2001. MEMS 2001. The 14th IEEE International Conference on , 21-25 Jan 2001, pp. 42 to 45.
- [26] Jun Zou, Chang Liu, Jose Schutt-Aine, Jinghoung Chen, and Sung-Mo Kang, "Development of a Wide Tuning Range MEMS Tunable Capacitor for Wireless Communication Systems", Device Research Conference, 2000. Conference Digest. 58th DRC , 19-21 June 2000 Page(s): 111 -112.

REFERENCES

- [27] Yongduk Kim, Samg-Geun Lee and Sekwang Park, "Design of the Two-Movable Plate Type MEMS Voltage Tunable Capacitor", Modeling and Simulation of Microsystems 2002.
- [28] Dan Cheol-Hyun, Kim Eun Sok, "Fabrication of piezoelectric acoustic transducers built on cantilever-like diaphragm", Micro Electro Mechanical Systems, 2001. MEMS 2001. The 14th IEEE International Conference on , 21-25 Jan 2001, pp 110 to 113.
- [29] Stephen D. Senturia, "Microsystem Design", Kluwer Academic Publishers, 2001, Chapter 9, page 217.
- [30] Daniel J. Inman, "Engineering Vibration", Prentice Hall, 1994, Chapter 1, pp. 39.
- [31] Warren C. Young, "Roark's "Formulas for Stress and Strain, 5th ed.", McGraw Hill, 1989, Chapter , pp. 100.
- [32] Stephen D. Senturia, "Microsystem Design", Kluwer Academic Publishers, 2001, Chapter 6, pp. 134 to 137.
- [33] Stephen D. Senturia, "Microsystem Design", Kluwer Academic Publishers, 2001, Chapter 9, pp. 218.
- [34] William B. Bickford, "Mechanics of Solids Concepts and Applications", Irwin, 1993, Chapter 7, pp. 392.

Appendix A

Program 1

%Program Name: clampedparallelplateSvsF111102.m

%Written by: James Sliepenbeek

%Date: Oct 22rd 2002.

%MEMS Microphone Simulation utilizing a 2 degree of freedom model.

%The MEMS microphone modeled here is based upon the paper "A High

%Sensitivity Polysilicon Diaphragm Condenser Microphone", by

%c. H. Mastrangelo.

%This program will calculate the Sensitivity vs Frequency with no

%electrostatic force. It is utilizing the correct mechanical model of the

%microphone

close all

clear all

clc

epsilon0=8.854e-12;

epsilonR=7.5; %SiN dielectric

epsilonA=1.0; %Air dielectric

etaair=17.1e-06; %Pa-sec, air viscosity

E=1.55e11; %Youngs modulus for silicon GPa.

%PApplied=1; %Applied Pressure 1 Pa.

NHoles=19*19; %Number of holes in the backplate

mew=0.28; %Poisson's ratio

sigmaR=20e06; %Residual Stress, Pa

davg=4.0e-06; %Average air gap distance

A. PROGRAM 1

```

vsound=343;           %Velocity of sound m/s
rHole=60e-06;        %radius of the vent holes
%rHole=sqrt((60e-06^2)/pi)
bphieght=13.0e-06;   %Back plate height, or lenght of vent holes
ParCapDiamThickness=2.4e-06; %Thickness of Parallel Plate Capacitor
                        %Diaphragm.
Diam=2600e-06;       %Diameter of the Diaphragm
DensitySi=2300;
DensityAir=1.21;     %kg/m^3
rho0=DensityAir;    %Density of air
EO=10.0;            %Volts.
fmax=30000;         %Maximum calculation frequency.

%For a Suspended Parallel Plate Capacitor.
ClampedParAreaTotal=Diam^2;
%Area of the clamped diaphragm holes(20 of them)
ClampedParHoleArea=rHole^2*NHoles;
%The hole density of the backplate
HoleDensity=NHoles/ClampedParAreaTotal;
%Surface fraction occupied by the holes
alfa=ClampedParHoleArea/ClampedParAreaTotal;

T=sigmaR*ParCapDiamThickness;
rho=(ClampedParAreaTotal*ParCapDiamThickness*DensitySi)/...
ClampedParAreaTotal;
D=E*ParCapDiamThickness^3/(12*(1-mew^2));
Mm=(pi^4*rho*(2*pi^2*D+Diam^2*T))/(64*T);
%Radiative mass due to acoustic impedance
Mr=(8*rho0*Diam^3)/(3*pi*sqrt(pi));
Mt=Mr+Mm;
%Viscosity loss in the air gap
Rg=((12*etaair*Diam^2)/(HoleDensity*davg^3*pi))*((alfa/2)-((alfa^2)/8)...
-(log(alfa)/4)-3/8));
Ca=davg/(rho0*vsound^2*alfa^2*Diam^2);           %Compliance of the air gap
Ka=(1/Ca);
Cm=(32*Diam^2)/(pi^6*(2*pi^2*D+Diam^2*T));
Km=(1/Cm);
%Viscosity loss of back plate holes
Rh=(8*etaair*bphieght*Diam^2)/(pi*HoleDensity*rHole^4);
Fe=0;
PApplied=1;
ForceClampedPar=PApplied*ClampedParAreaTotal;
%Estimated frequency response
FreqClampedPar=sqrt((1/rho)*((D*pi^2/Diam^4)+(T/(2*Diam^2))));

```

A. PROGRAM 1

```
%Pull in Voltage Estimate 80 % of expected
VpIdeal=sqrt((8*Km*davg^3)/(27*epsilon0*...
ClampedParAreaTotal))*0.8;%20% less than expected.
%The Capacitance of A fully Clamped Parallel Plate Capacitor with no
%displacement.
COClampedPar=(epsilon0*epsilonA*ClampedParAreaTotal)/davg;

%Now Calculate the change in capacitance due to the displacement for
%the Capacitor.
FreqResActClampedPar=0;
CorFact=10;
for m=2:(fmax)/CorFact;
    f(m)=(m-1)*CorFact;
    omega(m)=2*pi*f(m);
    s=j*omega(m);
%Radiative resistance for the air in contact with the vibrating diaphragm.
Rr1=(DensityAir*(Diam)^4*omega(m)^2)/(2*pi*vsound);
Rr=Rr1;
XClampedPar(m)=(ForceClampedPar+Fe)/(Mt*s^2+Rr*s+Km+(1/(1/(s*...
(Rg+Rh))+1/Ka)));
if((davg-abs(XClampedPar(m)))<=0)
    XClampedPar(m)=davg;
end
if(abs(XClampedPar(m))<davg)
    %New Capacitance.
    NewCapClampedPar(m)=COClampedPar*(davg/(davg-abs(XClampedPar(m))));
else
    NewCapClampedPar(m)=0;
end
%Sensitivity
if(VpIdeal<10)
    Va=VpIdeal*.90;    %90% for linearity.
else
    Va=10.0*.90;      %Maximum practical voltage
end
MClampedPar(m)=Va-((davg-abs(XClampedPar(m)))/davg)*Va;
if(m>1)
%Find the actual resonant frequency.
if(abs(XClampedPar(m-1))<abs(XClampedPar(m)))
    FreqResActClampedPar=m*CorFact;
end
end
end
%Effective Electrostatic Pressure, assuming 50% airgap displacement.
```

A. PROGRAM 1

```
Fen=(epsilon0*epsilonA*ClampedParAreaTotal*(VpIdeal)^2)/(davg*0.5)^2;
Pt=(Fen+ForceClampedPar)/ClampedParAreaTotal;
%Estimation of Maximum Stress.
SigmaBend=1.47*((Pt^2*Diam^2*E)/ParCapDiamThickness^2)^(1/3);
fprintf('COClampedPar = %.3e F\n',COClampedPar)
fprintf('Estimated Res Freq = %.3e Hz\n',FreqClampedPar)
fprintf('Actual Res Freq = %.3e Hz\n',FreqResActClampedPar)
%Sensitivity at 1000Hz, note:100=1000.
fprintf('MClampedParnew = %.3e V/Pa\n',MClampedPar(10))
figure
semilogx(f,abs(XClampedPar))
ylabel('Displacement (m)')
xlabel('Frequency (Hz)');
title('Displacement vs Frequency Mech Equiv');
figure
semilogx(f,MClampedPar*1000)
xlabel('Frequency (Hz)')
ylabel('Sensitivity (mV/Pa)');
title('Sensitivity vs Frequency Mech Equiv');
axis([min(f) max(f) min(MClampedPar)*1000 max(MClampedPar)*1000+1])
figure
semilogx(f,NewCapClampedPar)
xlabel('Frequency (Hz)')
ylabel('Capacitance (F)');
title('Capacitance vs Frequency Mech Equiv');
```

Appendix B

Program 2

%Program Name: finitedifference4.m
%Written by: James Sliepenbeek
%Date: July 25, 2003.

%This program will plot the diaphragm shape due to a applied voltage and
%pressure for a square parallel plate capacitive microphone via a finite
%difference algorithm

%The fundamental equation for the diaphragm is
% $D \cdot \Delta^4 w - T \cdot \Delta^2 w = P_a + P_e / (d_0 - z)^2$;

close all
clear all
clc

epsilon0=8.854e-12;	%Permitivity of free space
sigma=20e6;	%Residual Stress
Eyoung=1.3e11;	%Youngs Modulus
mew=0.18;	%Poisons ratio
DeltaZ=3e-6;	%Microphone thickness
Diam=2600e-06;	%Diaphragm Width
d0=4.0e-06;	%Air gap height
Pa=1;	%Air pressure difference
V0=1;	%Applied Voltage
Delta=40;	%The number of nodes along a given %line including edge nodes
Pe=(epsilon0*V0^2)/2;	%The electrostatic Constant

B. PROGRAM 2

```

Lambda=1.5; %Relaxation constant
ErrorStop=0.1; %Stopping error percent

deltaX=Diam/(Delta-1); %The distance between nodes
T=sigma*DeltaZ; %Tensile force
D=(Eyoung*DeltaZ^3)/(12*(1-mew^2)); %Flexural Rigidity

%This is a elliptic partial differential equation which can be solved by
%Liebmann's method incorporating Boundary Condition dw/dx=0 and w=0 at the
%plate edge. These boundary conditions correspond to a clamped plate.

Zold=zeros(Delta,Delta);
Z=Zold;
ErrorFlag=0;
NumIter=0;
skipboundary=0;
Const1=(-D/deltaX^4);
Const2=(T/deltaX^2);
Const3=(21*D/deltaX^4+4*T/deltaX^2)^-1;
Const4=(22*D/deltaX^4+4*T/deltaX^2)^-1;
Const5=(20*D/deltaX^4+4*T/deltaX^2)^-1;
while(ErrorFlag==0)
    NumIter=NumIter+1;
    for i=2:Delta-1
        for j=2:Delta-1
            temp1=2*Z(i+1,j-1)-8*Z(i+1,j)+2*Z(i+1,j+1)-8*Z(i,j-1)...
                -8*Z(i,j+1)+2*Z(i-1,j-1)-8*Z(i-1,j)+2*Z(i-1,j+1);
            temp2=Z(i+1,j)+Z(i,j-1)+Z(i-1,j)+Z(i,j+1);
            P=Pa+Pe/(d0-Zold(i,j))^2;
            if(skipboundary~=1)
                if(i<Delta-1&&i>2&&j==2) %Left side
                    Z(i,j)=Const3*(Const1*(temp1+Z(i+2,j)+Z(i,j+2)+Z(i-...
                        2,j))+Const2*temp2+P);
                elseif(i==2&&j==2) %Top Left corner
                    Z(i,j)=Const4*(Const1*(temp1+Z(i+2,j)+Z(i,j+2))+...
                        Const2*temp2+P);
                elseif(j<Delta-1&&j>2&&i==2) %Top side
                    Z(i,j)=Const3*(Const1*(temp1+Z(i+2,j)+Z(i,j-2)+...
                        Z(i,j+2))+Const2*temp2+P);
                elseif(i==2&&j==Delta-1) %Top Right corner
                    Z(i,j)=Const4*(Const1*(temp1+Z(i+2,j)+Z(i,j-2))+...
                        Const2*temp2+P);
                elseif(i<Delta-1&&i>2&&j==Delta-1) %Right Side
                    Z(i,j)=Const3*(Const1*(temp1+Z(i+2,j)+Z(i,j-2)+Z(i...

```

```

        -2,j))+Const2*temp2+P);
elseif(i==Delta-1&&j==Delta-1) %Bottom Right corner
    Z(i,j)=Const4*(Const1*(temp1+Z(i,j-2)+Z(i-2,j))+...
        Const2*temp2+P);
elseif(j<Delta-1&&j>2&&i==Delta-1) % Bottom side
    Z(i,j)=Const3*(Const1*(temp1+Z(i,j-2)+Z(i-2,j)+Z(i...
        ,j+2))+Const2*temp2+P);
elseif(i==Delta-1&&j==2) %Bottom Left corner
    Z(i,j)=Const4*(Const1*(temp1+Z(i,j+2)+Z(i-2,j))+...
        Const2*temp2+P);
    end
end
if(i>2&&j>2&&i<Delta-1&&j<Delta-1)
    Z(i,j)=Const5*(Const1*(temp1+Z(i+2,j)+Z(i,j-2)+Z(i,j+...
        2)+Z(i-2,j))+Const2*temp2+P);
end
if(Z(i,j)~=0)
    Z(i,j)=Lambda*Z(i,j)+(1-Lambda)*Zold(i,j);
    ErrorA(i,j)=abs((Z(i,j)-Zold(i,j))/Z(i,j))*100;
    if(max(max(ErrorA))<ErrorStop)
        ErrorFlag=1;
    end
    Zold(i,j)=Z(i,j);
end
end
end
end
C0=epsilon0*Diam^2/(d0);
CMax=epsilon0*Diam^2/(d0-max(max(Z)));
CapFD=0; %The capacitance for the microphone in
%its final deformed shape
count=0;
QOriginal=(epsilon0*deltaX^2/d0)*V0;
for i=2:Delta
    for j=2:Delta
        count=count+1;
        %The average value of Z for a given square
        ZAvgForASqr=(Z(i-1,j-1)+Z(i-1,j)+Z(i,j)+Z(i,j-1))/4;
        CSqrFD(i-1,j-1)=epsilon0*(deltaX^2)/(d0-ZAvgForASqr);
        CapFD=CapFD+CSqrFD(i-1,j-1);
        Q(i-1,j-1)=CSqrFD(i-1,j-1)*V0;
    end
end
end
fprintf('NumIter = %2.0f\n',NumIter)

```

B. PROGRAM 2

```
fprintf('MaxError= %0.3e (%)\n',max(max(ErrorA)))
fprintf('deltaX= %2.2e (m)\n',deltaX)
fprintf('Max Z = %2.3e (m)\n',max(max(Z)))
fprintf('Capacitance for an undeformed diaphragm %2.3e (F)\n',C0)
fprintf('Capacitance if max displacement is used %2.3e (F)\n',CMax)
fprintf('Capacitance for the deformed diaphragm %2.3e (F)\n',CapFD)
figure
mesh(Z)
title('Displacement vs Node Number')
xlabel('Node Number')
ylabel('Node Number')
zlabel('Displacement (m)')
figure
hold on
plot(diag(Z))
plot(Z(Delta/2,:), 'r')
hold off
title('Displacement for Diagonal and Cross Sections')
xlabel('Node Number')
ylabel('Displacement (m)')
legend('Diagonal', 'Cross Section')
figure
mesh(Q)
title('Charge Density vs Node Number')
xlabel('Node Number')
ylabel('Node Number')
zlabel('Charge (C)')
fprintf('Done')
```

Appendix C

Program 3

```
%Program Name: finitedifferencePOnly.m
%Written by: James Sliepenbeek
%Date: July 25, 2003.
```

```
%This program will plot the diaphragm shape due to a changing pressure
%for a square parallel plate capacitive microphone via a finite difference
%algorithm
```

```
%The fundamental equation for the diaphragm is
%D*Del^4w-T*Del^2w=Pa+Pe/(d0-z)^2;
```

```
%close all
clear all
clc
```

```
sigma=20e6; %Residual Stress
Eyoung=1.3e11; %Youngs Modulus
mew=0.18; %Poisons ratio
DeltaZ=3e-6; %Microphone thickness
Diam=2600e-06; %Diaphragm Width
d0=4.0e-06; %Air gap height
Pmax=1; %Maximum air pressure difference
%applied
```

```
Delta=60; %The number of nodes along a given
%line including edge nodes
Lambda=1.5; %Relaxation constant
ErrorStop=0.1; %Stopping error percent
```

C. PROGRAM 3

```

deltaX=Diam/(Delta-1);           %The distance between nodes
T=sigma*DeltaZ;                 %Tensile force
D=(Eyoung*DeltaZ^3)/(12*(1-mew^2)); %Flexural Rigidity

%This is a elliptic partial differential equation which can be solved by
%Liebmann's method incorporating Boundary Condition dw/dx=0 and w=0 at the
%plate edge. These boundary conditions correspond to a clamped plate.

h=0;
Zold=zeros(Delta,Delta);
Z=Zold;
Const1=(-D/deltaX^4);
Const2=(T/deltaX^2);
Const3=(21*D/deltaX^4+4*T/deltaX^2)^-1;
Const4=(22*D/deltaX^4+4*T/deltaX^2)^-1;
Const5=(20*D/deltaX^4+4*T/deltaX^2)^-1;
NumSteps=10;
PStepSize=Pmax/NumSteps;
for PApplied=0:PStepSize:Pmax
    ErrorFlag=0;
    h=h+1;
    P=PApplied;
    PPlot(h)=P;
    while(ErrorFlag==0&&P~=0)
        for i=2:Delta-1
            for j=2:Delta-1
                temp1=2*Z(i+1,j-1)-8*Z(i+1,j)+2*Z(i+1,j+1)-8*Z(i,j-1)-8*...
                    Z(i,j+1)+2*Z(i-1,j-1)-8*Z(i-1,j)+2*Z(i-1,j+1);
                temp2=Z(i+1,j)+Z(i,j-1)+Z(i-1,j)+Z(i,j+1);
                if(i<Delta-1&&i>2&&j==2) %Left side
                    Z(i,j)=Const3*(Const1*(temp1+Z(i+2,j)+Z(i,j+2)+Z(i-2,j))...
                        +Const2*temp2+P);
                elseif(i==2&&j==2) %Top Left corner
                    Z(i,j)=Const4*(Const1*(temp1+Z(i+2,j)+Z(i,j+2))+Const2*...
                        temp2+P);
                elseif(j<Delta-1&&j>2&&i==2) %Top side
                    Z(i,j)=Const3*(Const1*(temp1+Z(i+2,j)+Z(i,j-2)+Z(i,j+2))...
                        +Const2*temp2+P);
                elseif(i==2&&j==Delta-1) %Top Right corner
                    Z(i,j)=Const4*(Const1*(temp1+Z(i+2,j)+Z(i,j-2))+Const2*...
                        temp2+P);
                elseif(i<Delta-1&&i>2&&j==Delta-1) %Right Side
                    Z(i,j)=Const3*(Const1*(temp1+Z(i+2,j)+Z(i,j-2)+Z(i-2,j))...

```

```

        +Const2*temp2+P);
elseif(i==Delta-1&&j==Delta-1) %Bottom Right corner
    Z(i,j)=Const4*(Const1*(temp1+Z(i,j-2)+Z(i-2,j))+Const2*...
        temp2+P);
elseif(j<Delta-1&&j>2&&i==Delta-1) % Bottom side
    Z(i,j)=Const3*(Const1*(temp1+Z(i,j-2)+Z(i-2,j)+Z(i,j+2))...
        +Const2*temp2+P);
elseif(i==Delta-1&&j==2) %Bottom Left corner
    Z(i,j)=Const4*(Const1*(temp1+Z(i,j+2)+Z(i-2,j))+Const2*...
        temp2+P);
end
if(i>2&&j>2&&i<Delta-1&&j<Delta-1)
    Z(i,j)=Const5*(Const1*(temp1+Z(i+2,j)+Z(i,j-2)+Z(i,j+2)+...
        Z(i-2,j))+Const2*temp2+P);
end
if(Z(i,j)~=0)
    Z(i,j)=Lambda*Z(i,j)+(1-Lambda)*Zold(i,j);
    ErrorA(i,j)=abs((Z(i,j)-Zold(i,j))/Z(i,j))*100;
    if(max(max(ErrorA))<ErrorStop)
        ErrorFlag=1;
    end
    Zold(i,j)=Z(i,j);
end
end
end
end
ZPlot(:,:,h)=Z;
end
figure
axis manual
axis([10 Delta 0 max(max(max(ZPlot)))]])
hold on
for i=1:h
    plot(ZPlot(:,Delta/2,i))
end
axis auto
hold off
title('Displacement for Diagonal for Different P')
xlabel('Node Position')
ylabel('Displacement (m)')
%legend('Diagonal','Cross Section')
figure
hold on
view(-37.5,45)

```

C. PROGRAM 3

```
axis([0 Delta 0 Delta 0 6e-09])
  for i=1:h
    mesh(ZPlot(:,:,i))
  title('Displacement vs Mesh Nodes')
  xlabel('Node Position')
  ylabel('Node Position')
  pause
  end
hold off
axis auto
fprintf('Done')
```

Appendix D

Program 4

```
%Program Name: finitedifferenceVpwtMesh.m
%Written by: James Sliepenbeek
%Date: July 25, 2003.
%This program will estimate pull in voltage for a square parallel plate
%capacitive microphone via a finite difference algorithm
%An iterative approach is used to estimate Vp for different mesh sizes

%The fundamental equation for the diaphragm is
%D*Del^4z-T*Del^2z=Pa+Pe/(d0-z)^2;

close all
clear all
clc

epsilon0=8.854e-12;          %Permitivity of free space
sigma=20e6;                 %Residual Stress
Eyoung=1.3e11;             %Youngs Modulus
mew=0.18;                  %Poisons ratio
DeltaZ=3e-6;               %Microphone thickness
Diam=2600e-06;             %Diaphragm Width
d0=4.0e-06;                %Air gap height
Pa=1;                      %Air pressure difference

MinDelta=10;               %Minimum delta
MaxDelta=20;               %Maximum delta
g=0;                       %Count variable for Delta
Lambda=1.5;                %Relaxation constant
ErrorStop=0.1;            %Stopping error percent
```

D. PROGRAM 4

```

T=sigma*DeltaZ; %Tensile force
D=(Eyoung*DeltaZ^3)/(12*(1-mew^2)); %Flexural Rigidity
SkipBoundary=1;

for Delta=MinDelta:MaxDelta %The number of nodes along a line
                                %including edge nodes
    V0=0; %Initial Applied Voltage
    g=g+1;
    DeltaPlot(g)=Delta;
    deltaX=Diam/(Delta-1); %The distance between nodes

    %This is a elliptic partial differential equation which can be solved
    %by Liebmann's method incorporating Boundary Condition dw/dx=0 and w=0
    %at the plate edge. These boundary conditions correspond to a clamped
    %plate.

    Const1=(-D/deltaX^4);
    Const2=(T/deltaX^2);
    Const3=(21*D/deltaX^4+4*T/deltaX^2)^-1;
    Const4=(22*D/deltaX^4+4*T/deltaX^2)^-1;
    Const5=(20*D/deltaX^4+4*T/deltaX^2)^-1;
    CapConst=epsilon0*deltaX^2; %Constant for calculating capacitance
    Zold=zeros(Delta,Delta);
    Ctemp=zeros(Delta,Delta);
    VpFlag=0; %Pull in Voltage Flag, set when pull
                                %in is reached

    h=0;
    ResCount=1;
    while(VpFlag==0) %Applied Voltage
        h=h+1;
        Pe=(epsilon0*V0^2)/2; %The electrostatic Constant
        Z=Zold;
        ErrorFlag=0; %Error flag indicating when the
                                %desired error has been reached.

        while(ErrorFlag==0&&VpFlag==0)
            for i=2:Delta-1
                for j=2:Delta-1
                    temp1=2*Z(i+1,j-1)-8*Z(i+1,j)+2*Z(i+1,j+1)-8*Z(i,j-1)-8*...
                        Z(i,j+1)+2*Z(i-1,j-1)-8*Z(i-1,j)+2*Z(i-1,j+1);
                    temp2=Z(i+1,j)+Z(i,j-1)+Z(i-1,j)+Z(i,j+1);
                    P=Pa+Pe/(d0-Zold(i,j))^2;
                    if(SkipBoundary~=1)
                        if(i<Delta-1&&i>2&&j==2) %Left side
                            Z(i,j)=Const3*(Const1*(temp1+Z(i+2,j)+Z(i,j+2)+Z(i-2,...

```

```

        j))+Const2*temp2+P);
elseif(i==2&&j==2) %Top Left corner
    Z(i,j)=Const4*(Const1*(temp1+Z(i+2,j)+Z(i,j+2))+...
        Const2*temp2+P);
elseif(j<Delta-1&&j>2&&i==2) %Top side
    Z(i,j)=Const3*(Const1*(temp1+Z(i+2,j)+Z(i,j-2))+...
        Z(i,j+2))+Const2*temp2+P);
elseif(i==2&&j==Delta-1) %Top Right corner
    Z(i,j)=Const4*(Const1*(temp1+Z(i+2,j)+Z(i,j-2))+...
        Const2*temp2+P);
elseif(i<Delta-1&&i>2&&j==Delta-1) %Right Side
    Z(i,j)=Const3*(Const1*(temp1+Z(i+2,j)+Z(i,j-2))+...
        Z(i-2,j))+Const2*temp2+P);
elseif(i==Delta-1&&j==Delta-1) %Bottom Right corner
    Z(i,j)=Const4*(Const1*(temp1+Z(i,j-2)+Z(i-2,j))+...
        Const2*temp2+P);
elseif(j<Delta-1&&j>2&&i==Delta-1) % Bottom side
    Z(i,j)=Const3*(Const1*(temp1+Z(i,j-2)+Z(i-2,j))+...
        Z(i,j+2))+Const2*temp2+P);
elseif(i==Delta-1&&j==2) %Bottom Left corner
    Z(i,j)=Const4*(Const1*(temp1+Z(i,j+2)+Z(i-2,j))+...
        Const2*temp2+P);
end
end
if(i>2&&j>2&&i<Delta-1&&j<Delta-1)
    Z(i,j)=Const5*(Const1*(temp1+Z(i+2,j)+Z(i,j-2))+...
        Z(i,j+2)+Z(i-2,j))+Const2*temp2+P);
end
if(Z(i,j)~=0)

    Z(i,j)=Lambda*Z(i,j)+(1-Lambda)*Zold(i,j);
    ErrorA(i,j)=abs((Z(i,j)-Zold(i,j))/Z(i,j))*100;
    if(max(max(ErrorA))<ErrorStop)
        ErrorFlag=1;
        break
    end
    if(Z(i,j)<d0)
        Zold(i,j)=Z(i,j);
    else
fprintf('Vp reached at %2.3f V with a mesh size of %2.0f Nodes\n'...
,V0,Delta)

        Vp(g)=V0;
        VpFlag=1;
        break

```

```
figure
plot(DeltaPlot,Vp)
title('Pull in Voltage vs Number of Nodes')
xlabel('Delta')
ylabel('Pull in Voltage (V)')
fprintf('Done')
```

Appendix E

Program 5

```
%Program Name: clampedparallelplateXvsVnewidea072503.m
%Written by: James Sliepenbeek
%Date: July 25, 2003.
```

```
%The Effect of Pressure on Pull in Voltage
%This program will determine the effect of air pressure on pull in voltage
%for a clamped plates and a spring supported plates pull in voltage.
```

```
close all
clear all
clc
```

```
%Calculate the capacitance of the mems microphones
```

```
epsilon0=8.854e-12;
epsilonR=7.5;           %SiN dielectric
epsilonA=1.0;          %Air dielectric
etaair=17.1e-06;      %Pa-sec, air viscosity
E=1.69e11;            %Youngs modulus for silicon GPa.
NHoles=289;           %Number of holes in the backplate
mew=0.28;             %Poisson's ratio
vsound=343;           %Velocity of sound m/s
rHole=60e-06;         %radius of the vent holes originally
bphieght=13.0e-06;    %Back plate height, or length of vent holes
ParCapDiamThickness=3.0e-06;%Thickness of Suspended/Clamped Parallel Plate
                        %Capacitor Diaphragm
Diam=2600e-06;        %Diameter of the Diaphragm
DensitySi=2300;       %Density of polysilicon kg/m^3
```

E. PROGRAM 5

```

DensityAir=1.21;           %Density of air kg/m^3
AirGap=4.0e-06;          %The average air gap distance
sigmaR=20e06;            %Residual Stress,Pa

%These parameters will be used to model the suspended parallel plate
%microphone
NumSprings=4;            %The number of springs used to support the
                          %diaphragms
W=30e-06;                %Spring width
H=3.0e-06;               %Spring height
BeamLSusPar=200e-06;     %Length of spring
kSusPar=((E*W*H^3)/(BeamLSusPar^3));%Guided spring constant

%For a Suspended Parallel Plate Capacitor.

ClampedParAreaTotal=Diam^2;
ClampedParVolume=ClampedParAreaTotal*ParCapDiamThickness;
ClampedParMass=ClampedParVolume*DensitySi;
ClampedParHoleArea=rHole^2*NHoles; %Area of the clamped diaphragm holes
HoleDensity=NHoles/ClampedParAreaTotal; %The hole density of the backplate
alfa=ClampedParHoleArea/ClampedParAreaTotal;%Surface fraction occupied by
                          %the holes

T=sigmaR*ParCapDiamThickness;
rho=(ClampedParAreaTotal*ParCapDiamThickness*DensitySi)/...
ClampedParAreaTotal;
D=E*ParCapDiamThickness^3/(12*(1-mew^2));
Mm=(pi^4*rho*(2*pi^2*D+Diam^2*T))/(64*T);
Mr=(8*DensityAir*Diam^3)/(3*pi*sqrt(pi)); %Radiative mass due to acoustic
                                          %impedance

Mt=Mr+Mm;
%Viscosity loss in the air gap
Rg=(((12*etaair*Diam^2)/(HoleDensity*AirGap^3*pi))*((alfa/2)-((alfa^2)/...
8)-(log(alfa)/4)-3/8));
Ca=AirGap/(DensityAir*vsound^2*alfa^2*Diam^2); %Compliance of the air gap
Ka=(1/Ca); %The spring constant of the air gap
Cm=(32*Diam^2)/(pi^6*(2*pi^2*D+Diam^2*T)); %The compliance of the diaphragm
Km=(1/Cm); %The spring constant of the diaphragm
%Viscosity loss of back plate holes
Rh=(8*etaair*bphiight*Diam^2)/(pi*HoleDensity*rHole^4);
%The Capacitance of A fully Clamped Parallel Plate Capacitor with no
%displacement.
COClampedPar=(epsilon0*epsilonA*(ClampedParAreaTotal))/AirGap;
%Frequency estimate for clamped parallel capacitor microphone

```

```

FreqSqrClampedPar=(1/(2*pi))*sqrt((Km+Ka)/(ClampedParMass+Mr));
%Frequency estimate for a clamped parallel capacitor microphone based on
%Mastrangelo paper
FreqSqrClampedParMast=sqrt((1/rho)*((D*pi^2)/Diam^4+T/(2*Diam^2)));
%Frequency estimate for a suspended parallel plate capacitor microphone
FreqSqrSuspendPar=(1/(2*pi))*sqrt((NumSprings*kSusPar)/(ClampedParMass+...
Mr));

%Design 1 corresponds to a clamped, design 2 a suspended microphone
Design=2;
Pmax=1; %Set this for the max pressure applied
PNumSteps=1; %Set this for the number of steps
%By default there is always 1Pa applied
PStepSize=Pmax/PNumSteps;
Vmax=40;
VNumSteps=1000;
VStepSize=Vmax/VNumSteps;
for nn=1:PNumSteps+1;
    PApplied(nn)=(nn-1)*PStepSize;
    ForceP=PApplied(nn)*(ClampedParAreaTotal);
    flag1=0;
    for n=1:VNumSteps;
        V(n)=n*VStepSize;
        if(Design==1) %Clamped Plate
            C=[Km -2*AirGap*Km-ForceP AirGap^2*Km+2*ForceP*AirGap -ForceP*...
                AirGap^2-epsilon0*epsilonA*ClampedParAreaTotal*V(n)^2/2];
        end
        if(Design==2) %Suspended Plate
            K=kSusPar;
            C=[K -2*AirGap*K-ForceP AirGap^2*K+2*ForceP*AirGap -ForceP*...
                AirGap^2-epsilon0*epsilonA*ClampedParAreaTotal*V(n)^2/2];
        end
        temp1=(roots(C)); %Load the roots
        if(flag1==1)
            RXClampedPar(nn,n,1)=temp1(1,1);
            RXClampedPar(nn,n,2)=AirGap*0.9999;
            RXClampedPar(nn,n,3)=AirGap*0.9999;
            NewCapClampedPar(nn,n)=0;
        end
        if(flag1==0)
            RXClampedPar(nn,n,1)=temp1(1,1);
            RXClampedPar(nn,n,2)=temp1(2,1);
            RXClampedPar(nn,n,3)=temp1(3,1);
            %New Capacitance.

```

E. PROGRAM 5

```
NewCapClampedPar(nn,n)=COClampedPar*(AirGap/(AirGap-...
                                abs(RXClampedPar(nn,n,3))));
end
if(abs(RXClampedPar(nn,n,2))==abs(RXClampedPar(nn,n,3))&&flag1==0)
    Vp(nn)=V(n);
    fprintf('RXClampedPar at %4.2f V is %d m\n',V(n),RXClampedPar...
            (nn,n,3));
    flag1=1;
end
end
end
for nn=1:PNumSteps+1;
    for xn=1:VNumSteps
        x(xn)=xn*AirGap*0.75/VNumSteps;
        Fe(nn,xn)=(epsilon0*epsilonA*ClampedParAreaTotal*(0.6*Vp(nn))^2)/...
                    (AirGap-x(xn))^2;
        Fk(xn)=Km*x(xn);
    end
end
for n=1:PNumSteps+1
    fprintf('Vp is = %4.2f V at %4.2f Pa\n',Vp(n),PApplied(n))
end

%Output Section of Matlab code
fprintf('Estimated frequency for the clamped microphone %4.2f Hz\n',...
FreqSqrClampedPar)
fprintf(...
'Estimated frequency for the suspended plate microphone %4.2f Hz\n'...
,FreqSqrSuspendPar)
fprintf('Estimated frequency from the Mastrangelo paper %4.2f Hz\n'...
,FreqSqrClampedParMast)
figure
hold on
for n=1:PNumSteps+1
    plot(V,NewCapClampedPar(n,:)*1e12,'LineWidth',2)
end
hold off
xlabel('Volts (V)')
ylabel('Capacitance (pF)');
title('Capacitance vs Volts');
axis([0 max(max(Vp))+1 COClampedPar*1e12 max(max(NewCapClampedPar))*1e12])
figure
hold on
for n=1:PNumSteps+1
```

```
    plot(V,AirGap-abs(RXClampedPar(n,:,1)), 'b',V,AirGap-abs(RXClampedPar...
(n,:,2)), 'g',V,AirGap-abs(RXClampedPar(n,:,3)), 'r', 'LineWidth',2);
end
hold off
xlabel('Volts (V)')
ylabel('Displacement (m)');
title('Displacement vs Volts');
axis([0 max(max(Vp))+1 -5e-06 AirGap])
figure
hold on
for n=1:PNumSteps+1
    plot(x/max(x),Fe(n,:)/max(Fe(n,:)), 'b',x/max(x),Fk/max(Fk), 'r')
end
hold off
ylabel('Normalized Force');
xlabel('Normalized Displacement (m)');
title('Electrical and Spring Forces vs Displacement');
figure
semilogy(V,Fe)
xlabel('Volts (V)')
ylabel('Electrostatic Force (N)');
title('Electrostatic Force vs Volts');
```

Appendix F

Program 6

%Program Name: clampedparallelplateXvsVT072503.m

%Written by: James Sliepenbeek

%Date: July 25, 2003.

%The Effect of Residual Tension on Pull in Voltage

%This program will determine the effect of air pressure on pull in voltage

%for a clamped plates and a spring supported plates pull in voltage.

close all

clear all

clc

%Calculate the capacitance of the mems microphones

epsilon0=8.854e-12;

epsilonR=7.5; %SiN dielectric

epsilonA=1.0; %Air dielectric

etaair=17.1e-06; %Pa-sec, air viscosity

E=1.69e11; %Youngs modulus for silicon GPa.

NHoles=289; %Number of holes in the backplate

mew=0.28; %Poisson's ratio

vsound=343; %Velocity of sound m/s

rHole=60e-06; %radius of the vent holes originally

bphieght=13.0e-06; %Back plate height, or length of vent holes

ParCapDiamThickness=3.0e-06; %Thickness of Suspended/Clamped Parallel Plate

%Capacitor Diaphragm

Diam=2600e-06; %Diameter of the Diaphragm

DensitySi=3200; %Density of polysilicon kg/m³

F. PROGRAM 6

```

DensityAir=1.21;           %Density of air kg/m^3
AirGap=4.0e-06;          %The average air gap distance

%For a Suspended Parallel Plate Capacitor.

ClampedParAreaTotal=Diam^2;
ClampedParVolume=ClampedParAreaTotal*ParCapDiamThickness;
ClampedParMass=ClampedParVolume*DensitySi;
ClampedParHoleArea=rHole^2*NHoles; %Area of the clamped diaphragm holes
HoleDensity=NHoles/ClampedParAreaTotal; %The hole density of the backplate
alfa=ClampedParHoleArea/ClampedParAreaTotal;%Surface fraction occupied by
%the holes

%The Capacitance of A fully Clamped Parallel Plate Capacitor with no
%displacement.
COClampedPar=(epsilon0*epsilonA*(ClampedParAreaTotal))/AirGap;
PApplied=1; %Applied pressure
sigmaRMax=100e06; %Set this for the max stress applied
sigmaRNumSteps=3; %Set this for the number of steps
sigmaRStepSize=sigmaRMax/sigmaRNumSteps;
for nn=1:sigmaRNumSteps;
sigmaR(nn)= sigmaRStepSize*nn; %Residual Stress,Pa
T=sigmaR(nn)*ParCapDiamThickness;
rho=(ClampedParAreaTotal*ParCapDiamThickness*DensitySi)/...
ClampedParAreaTotal;
D=E*ParCapDiamThickness^3/(12*(1-mew^2));
Mm=(pi^4*rho*(2*pi^2*D+Diam^2*T))/(64*T);
Mr=(8*DensityAir*Diam^3)/(3*pi*sqrt(pi)); %Radiative mass due to acoustic
%impedance

Mt=Mr+Mm;
%Viscosity loss in the air gap
Rg((((12*etaair*Diam^2)/(HoleDensity*AirGap^3*pi))*((alfa/2)-((alfa^2)/...
8)-(log(alfa)/4)-3/8));
Ca=AirGap/(DensityAir*vsound^2*alfa^2*Diam^2); %Compliance of the air gap
Ka=(1/Ca); %The spring constant of the air gap
Cm=(32*Diam^2)/(pi^6*(2*pi^2*D+Diam^2*T));%The compliance of the
%diaphragm
Km=(1/Cm); %The spring constant of the diaphragm
%Viscosity loss of back plate holes
Rh=(8*etaair*bphieght*Diam^2)/(pi*HoleDensity*rHole^4);

Vmax=55;
VNumSteps=1000;
VStepSize=Vmax/VNumSteps;
ForceP=PApplied*(ClampedParAreaTotal);

```

```

flag1=0;
for n=1:VNumSteps;
    V(n)=n*VStepSize;
    C=[Km -2*AirGap*Km-ForceP AirGap^2*Km+2*ForceP*AirGap -ForceP*...
        AirGap^2-epsilon0*epsilonA*ClampedParAreaTotal*V(n)^2/2];
    temp1=(roots(C)); %Load the roots
    if(flag1==1)
        RXClampedPar(nn,n,1)=temp1(1,1);
        RXClampedPar(nn,n,2)=AirGap*0.9999;
        RXClampedPar(nn,n,3)=AirGap*0.9999;
    end
    if(flag1==0)
        RXClampedPar(nn,n,1)=temp1(1,1);
        RXClampedPar(nn,n,2)=temp1(2,1);
        RXClampedPar(nn,n,3)=temp1(3,1);
    end
    if(abs(RXClampedPar(nn,n,2))==abs(RXClampedPar(nn,n,3))&&flag1==0)
        Vp(nn)=V(n);
        fprintf('RXClampedPar at %4.2f V is %d m\n',V(n),RXClampedPar...
            (nn,n,3));
        flag1=1;
    end
end
end
end
for n=1:sigmaRNumSteps
    fprintf('Vp is = %4.2f V at SigmaR= %4.2e Pa\n',Vp(n),sigmaR(n))
end

%Output Section of Matlab code
figure
hold on
for n=1:sigmaRNumSteps
    plot(V,AirGap-abs(RXClampedPar(n,:,1)), 'b',V,AirGap-abs(RXClampedPar...
        (n,:,2)), 'g',V,AirGap-abs(RXClampedPar(n,:,3)), 'r');
end
hold off
xlabel('Volts (V)')
ylabel('Displacement (m)');
title('Displacement vs Volts for Various Residual Tensions');
axis([0 max(max(Vp))+1 -5e-06 AirGap])

```

Appendix G

Program 7

```
%Program Name: ClampedDesignSpace.m
%Written by: James Sliepenbeek
%Date: August 4th 2003.
%MEMS Microphone Simulation utilizing a 2 degree of freedom model.
%This program will explore the design space for a parallel plate
%capacitor and search for the optimal design to give the best
%sensitivity

close all
clear all
clc

epsilon0=8.854e-12;
epsilonR=7.5;           %SiN dielectric
epsilonA=1.0;          %Air dielectric
etaair=17.1e-06;      %Pa-sec, air viscosity
E=1.69e11;            %Youngs modulus for silicon GPa.

mew=0.28;              %Poisson's ratio
vsound=343;           %Velocity of sound m/s
bphieght=13.0e-06;    %Back plate height, or length of vent holes
DensitySi=2300;       %Density of Silicon
DensityAir=1.21;      %kg/m^3
rho0=DensityAir;      %Density of air
E0=10.0;              %Applied Voltage.
fmax=30000;           %Maximum calculation frequency.

NumDiamSteps=60;
```

G. PROGRAM 7

```

StartDiam=100e-06;           %Diam=StartDiam+NumDiamSteps*100e-06;
NumrHolesSteps=20;
StartrHole=10e-06;         %rHole=StartrHole+NumrHolesSteps*10e-06;
NumNHolesSteps=30;
StartNHoles=100;          %NHoles=StartNHoles+NumNHolesSteps*20;
NumParCapDiamThicknessSteps=30;
StartParCapDiamThickness=0.2e-06; %ParCapDiamThickness=
                               %StartParCapDiamThickness+
                               %NumParCapDiamThicknessSteps*0.1e-06;

NumdavgSteps=20;
Startdavg=3.0e-06;        %davg=Startdavg+0.2e-06*NumdavgSteps;
NumsigmaSteps=20;
StartsigmaR=1e06;

MaxM=0;
MaxFreq=0;

for a=0:NumDiamSteps
Diam=StartDiam; %+a*100e-06;
%For a Suspended Parallel Plate Capacitor.
ClampedParAreaTotal=Diam^2;
for b=0:NumrHolesSteps
rHole=StartrHole+b*10e-06;
%Area of the clamped diaphragm holes(20 of them)
for c=0:NumNHolesSteps
NHoles=StartNHoles+c*20;
ClampedParHoleArea=pi*rHole^2*NHoles;
%The hole density of the backplate
HoleDensity=NHoles/ClampedParAreaTotal;
%Surface fraction occupied by the holes
alfa=ClampedParHoleArea/ClampedParAreaTotal;
for d=0:NumParCapDiamThicknessSteps
ParCapDiamThickness=StartParCapDiamThickness+d*0.1e-06;
for sigmaR=1:NumsigmaSteps           %Residual Stress, Pa
T=sigmaR*StartsigmaR*ParCapDiamThickness;
rho=(ClampedParAreaTotal*ParCapDiamThickness*DensitySi)/...
ClampedParAreaTotal;
D=E*ParCapDiamThickness^3/(12*(1-mew^2));
Mm=(pi^4*rho*(2*pi^2*D+Diam^2*T))/(64*T);
%Radiative mass due to acoustic impedance
Mr=(8*rho0*Diam^3)/(3*pi*sqrt(pi));
Mt=Mr+Mm;
for e=0:NumdavgSteps
davg=Startdavg+0.2e-06*e;

```

```

%Viscosity loss in the air gap
Rg=((12*etaair*Diam^2)/(HoleDensity*davg^3*pi))*((alfa/2)-((alfa^2)/8)...
-(log(alfa)/4)-3/8));
Ca=davg/(rho0*vsound^2*alfa^2*Diam^2);           %Compliance of the air gap
Ka=(1/Ca);
Cm=(32*Diam^2)/(pi^6*(2*pi^2*D+Diam^2*T));
Km=(1/Cm);
%Viscosity loss of back plate holes
Rh=(8*etaair*bphieght*Diam^2)/(pi*HoleDensity*rHole^4);
Fe=0;
PApplied=1;
ForceClampedPar=PApplied*ClampedParAreaTotal;
%Estimated frequency response
FreqClampedPar=sqrt((1/rho)*((D*pi^2/Diam^4)+(T/(2*Diam^2))));

%The Capacitance of A fully Clamped Parallel Plate Capacitor with no
%displacement.
COClampedPar=(epsilon0*epsilonA*ClampedParAreaTotal)/davg;

%Now Calculate the change in capacitance due to the displacement for
%the Capacitor.
%Pull in Voltage Estimate
VpIdeal=sqrt((8*Km*davg^3)/(27*epsilon0*ClampedParAreaTotal));
VpIdeal=VpIdeal*0.8; %Expected to be 20% less from model
%Effective Electrostatic Pressure, assuming 50% airgap displacement.
Fen=(epsilon0*epsilonA*ClampedParAreaTotal*(VpIdeal)^2)/(davg*.05)^2;
Pt=(Fen+ForceClampedPar)/ClampedParAreaTotal;
%Estimation of Maximum Stress.
SigmaBend=1.47*((Pt^2*Diam^2*E)/ParCapDiamThickness^2)^(1/3);
TotalStress=SigmaBend+sigmaR;
if(TotalStress<1.2e09)
Ftest=20e03; %The minimum desired resonant frequency.
Fmax=40000;
NumFSteps=Fmax/10;
FreqRes=Fmax/NumFSteps;
FreqResActClampedPar=FreqRes;
if(VpIdeal>5.0)
if(ClampedParAreaTotal>ClampedParHoleArea)
%Check to see if the resonant freq ftest.
if(FreqClampedPar>=Ftest&&FreqClampedPar<Fmax);
if(COClampedPar>1e-12) %Check for CO > 1 pF.
for m=2:NumFSteps;
    f(m)=(m-1)*FreqRes;
    omega(m)=2*pi*f(m);

```

G. PROGRAM 7

```

    s=j*omega(m);
    %Radiative resistance for the air in contact with the vibrating diaphragm.
    Rr1=(DensityAir*(Diam)^4*omega(m)^2)/(2*pi*vsound);
    Rr=Rr1;
    XClampedPar(m)=(ForceClampedPar+Fe)/(Mt*s^2+Rr*s+Km+(1/(1/(s*...
    (Rg+Rh))+1/Ka)));
    if((davg-abs(XClampedPar(m)))<=0)
        XClampedPar(m)=davg;
    end
    %Sensitivity
    if(m==(1000/FreqRes))
    if(VpIdeal<10)
    Va=VpIdeal*0.90; %Applied voltage will be 10 % less for linearity.
    else
    Va=10.0*0.90;
    end
    MClampedPar=Va-((davg-abs(XClampedPar(m)))/davg)*Va;
    end

    if(m>1)
    %Find the actual resonant frequency.
    if(abs(XClampedPar(m-1))<abs(XClampedPar(m)))
        FreqResActClampedPar=m*FreqRes;
    end
    end
end
%
if(MClampedPar>MaxM&&(FreqResActClampedPar>FreqRes&&...
abs(XClampedPar(FreqResActClampedPar/FreqRes))...
<=abs(XClampedPar(1e03/FreqRes))*1.10&&FreqResActClampedPar...
<Fmax)|| (FreqResActClampedPar...
==FreqRes&&abs(XClampedPar(Ftest/FreqRes))>=...
abs(XClampedPar(1e03/FreqRes))*0.30))
    MaxM=MClampedPar;
    MaxFreq=FreqResActClampedPar;
    tMax=ParCapDiamThickness;
    DMax=Diam;
    davgMax=davg;
    NumHolesMax=NHoles;
    rHolesMax=rHole;
    sigmaRMax=sigmaR*StartsigmaR;
    CMax=COClampedPar;
    StessMax=TotalStress;
fprintf('MaxM= %.3e (V/Pa) at MaxF= %.3e (Hz) ',MaxM,MaxFreq)

```

Appendix H

Program 8

```
%Program: susparallelplate102402.m
%Written by: James Sliepenbeek
%Date: Sept 2nd 2002.
```

```
%This capacitive microphone consists of a parallel plate type of capacitor
%in which the distance between the plates changes due to air pressure. It
%is supported NumSprings springs and is not clamped.
```

```
close all
clear all
clc
```

```
%Calculate the capacitance of the mems microphones
```

```
epsilon0=8.854e-12;
epsilonR=7.5;           %SiN dielectric
epsilonA=1.0;          %Air dielectric
etaair=17.1e-06;       %Pa-sec, air viscosity
E=1.69e11;            %Youngs modulus for silicon GPa.
PApplied=1;           %Applied Pressure 1 Pa.

NumSprings=4;         %The number of springs used to support the diaphragms.
W=4.0e-06;            %Spring width.
H=3.0e-06;            %Spring hieght
BeamLSusPar=200e-06; %Spring Length
NHoles=1000;          %Number of vent holes in the backplate
rHole=8.0e-06;        %Radius of the vent holes
mew=0.28;             %Poisson's ratio
```

H. PROGRAM 8

```

davg=5.0e-06;           %Air gap distance
vsound=343;           %Velocity of sound m/s

bphieght=13.0e-06;    %Back plate height, or lenght of vent holes

%Thickness of Suspended Parallel Plate Capacitor Diaphragm.
SusParCapDiamThickness=1.0e-06;
Diam=900e-06;         %Diameter of the Diaphragm
DensitySi=2300;
DensityAir=1.21;     %kg/m^3
row0=DensityAir;     %Density of air
fmax=25000;          %Maximum calculation frequency.

%For a Suspended Parallel Plate Capacitor.
SusParAreaTotal=Diam^2;
SusParHoleArea=rHole^2*NHoles;      %Area of the clamped diaphragm holes
HoleDensity=NHoles/SusParAreaTotal; %The hole density of the backplate
%Surface fraction occupied by the holes
alfa=SusParHoleArea/SusParAreaTotal;
SusParVolume=SusParAreaTotal*SusParCapDiamThickness;
SusParMass=SusParVolume*DensitySi;
%Stiffening mass, a square ring top only
sw=5e-06;
sh=6e-06;
SA=(Diam*sw*sh);
SB=((Diam-3*sw)/2)*sh*sw;
Ms=2*(3*SA+6*SB)*DensitySi;
%Radiative mass due to acoustic impedance
Mr=(8*row0*Diam^3)/(3*pi*sqrt(pi));
Mt=Mr+Ms+SusParMass;
%Viscosity loss in the air gap
Rg=((12*etaair*Diam^2)/(HoleDensity*davg^3*pi))*((alfa/2)-((alfa^2)/8)...
-(log(alfa)/4)-3/8);
%Compliance of the air gap
Ca=davg/(row0*vsound^2*alfa^2*Diam^2);
Ka=(1/Ca);           %Equivalent Spring constant
%Viscosity loss of back plate holes
Rh=((8*etaair*bphieght*Diam^2)/(pi*HoleDensity*rHole^4));

ForceSusPar=PApplied*SusParAreaTotal;

kSusPar=((E*W*H^3)/(BeamLSusPar^3)); %Guided Cantalever beam
OmeganSusPar=sqrt((kSusPar*NumSprings)/Mt);
FreqSusPar=(1/(2*pi))*OmeganSusPar; %Estimated frequency response

```

```

%The Capacitance of Suspended Parallel Plate Capacitor with no
%displacement.
COSusPar=(epsilon0*epsilonA*SusParAreaTotal)/davg;
%The ideal pull in voltage
VpIdeal=sqrt((8*kSusPar*NumSprings*davg^3)/(27*...
epsilon0*SusParAreaTotal))*0.80;%20% less expected.
%Now Calculate the change in capacitance due to the displacement for the
%Capacitor.
FreqResActSusPar=0;
for m=1:fmax/10;
    f(m)=m*10;
    omega(m)=2*pi*f(m);
    s=j*omega(m);
%Radiative resistance for the air in contact with the vibrating diaphragm.
Rr=(DensityAir*(Diam)^4*omega(m)^2)/(2*pi*vsound);
XSusPar(m)=ForceSusPar/(Mt*s^2+Rr*s+kSusPar*NumSprings+(1/((Rg+Rh)...
*s)^-1+Ka^-1)));
%New Capacitance.
NewCapSusPar(m)=COSusPar*(davg/(davg-abs(XSusPar(m))));
if(VpIdeal<10.0)
    Va=VpIdeal*0.90;%10% less for linearity.
else
    Va=10.0*0.90;
end
MSusParnew(m)=Va-((davg-abs(XSusPar(m)))/davg)*Va;           %Sensitivity.
if(m>1)
%Find the actual resonant frequency.
if(abs(XSusPar(m-1))<abs(XSusPar(m)))
    FreqResActSusPar=m*10;
end
end
end
fprintf('COSusPar = %.3e F\n',COSusPar)
fprintf('Estimated Res Freq = %4.2f Hz\n',FreqSusPar)
fprintf('Actual Res Freq = %.3e Hz\n',FreqResActSusPar)
fprintf('Vp ideal = %.3d\n',VpIdeal)
%Sensitivity at 1000Hz, note:100=1000.
fprintf('MSusParnew = %.3e V/Pa\n',MSusParnew(100))
figure
semilogx(f,MSusParnew)
xlabel('Frequency (Hz)')
ylabel('Sensitivity (V/Pa)');
title('Sensitivity vs Frequency');

```

```
figure
semilogx(f,abs(XSusPar),'r')
xlabel('Frequency (Hz)')
ylabel('Displacement (m)');
title('Displacement vs Frequency');
figure
semilogx(f,NewCapSusPar,'b')
xlabel('Frequency (Hz)')
ylabel('Capacitance (F)');
title('Capacitance vs Frequency');
```

Appendix I

Program 9

```
%Program: SuspendedCapDesignSpace.m
%Written by: James Sliepenbeek
%Date: April 16th 2002.

%This program will search the design space for a modified parallel plate
%capacitor.

close all
clear all
clc

%Calculate the capacitance of the mems microphones

epsilon0=8.854e-12;
epsilonR=7.5;           %SiN dielectric
epsilonA=1.0;           %Air dielectric
etaair=17.1e-06;        %Pa-sec, air viscosity
E=1.69e11;              %Youngs modulus for silicon GPa.
PApplied=1;             %Applied Pressure 1 Pa.

%The number of springs used to support the diaphragms this is fixed for the
%design space.
NumSprings=4;
%Back plate height, or length of vent holes this will be fixed for this
%analysis.
bphieght=13.0e-06;

%r=Diam/2;
```

I. PROGRAM 9

```
DensitySi=2300;          %kg/m^3
DensityAir=1.21;        %kg/m^3
rho0=DensityAir;        %kg/m^3
vsound=343;             %m/s

%Now Calculate the frequency response at 1KHz for every variable in the
%design space.
Fmax=30000;
NumLSteps=5;
StartL=100e-06;
NumWSteps=10;
StartW=1e-06;
NumHSteps=5;
StartH=1.0e-06;
NumDiamSteps=30;
StartDiam=100e-06;
NumtSteps=5;
Startt=1.0e-06;
NumHolesSteps=15;
StartNumHoles=100;
NumrHoleSteps=20;
StartrHoles=1e-06;
NumdavgSteps=10;
Startdavg=0.5e-06;
MaxM=0;
for a=1:NumLSteps
    BeamLSusPar=a*StartL;    %Spring length
for b=1:NumWSteps
    W=b*StartW;             %Spring width.
for c=1:NumHSteps
    H=StartH*c;             %Spring hieght or thickness of the springs
for d=1:NumtSteps
    CapLength=d*Startt;     %Length of modified parallel plate SusPar
                                %Capacitor microphone otherwise know as the
                                %thickness.
for e=1:NumDiamSteps
    Diam=e*StartDiam;        %The diameter or cross sectional width of
                                %the capacitor

    SusParAreaTotal=Diam^2;
    SusParVolume=SusParAreaTotal*CapLength;
    SusParMass=SusParVolume*DensitySi;
    ForceSusPar=PApplied*SusParAreaTotal;
    %Stiffening mass, a square ring top only
    sw=5e-06;
```

I. PROGRAM 9

```

sh=6e-06;
SA=(Diam*sw*sh);
SB=((Diam-3*sw)/2)*sh*sw;
Ms=2*(3*SA+6*SB)*DensitySi;
Mr=(8*DensityAir*(Diam)^3)/(3*pi*sqrt(pi));
Mt=SusParMass+Mr+Ms;
for f=1:NumHolesSteps
    NHoles=StartNumHoles*f;    %Number of holes in the backplate
for g=1:NumrHoleSteps
    rHole=g*StartrHoles;    %radius of the vent holes
    kSusPar=(E*W*H^3)/(BeamLSusPar^3);    %Guided cantilever beams
    OmeganSusPar=sqrt((kSusPar*NumSprings)/Mt);
    %The estimated resonant frequency of the microphone
    FreqSusPar=(1/(2*pi))*OmeganSusPar;
%Test to see if the hole area is less than 25% the size of the microphone
if(NHoles*pi*rHole^2<0.25*Diam^2&FreqSusPar>=10e03&BeamLSusPar<Diam)
    SusParHoleArea=rHole^2*NHoles;    %Area of the clamped diaphragm holes
    %Surface fraction occupied by the holes
    alfa=SusParHoleArea/SusParAreaTotal;
    %The hole density of the backplate
    HoleDensity=NHoles/SusParAreaTotal;
for h=1:NumdavgSteps
    davg=h*Startdavg;
%The Capacitance of Suspended Parallel Plate Capacitor with no
%displacement.
COSusPar=(epsilon0*epsilonA*SusParAreaTotal)/davg;
if(COSusPar>=10e-12) %Check for sufficient capacitance.
    VpIdeal=sqrt((8*kSusPar*NumSprings*davg^3)/(27*epsilon0*...
        SusParAreaTotal))*0.80;%Expected to be 20% less.
    Ka=(davg/(rho0*vsound^2*alfa^2*Diam^2))^-1; %Compliance of the air gap
    Rg=(((12*etaair*Diam^2)/(HoleDensity*davg^3*pi))*((alfa/2)-...
        ((alfa^2)/8)-(log(alfa)/4)-3/8));    %Viscosity loss in the air gap
%Viscosity loss of back plate holes
    Rh=(8*etaair*bphieght*Diam^2)/(pi*HoleDensity*rHole^4);
    omega=2*pi*1000;    %Evaluate the frequency response at 1KHz.
    s=j*omega;
    Rr=(DensityAir*(Diam)^4*(omega)^2)/(2*pi*vsound);
    XSusPar1K=ForceSusPar/(Mt*s^2+Rr*s+kSusPar*NumSprings+...
        (1/(((Rg+Rh)*s)^-1+Ka^-1)));
%Evaluate the frequency response at the estimated resonant frequency.
    omega=2*pi*FreqSusPar;
    s=j*omega;
    Rr=(DensityAir*(Diam)^4*(omega)^2)/(2*pi*vsound);
    XSusParRes=ForceSusPar/(Mt*s^2+Rr*s+kSusPar*NumSprings+...

```

```

                (1/(((Rg+Rh)*s)^-1+Ka^-1)));
if((davg-(abs(XSusPar1K)))>0)
    Lnew=davg-abs(XSusPar1K);
else
    Lnew=0;
end
if(VpIdeal<10)
Va=VpIdeal*.90; %10% less for linearity.
else
Va=10.0*0.90;      %Also 10 % less for linearity.
end
MSusPar=Va-(Lnew/davg)*Va;                                %Sensitivity.
if(MSusPar>MaxM&abs(XSusParRes)<abs(XSusPar1K)*1.10)
    MaxM=MSusPar;
    MaxFreq=FreqSusPar;
    if(XSusParRes>XSusPar1K)
        XSusParMax=abs(XSusParRes);
    else
        XSusParMax=abs(XSusPar1K);
    end
    LMax=BeamLSusPar;
    WMax=W;
    HMax=H;
    tMax=CapLength;
    DMax=Diam;
    NHolesMax=NHoles;
    rHolesMax=rHole;
    davgMax=davg;
    CMax=COSusPar;
    VpIdealMax=VpIdeal;
end
end %End of if capacitance check
end
end %End of if area check
end
end
end
end
end
end
end
MaxStress=(3*E*HMax*abs(XSusParMax))/(2*LMax^2);
fprintf('Range for Spring Length %.3e to %.3e (m)\n',StartL,...
NumLSteps*StartL)

```

I. PROGRAM 9

```
fprintf('Range for Spring Width %.3e to %.3e (m)\n',StartW,...
NumWSteps*StartW)
fprintf('Range for Spring Hieght %.3e to %.3e (m)\n',StartH,...
NumHSteps*StartH)
fprintf('Range for Diaphram thickness %.3e to %.3e (m)\n',Startt,...
NumtSteps*Startt)
fprintf('Range for Diamater %.3e to %.3e (m)\n',StartDiam,...
NumDiamSteps*StartDiam)
fprintf('Range for the number of holes %.3d to %.3d\n',StartNumHoles,...
NumHolesSteps*StartNumHoles)
fprintf('Range for the radius of the holes %.3e to %.3e (m)\n',...
StartrHoles,NumrHoleSteps*StartrHoles)
fprintf('MaxM= %.3e (V/Pa) at MaxF= %.3e (Hz)\n',MaxM,MaxFreq)
fprintf('L= %.1e W= %.1e H= %.1e t= %.1e Diam= %.2e\n',LMax,WMax,...
HMax,tMax,DMax)
fprintf('NumHoles= %.3d rHoles= %.1e Maxdavg= %.3e\n',NHolesMax,...
rHolesMax,davgMax)
fprintf('MaxStress= %.3e (Pa) COSusPar= %.3e (F) ',MaxStress,CMax)
fprintf('Vp Ideal = %2.2f (V)\n',VpIdealMax)
fprintf('done')
```

Appendix J

Program 10

```
%Program name: modcapcircularrings2.m
%Written by: James Sliepenbeek
%Date: August 8th, 2003
%This program will explore the behaviour of a cylindrical capacitor
%that consists of a series of rings supported by 3 springs.
%This microphone does not have vent holes in the backplate since
%the back plate only exists under each ring. The only source of dampening
%is electrostatic forces viscosity loss in the air gap and Couette type
%dampening. There is a squeeze film between the rings and the back plate.

close all
clear all
clc

epsilon0=8.854e-12;
epsilonR=7.5;      %SiN dielectric
epsilonA=1.0;      %Air dielectric
etaair=17.1e-06;   %Pa-sec, air viscosity
E=1.69e11;         %Youngs modulus for silicon GPa.
PApplied=1;        %Applied Pressure 1 Pa.
P0=101.1e03;       %Average atmospheric pressure

NumSprings=3;      %The number of springs used to support the diaphragms.
BeamLCylRing=200e-06;%Spring beam length
W=10.0e-06;        %Spring width.
H=5.0e-06;         %Spring height
CapLength=1.0e-06; %Length of CylRing Capacitor.
condwidth=1.0e-06; %The stationary electrode
```

```

movcondwidth=35.0e-06;%The conducting electrode part of the microphone
                        %capacitance that is displaced by the sound wave

dielwidth=1.0e-06;
airgapwidth=1.0e-06;
Diam=2600e-06;
r=Diam/2;
DensitySi=2320;        %kg/m^3
DensityAir=1.21;       %kg/m^3
E0=3.0;                %Volts.
vsound=343;
rho0=DensityAir;
davg=4.0e-06;

Maxnumrings=round((Diam/2)/(movcondwidth+2*airgapwidth+2*dielwidth+...
condwidth))

%For a CylRing Capacitor.
%Total surface area of cylindrical Capacitor.
CylRingAreaTotal=0;
CylRingIntA=0;
for n=1:Maxnumrings;
    CylRingAreaTotal=CylRingAreaTotal+pi*((n*movcondwidth+3*(...
airgapwidth+dielwidth+0.5*condwidth))^2-((n-1)*movcondwidth...
+3*(airgapwidth+dielwidth+0.5*condwidth))^2);
    CylRingIntA=CylRingIntA+(2*pi*CapLength*(n*movcondwidth+2*n*...
airgapwidth+2*n*dielwidth+n*condwidth));
end
CylRingVolume=CylRingAreaTotal*CapLength;
CylRingMass=CylRingVolume*DensitySi;
%The Capacitance of the CylRing Capacitor with no displacement.
CylRingC0=0;
%CapLength/2 since only 1/2 is used per capacitor.
for n=1:Maxnumrings
    D1=(n-1)*movcondwidth+n*airgapwidth+(2*n-1)*dielwidth+0.5*(2*n-1)*...
condwidth;
    N1=D1+airgapwidth;
    N2=D1;
    D2=N2-dielwidth;
    D3=D1+airgapwidth+movcondwidth;
    N3=D3+airgapwidth;
    D4=N3;
    N4=D4+dielwidth;
    CCylRingIA=(2*pi*epsilon0*epsilonA*CapLength/2)/log(N1/D1);
    CCylRingIR=(2*pi*epsilon0*epsilonR*CapLength/2)/log(N2/D2);

```

```

    CCylRingOA=(2*pi*epsilon0*epsilonA*CapLength/2)/log(N3/D3);
    CCylRingOR=(2*pi*epsilon0*epsilonR*CapLength/2)/log(N4/D4);
    CylRingCO=CylRingCO+((1/(1/CCylRingIA+1/CCylRingIR))+1/(1/CCylRingOA+...
        1/CCylRingOR));
end
%The capacitance of a equivalent square capacitor, for comparision,
%assuming an air gap or 3um.
CSquare=epsilon0*Diam^2/davg;

%Now Calculate the change in capacitance due to the displacement for the
%CylRing Capacitor.

RCouetteCylRing=(etaair*CylRingIntA)/airgapwidth;
RPoiseuille=(12*etaair*CapLength)/((CylRingIntA/CapLength)*airgapwidth^3);
Fe=-4*epsilon0*CylRingIntA*E0^2/(airgapwidth/epsilonA+dielwidth/epsilonR);
ForceCylRing=PApplied*CylRingAreaTotal;
Mr=(8*DensityAir*(Diam)^3)/(3*pi*sqrt(pi));
Mt=CylRingMass+Mr;
BeamMass=BeamLCylRing*W*H*DensitySi*3;
kCylRing=(E*W*H^3)/(BeamLCylRing^3); %Guided cantaliver beam
OmeganCylRing=sqrt((kCylRing*NumSprings)/Mt);
FreqCylRing=(1/(2*pi))*OmeganCylRing;
CCriticalCylRing=2*CylRingMass*OmeganCylRing;
ZetaCylRing=(RCouetteCylRing)/CCriticalCylRing;
%Squeeze film dampening
bairgap=(96*etaair*CylRingAreaTotal*movcondwidth^2)/(pi^4*davg^3);
omegac=(pi^2*davg^2*P0)/(12*etaair*movcondwidth^2);
%Airgap spring constant
Ka=bairgap*omegac;
%Now Calculate the change in capacitance due to the displacement for the
%CylRing Capacitor.
Fmax=50000;
NumFSteps=Fmax/10;
FreqRes=Fmax/NumFSteps;
FreqResAct=0;
for m=1:NumFSteps;
    f(m)=m*FreqRes;
    omega(m)=2*pi*f(m);
    s=j*omega(m);
    Rr=(DensityAir*(Diam)^4*(omega(m))^2)/(2*pi*vsound);
    XCylRing(m)=(ForceCylRing+Fe)/(Mt*s^2+(Rr+RCouetteCylRing)*s+...
        kCylRing*NumSprings+(1/(1/(s*bairgap)+1/Ka)));
    if((CapLength-(abs(XCylRing(m))))>0)
        NewCylRingCapLength=CapLength-abs(XCylRing(m));
    end
end

```

```

        Lnew=abs(XCylRing(m));
    else
        NewCylRingCapLength=0;
        Lnew=0;
    end
    NewCapCylRing(m)=CylRingC0*(NewCylRingCapLength/CapLength);
    MCylRing(m)=(CapLength/(CapLength-Lnew))*E0-E0;           %Sensitivity.
    if(m>1)
    if(abs(XCylRing(m-1))<abs(XCylRing(m)))
        FreqResAct=m*FreqRes;
    end
    end
end
fprintf('Maxnumrings= %.2i\n',Maxnumrings)
fprintf('CylRingC0 = %.3e F\n',CylRingC0)
fprintf('CSquare Equivalent = %.3e F\n',CSquare)
fprintf('Estimated Res Freq = %.3e Hz\n',FreqCylRing)
fprintf('Actual Res Freq = %.3e Hz\n',FreqResAct)
fprintf('Beam Length = %.3e m\n',BeamLCylRing)
fprintf('MCylRing = %.3e V/Pa at 1kHz\n',MCylRing(round(1000/FreqRes)))
fprintf('max MCylRing = %.3e V/Pa\n',max(MCylRing))
fprintf('RCouetteCylRing = %d\n',RCouetteCylRing)
fprintf('CCriticalCylRing = %d\n',CCriticalCylRing);
fprintf('Zeta = %d\n',ZetaCylRing);
figure
semilogx(f,MCylRing)
xlabel('Frequency (Hz)');
ylabel('Sensitivity (V/Pa)');
title('Sensitivity vs Frequency');
figure
plot(f,abs(XCylRing),'r')
xlabel('Frequency (Hz)');
ylabel('Amplitude');
title('Displacement vs Frequency');
figure
plot(f,NewCapCylRing)
xlabel('Frequency (Hz)');
ylabel('Capacitance (F)');
title('Capacitance vs Frequency');

```

Appendix K

Program 11

```
%Program Name: modparallelcircularringsdesignspace2.m
%Written by: James Sliepenbeek
%Date: August 13th, 2003.
%This program will explore the design space of a cylindrical capacitor
%that consists of a series of rings supported by 3 springs.
%This microphone does not have vent holes in the back plate since
%the back plate only exists under each ring. The only source of dampening
%is electrostatic forces, viscosity loss in the air gap and Couette type
%dampening. There is a squeeze film between the rings and the back plate.
%This version will use a different ring width varying technique.
```

```
close all
clear all
clc
```

```
epsilon0=8.854e-12;
epsilonR=7.5;           %SiN dielectric
epsilonA=1.0;           %Air dielectric
etaair=17.1e-06;       %Pa-sec, air viscosity
E=1.69e11;             %Youngs modulus for silicon GPa.
PApplied=1;            %Applied Pressure 1 Pa.
P0=101.1e03;           %Average atmospheric pressure

NumSprings=3;          %The number of springs used to support the
%diaphragms.
dielwidth=1.0e-06;
airgapwidth=1.0e-06;
DensitySi=2320;        %kg/m^3
```

K. PROGRAM 11

```

DensityAir=1.21;          %kg/m^3
EO=3.0;                  %Volts.
vsound=343;
rho0=DensityAir;

NumLSteps=5;
StartL=190e-06;          %BeamLCylRing=NumLSteps*10e-06+StartL;
NumWSteps=5;
StartW=9.0e-06;          %W=NumWSteps*1e-06+StartW;
NumHSteps=5;
StartH=4.5e-06;          %H=StartH+NumHSteps*0.5e-06;
NumDiamSteps=5;
StartDiam=2550e-06;      %Diam=NumDiamSteps*50e-06+StartDiam;
NumMovCondWidthSteps=10;
StartMovCondWidth=34.5e-06; %movcondwidth=0.5e-06*NumMovCondWidthSteps
                               %+StartMovCondWidth;

NdavgSteps=10;
Startdavg=3.9e-06;       %davg=NdavgSteps*0.1e-06+Startdavg;
NumCapLengthSteps=1;
CapLengthStart=1.0e-06; %CapLength=NumCapLengthSteps*CapLengthStart;
MaxM=0;
MaxFreq=0;
Fmax=30000;
NumFSteps=Fmax/10;
FreqRes=Fmax/NumFSteps;
condwidth=1e-06;         %Fixed conductor width
for e=0:NumMovCondWidthSteps
    %The conducting electrode part of the microphone capacitance that is
    %displaced by the sound wave
    movcondwidth=0.5e-06*e+StartMovCondWidth;
for a=0:NumDiamSteps
    Diam=a*50e-06+StartDiam;          %The diameter of the capacitor
    Maxnumrings=round((Diam/2)/(movcondwidth+2*airgapwidth+2*dielwidth...
    +condwidth));
for cl=1:NumCapLengthSteps
    CapLength=cl*CapLengthStart;
%For a CylRing Capacitor.
%Total surface area of cylindrical Capacitor.
CylRingAreaTotal=0;
CylRingIntA=0;
for n=1:Maxnumrings;
    CylRingAreaTotal=CylRingAreaTotal+pi*((n*movcondwidth+3*(...
    airgapwidth+dielwidth+0.5*condwidth))^2-((n-1)*movcondwidth...
    +3*(airgapwidth+dielwidth+0.5*condwidth))^2);

```

K. PROGRAM 11

```

    CylRingIntA=CylRingIntA+(2*pi*CapLength*(n*movcondwidth+2*n...
    *airgapwidth+2*n*dielwidth+n*condwidth));
end
CylRingVolume=CylRingAreaTotal*CapLength;
CylRingMass=CylRingVolume*DensitySi;
CylRingC0=0;
%CapLength/2 since only 1/2 is used per capacitor.
for n=1:Maxnumrings
    D1=(n-1)*movcondwidth+n*airgapwidth+(2*n-1)*dielwidth+0.5*(2*n-1)...
    *condwidth;
    N1=D1+airgapwidth;
    N2=D1;
    D2=N2-dielwidth;
    D3=D1+airgapwidth+movcondwidth;
    N3=D3+airgapwidth;
    D4=N3;
    N4=D4+dielwidth;
    CCylRingIA=(2*pi*epsilon0*epsilonA*CapLength/2)/log(N1/D1);
    CCylRingIR=(2*pi*epsilon0*epsilonR*CapLength/2)/log(N2/D2);
    CCylRingOA=(2*pi*epsilon0*epsilonA*CapLength/2)/log(N3/D3);
    CCylRingOR=(2*pi*epsilon0*epsilonR*CapLength/2)/log(N4/D4);
    CylRingC0=CylRingC0+((1/(1/CCylRingIA+1/CCylRingIR))+1/(1/CCylRingOA...
    +1/CCylRingOR));
end
if(CylRingC0>=1e-12)
for f=1:NdavgSteps
    davg=f*0.1e-06+Startdavg;
    %Squeeze film dampening
    baairgap=(96*etaair*CylRingAreaTotal*movcondwidth^2)/(pi^4*davg^3);
    omegac=(pi^2*davg^2*P0)/(12*etaair*movcondwidth^2);
    Ka=baairgap*omegac;          %Airgap spring constant
    RCouetteCylRing=(etaair*CylRingIntA)/airgapwidth;
    RPoiseuille=(12*etaair*CapLength)/((CylRingIntA/CapLength)*airgapwidth^3);
    Fe=-4*epsilon0*CylRingIntA*E0^2/(airgapwidth/epsilonA+dielwidth/epsilonR);
    ForceCylRing=PApplied*CylRingAreaTotal;
    Mr=(8*DensityAir*(Diam)^3)/(3*pi*sqrt(pi));

    Mt=CylRingMass+Mr;
    for b=0:NumLSteps
        BeamLCylRing=b*10e-06+StartL;    %Spring length
    for c=0:NumWSteps
        W=c*1e-06+StartW;                %Spring width.
    for d=0:NumHSteps
        H=StartH+d*0.5e-06;              %Spring hieght or thickness of the springs

```

```

kCylRing=(E*W*H^3)/(BeamLCylRing^3);           %Guided cantaliver beam
OmeganCylRing=sqrt((kCylRing*NumSprings)/Mt);
FreqCylRing=(1/(2*pi))*OmeganCylRing;
%Now Calculate the change in capacitance due to the displacement for the
%CylRing Capacitor.
FreqResAct=FreqRes;           %Start at the lowest frequency
if(FreqCylRing>=10e03)
for m=1:NumFSteps;
    freq(m)=m*FreqRes;
    omega(m)=2*pi*freq(m);
    s=j*omega(m);
    Rr=(DensityAir*(Diam)^4*omega(m)^2)/(2*pi*vsound);
    XCylRing(m)=(ForceCylRing+Fe)/(Mt*s^2+(Rr+RCouetteCylRing)*s+...
        kCylRing*NumSprings+(1/(1/(s*bairgap)+1/Ka)));
    if(m==(1000/FreqRes))
        if((CapLength-(abs(XCylRing(m))))>0)
            NewCylRingCapLength=CapLength-abs(XCylRing(m));
            Lnew=abs(XCylRing(m));
        else
            NewCylRingCapLength=0;
            Lnew=0;
        end
        MCylRing=(CapLength/(CapLength-Lnew))*E0-E0;           %Sensitivity
    end
    if(m>1)
    if(abs(XCylRing(m-1))<abs(XCylRing(m)))
        FreqResAct=m*FreqRes;
    end
    end
end
end
if(MCylRing>MaxM&&abs(XCylRing(FreqResAct/FreqRes))<=...
    abs(XCylRing(1000/FreqRes))*1.10)
    MaxM=MCylRing;
    MaxFreq=FreqResAct;
    LMax=BeamLCylRing;
    WMax=W;
    HMax=H;
    CLMax=CapLength;
    DMax=Diam;
    CondMax=movcondwidth;
    davgMax=davg;
    CMax=CylRingC0;
fprintf('Best MaxM= %.3e (V/Pa) at MaxF= %.3e (Hz) with L= %.1e ',...
    MaxM,MaxFreq,LMax)

```

K. PROGRAM 11

```
fprintf('W= %.1e H= %.1e CapLength= %.1e D= %.2e MovCondWidth= %.3e ',...
WMax,HMax,CLMax,DMax,CondMax)
fprintf('davg = %.3e Cmax= %.3d (F)\n',davgMax,CMax)
end
end
end
end
end
end
end
end
end
end

fprintf('done')
```

VITA AUCTORIS

Name: James Sliepenbeek
Place of Birth: Windsor, Ontario
Year of Birth: 1971
Education: B.A.Sc. Electrical Engineering,
University of Windsor, 1996
M.A.Sc. Electrical Engineering,
University of Windsor, 2003